University of California,

Irvine

Extraction Kinetics and Hydrodynamics in a Miniature Annular Centrifugal Contactor

DISSERTATION

Tro Babikian

Submitted in partial satisfaction of the requirements

for the degree of

DOCTOR OF PHILOSOPHY

in Chemical Engineering

by

Tro Babikian

Dissertation Committee:
Professor Mikael Nilsson, Chair
Professor Nancy Da Silva
Professor John LaRue

2019

DEDICATION

I would like to dedicate this work to my parents and particularly to my beloved wife who has always been the biggest supporter every step of the way.

TABLE OF CONTENTS

	Page
LIST OF FIGURES	v
LIST OF TABLES	ix
ACKNOWLEDGMENTS	x
CURRICULEM VUTAE	xi
ABSTRACT OF THE DISSERTATION	xii
INTRODUCTION	1
CHAPTER 1: Solvent Extraction	7
Project Aim	17
Process Efficiency	18
Approach	21
CHAPTER 2: Equilibrium Studies	22
Experiments and Discussion	26
Contactor Characterization	31
Experiments and Discussion	33
CHAPTER 3: Residence Time Distribution Analysis	44
Experiments and Discussion	47
CHAPTER 4: Extraction Kinetics	60
Theory	64
Stirred Cells	72
Results and Discussion	80
CHAPTER 5: Mixing and Droplet Formation	96
Final Analysis	106

CHAPTER 6: Summary and Conclusion 113

NOMENCLATURE 115

REFERENCES 118

LIST OF FIGURES

Page

Figure 1 Energy density of various fossil fuels given by the US Department of Energy 1

Figure 2 CO_2 Emission levels given by the Carbon Dioxide Information Analysis Center at Oak Ridge National Laboratory 2

Figure 3 The fission of uranium-235 upon capturing a thermal neutron 3

Figure 4 Composition of spent nuclear fuel after 10 years of cooling 5

Figure 5 A schematic representation of the process of solvent extraction 7

Figure 6 A schematic representation for a typical extraction flowsheet 9

Figure 7 Schematic cross-section representation of the CINC centrifugal Contactor 12

Figure 8 Robatel BXP012. Entire assembly 17

Figure 9 A generic example of a phosphinic acid (A) and a Phosphonic acid ester (B) 23

Figure 10 A schematic representation of the HEH[EHP] molecule 23

Figure 11 Average logarithm of distribution ratios vs equilibrium concentration of hydronium ions at 0.1 mM dysprosium nitrate and 0.2 M C572 at 20.0 C 26

Figure 12 Average distribution ratios vs initial concentration of dysprosium metal ions at 0.2 M C572 and 0.1 M nitric acid at 20.0 C 27

Figure 13 Average logarithm distribution ratios vs equilibrium concentration of unreacted HEH[EHP] at 0.1 M nitric acid at 20.0 C 28

Figure 14 Average distribution ratio vs total flowrate of aqueous and organic phases in Robatel BXP012 at 4500 RPM and room temperature 34

Figure 15 Average distribution ratio vs total flowrate of aqueous and organic phases in Robatel BXP012 at 4000 RPM and room temperature 35

Figure 16 Average distribution ratio vs total flowrate of aqueous and organic phases in Robatel BXP012 at 3500 RPM and room temperature 35

Figure 17 3D printed Robatel BXP012 housing 36

Figure 18 Height of the aqueous phase liquid column in the mixing zone in absence of organic phase. The fluid height reduces over time 37

Figure 19 Height of fluid column in the mixing zone at 3500 RPM on the left and 4500 RPM on the right 37

Figure 20 ANL contactors. a) 10 mm. b) 20 mm (extended mixing zone to the left) 39

Figure 21 Average distribution ratio vs total flowrate 3600 RPM and room temperature. Comparison of varies sizes of contactors at a/o =1 39

Figure 22 Average distribution ratio vs total flowrate 3600 RPM and room temperature. Comparison of varies sizes of contactors at a/o =2 40

Figure 23 Concentration of UO_2^{2+} in the organic effluent as a function of operation time at a/o =2. The first point was collected when both phases start exiting the contactor 41

Figure 24 Concentration of UO_2^{2+} in the organic effluent as a function of operation time at a/o =3. The first point was collected when both phases start exiting the contactor 42

Figure 25 Uranyl concentration of the organic phase in the mixing, separating zones of the 20 mm ANL contactors relative to the effluent concentration 43

Figure 26 The change in concentration vs time following an injection of a tracer in a perfectly-mixed ideal CSTR 45

Figure 27 Concentration of the tracer in the aqueous phase leaving the Robatel BXP012 contactor as a function of time for A/O=1 and 3500 RPM 48

Figure 28 Concentration of the tracer in the aqueous phase leaving the Robatel BXP012 contactor as a function of time for A/O=1 and 4000 RPM 49

Figure 29 Concentration of the tracer in the aqueous phase leaving the Robatel BXP012 contactor as a function of time for A/O=1 and 4500 RPM 49

Figure 30 Concentration of the tracer in the organic phase leaving the Robatel BXP012 contactor as a function of time for A/O=1 and 3500 RPM 51

Figure 31 Concentration of the tracer in the organic phase leaving the Robatel BXP012 contactor as a function of time for A/O=1 and 4000 RPM 52

Figure 32 Concentration of the tracer in the organic phase leaving the Robatel BXP012 contactor as a function of time for A/O=1 and 4500 RPM 52

Figure 33 Concentration of the tracer in the aqueous phase leaving the ANL 20 mm ACC with non-extended mixing zone as a function of time for A/O=1 at 3600 RPM 55

Figure 34 A schematic representation of a rising-falling bubble apparatus, left, and an organic droplet, right 60

Figure 35 The Kenics centrifugal contactor-centrifuge. A and B are the inlets to the contactor, C is the Kenics mixer and D is the centrifugal separator 61

Figure 36 A schematic representation of a microfluidic device 62

Figure 37 A schematic representation of the Lewis stirred cell 63

Figure 38 A schematic representation of the hydrodynamics in a Lewis cell, right, the stagnant layers, left 67

Figure 39 Dependence of flux on stirring speed in Lewis cells 73

Figure 40 Stirred beaker, left, stirrers, right 76

Figure 41 The Nitsch cell designed at the Karlsruhe Institute of Technology 77

Figure 42 On the left are the vertical baffles on which the inner cylinder is placed. On the right is the three bladed pitched stirrers 77

Figure 43 The stepper motors connected to the control circuit 78

Figure 44 Dysprosium concentration profile in the aqueous phase as a function of time 80

Figure 45 Concentration of dysprosium ions in the aqueous phase as a function of time. The initial rate fits first order kinetics 80

Figure 46 Natural logarithm of the remaining concentration in the aqueous phase as function of time in the Lewis cell 82

Figure 47 The flux of dysprosium into the organic phase as a function of stirring speed 82

Figure 48 The mass transfer coefficient in the aqueous phase as a function of stirring speed 83

Figure 49 Aluminum mesh, right, used in the high RPM experiment and a thin layer of PMMA, left, used in the interfacial area reduction experiment 84

Figure 50 Comparison of the reaction observed rate constant between the highest possible stirring without the addition of meshes and higher stirring speed with the presence of meshes 84

Figure 51 0.1 mM $Dy(NO_3)_3$ in 0.1 M HNO_3 and 0.2 M C572 in Isopar l at 20.0 °C 85

Figure 52 0.1 mM $Dy(NO_3)_3$ in 0.1 M HNO_3 HEH[EHP] in dodecane at 20.0 °C 87

Figure 53 In the plateau region $Dy(NO_3)_3$ in 0.1 M HNO_3 HEH[EHP] in dodecane at 20.0 °C 87

Figure 54 shows the rate of surface renewal as a function of stirring speed 89

Figure 55 Overall mass transfer coefficient of dysprosium extraction from the aqueous to organic phase as a function of ligand concentration 89

Figure 56 Interfacial Tension of HEH[EHP] in Dodecane with 0.1 M HNO3 91

Figure 57 Number of molecules per unit interface area calculated using the Gibbs adsorption Isotherm 91

Figure 58 Natural logarithm of the concentration of ligand as a function of observed rate constant 92

Figure 59 Initial rate of extraction as a function of initial ligand concentration for 0.1 mM initial dysprosium concentration 93

Figure 60 Initial rate of extraction as a function of initial ligand concentration for 1.0 mM initial dysprosium concentration 93

Figure 61 Initial rate of extraction as a function of initial ligand concentration for 10 mM initial dysprosium concentration 94

Figure 62 Sauter and maximum droplet diameter in the mixing zone of the Robatel BXP012 at a/o =1 as a function of rotor speed 103

Figure 63 Sauter and maximum droplet diameter in the mixing zone of the 20 mm ANL ACC as a function of total flow rate 103

Figure 64 The organic holdup volume in the mixing zone as a function of total flowrate for the Robatel contactor at 3500 RPM using the mass transfer coefficient obtained from the Nitsch cell 108

Figure 65 The organic holdup volume in the mixing zone as a function of total flowrate for the Robatel contactor at 4000 RPM using the mass transfer coefficient obtained from the Nitsch cell 108

Figure 66 The organic holdup volume in the mixing zone as a function of total flowrate for the Robatel contactor at 4500 RPM using the mass transfer coefficient obtained from the Nitsch cell 109

Figure 67 The organic holdup volume in the mixing zone as a function of total flowrate for the Robatel contactor at 3500 RPM 111

Figure 68 The organic holdup volume in the mixing zone as a function of total flowrate for the Robatel contactor at 4000 RPM 111

Figure 69 The organic holdup volume in the mixing zone as a function of total flowrate for the Robatel contactor at 4500 RPM 112

LIST OF TABLES

Page

Table 1: Physical dimensions of the Robatel BXP012 31

Table 2. Summary of the aqueous phase RTD results at 4000 RPM 50

Table 3. Summary of the organic phase RTD results 53

Table 4: Holdup volume of the organic phase in the mixing zone of the 20 mm ANL contactors under varying parameters. The error represents the standard deviation of multiple runs 57

Table 5: Holdup volume of the organic phase in the mixing zone of the 20 mm ANL contactors under varying parameters. The error represents the standard deviation of multiple runs 58

Table 6: Comparison between the Robatel and the Argonne contactors in terms of non-dimensional quantities 106

ACKNOWLEDGMENTS

I would like to extend my sincerest gratitude and appreciation to Professor Nilsson for his mentorship, guidance, and continuous support leading to the successful completion of this project. I would like to acknowledge and thank Professors Nancy Da Silva, John LaRue, Hung Nguyen, and Diego Rosso, for taking the time to serve on my advancement to candidacy and defense committees. I would also like to thank the members of the Nilsson lab for their help and support and Jonathan Wallick for his continuous assistance at the UCI TRIGA nuclear reactor. In addition, I would like to acknowledge the U.S. Department of Energy U.S. DOE, Nuclear Energy University Program, NEUP, for the financial support under contract # DE-NE0008288. Finally, I would like to acknowledge and thank Dr. Kent Wardle and Professor Andreas Geist for their help and guidance with specifics pertaining to this study.

CURRICULUM VITAE

Tro Babikian

2013 B.S. in Chemical Engineering, University of California, Irvine

2015 M.S. in Chemical Engineering, University of California, Irvine

2019 Ph.D. in Chemical Engineering, University of California, Irvine

FIELD OF STUDY

Extraction Kinetics and Hydrodynamics in a Miniature Annular Centrifugal Contactor

ABSTRACT OF THE DISSERTATION

Extraction Kinetics and Hydrodynamics in a Miniature Annular Centrifugal Contactor

By

Tro Babikian

Doctor of Philosophy in Chemical Engineering and Materials Science Engineering

University of California, Irvine, 2019

Professor Mikael Nilsson, Chair

Annular centrifugal contactors have become attractive equipment for the separation step in the recycling process of spent nuclear fuel due to their high efficiency, high throughput, and rapid operational properties relative to other recycling equipment such as mixer-settlers and pulsed columns. Various sizes of contactors ranging from laboratory scale to commercial scale have been developed for different needs and process scales. As in all solvent extraction equipment, the efficiency of a single stage will depend on residence time and interfacial area. A characteristic to centrifugal contactors is the free interface of their mixing zone causing the holdup volume to change depending on the operational parameters. To successfully simulate and model the separation process in a centrifugal contactor, certain aspects of the hydrodynamics must be known. In this work, the holdup volume of the dispersed phase in the mixing zone of the lab-scale Robatel BXP012 centrifugal contactor was investigated by two approaches. First, residence time

distribution (RTD) measurements of both the aqueous and the organic phases by the method of a pulse input was performed. The aqueous phase was found to have a longer residence time suggesting a larger holdup. The interfacial mass transfer kinetics for the extraction of dysprosium ions from a nitric acid medium with both cyanex 572 and HEH[EHP] was studied with the use of a Nitsch cell. A forward extraction rate law was suggested having a first order and half order dependence on the metal ion in the aqueous phase and the extracting ligand in the organic phase, respectively. Mass transfer coefficients were obtained from both the Nitsch cell and a similar centrifugal contactor and the method of a chemical reaction was applied to the Robatel BXP012 to estimate its organic holdup volume. The holdup volume in the contactor mixing zone was found to increase with total flow rate ranging from 0.1 ml to about 0.5 ml when a constant mass transfer coefficient is used

Introduction and Background

Since their existence, humans have always strived for energy. They used the chemical energy in food to stay alive, the thermal energy contained in wood to stay warm, and the mechanical energy in rivers to travel, for instance. [1] However, the discovery of fossil fuels such as coal and petroleum, characterized with high energy densities figure 1, along with the industrial revolution in Europe in the 18th century provided significant improvement to people's quality of life. Starting with the steam engine to the creation of electricity and the internal combustion engines, energy was no longer merely a means for surviving but it provided convenience and luxury to humanity.

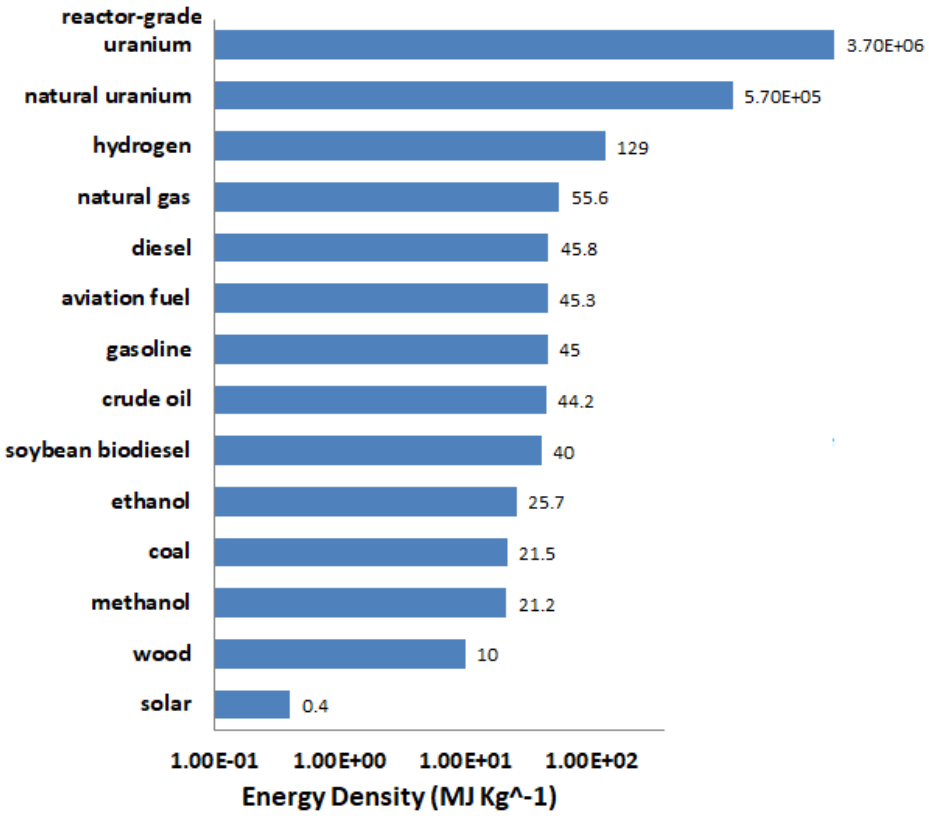

Fig. 1. Energy density of various fossil fuels given by the US Department of Energy [2]

As a result, the population of the planet started to rapidly increase over the last few decades reaching exponential rates. In addition, both industrial and technological advancements in highly populated developing countries such as India and China have led to enormous need for energy globally. According to the International Energy Outlook 2013 report, the world's energy is projected to increase by 56% by the year 2040 with 90% increase in non- Organization for Economic Cooperation and Development (non-OECD) Countries. [3] To meet this ever-increasing demand for energy, more coal and natural gas is burned for their high energy density, 30 GJ/m^3 and 40 MJ/m^3 respectively. [4] This tremendous extraction of energy to maintain a modern quality of life, however, is rapidly and permanently degrading our environment. Burning fossil fuels comes at the price of releasing pollutants, and greenhouse gasses (GHG), primarily CO_2, see figure 2, into the atmosphere. Over the course of the past few decades this has significantly contributed to global warming and has even caused significant drought in countries like China.

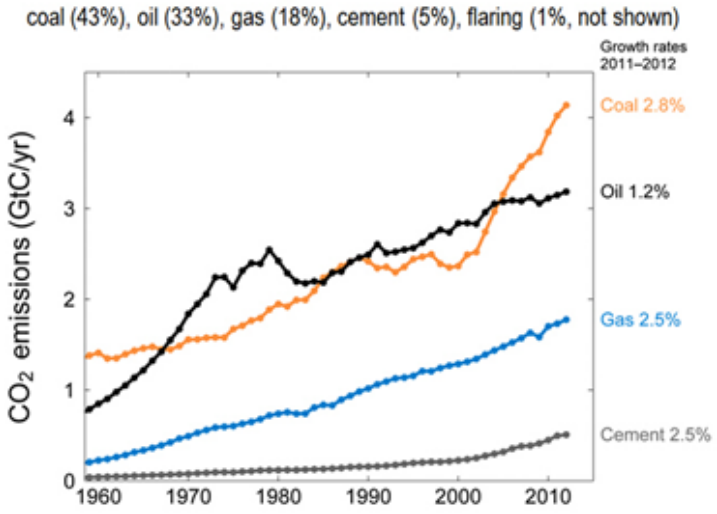

Fig. 2. CO_2 Emission levels given by the Carbon Dioxide Information Analysis Center at Oak Ridge National Laboratory [5]

According to Greenpeace, a non-governmental environmental organization, coal power plants annually consume water enough to meet the basic needs of almost one billion people. [6] In recent years, alternative power production methods, the so-called renewables such as photo voltaic solar cells and windmills, have been developed to assist in lowering the levels of GHG in the atmosphere. The major advantage of renewables besides having net-zero CO_2 emissions is their use of inexhaustible "fuel". Neither the sun nor the wind will vanish any time soon. Nevertheless, a major drawback is their inability to produce energy that is comparable to today's need. [4] Not to mention, their performance is affected primarily by weather conditions, which are not always predictable. These considerations emphasize the necessity of having a clean source of energy that will not further damage the environment and yet be able to produce enough energy to meet the increasing demand. Nuclear fission is perhaps the most significant source of energy on the planet Earth. [4, 7, 8]Nuclear fission occurs when a heavy nuclide captures a neutron and due to its instability splits into two lighter nuclides releasing tremendous energy in the form of radiation and fragment kinetic energy that is converted to thermal energy for use. The most common example is the fission of ^{235}U, shown in figure 3, producing about 200 MeV of energy per fission.

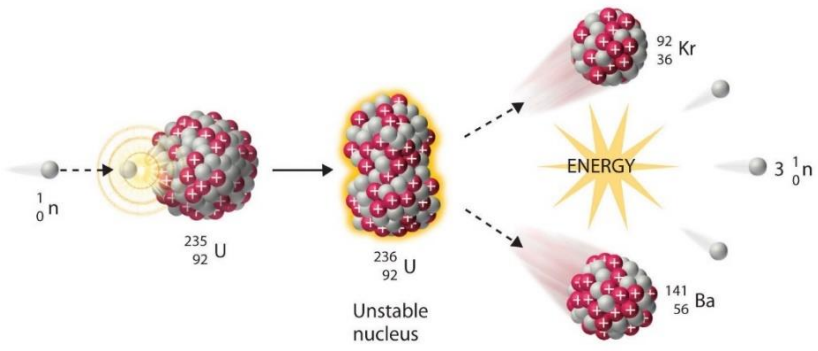

Fig. 3. The fission of uranium-235 upon capturing a thermal neutron[9]

In addition to the enormous energy that could be recovered from the fission process, another major advantage of nuclear power is its relatively negligible CO_2 and GHG pollutants emissions [10]. It has been calculated that globally about 1.8 billion pollutant-related deaths and release of over 64 Gtons of CO_2 equivalent GHG have been prevented by the current nuclear power generating plants. [11, 12]It is also worth mentioning that the energy returned on energy invested for nuclear power dominates the list at a value of 75 compared to 30, 28, 9, and 3.9 for coal, natural gas, solar, and wind, respectively.[13] The nuclear fuel cycle can be described in two major stages. The front-end stage consists of mining, milling, converting, and enriching the uranium to be used in the nuclear reactor. The back-end stage is where the used nuclear fuel (UNF) is either entirely kept in final repositories (this is called a once –through cycle) or has first been recycled to recover the unfissioned uranium and then the remaining high level waste (HLW) is sent to final repositories. [8, 14, 15]Unfortunately, since 1976 the US has deferred all commercial reprocessing of UNF over proliferation concerns adopting the once-through cycle. As a result of this policy, there is about 90,000 metric tons of HLW stored on site and increasing by about 2,400 metric tons per year. Reprocessing the UNF has many advantages over the once-through cycle. As shown in figure 4 over 95% of the uranium will still be present when the fuel is removed from the reactor. At the time of removal, the concentration of neutron poisons, non-fissile nuclides with high neutron capture cross section, accumulated in the fuel prevents further fission and render it unusable.

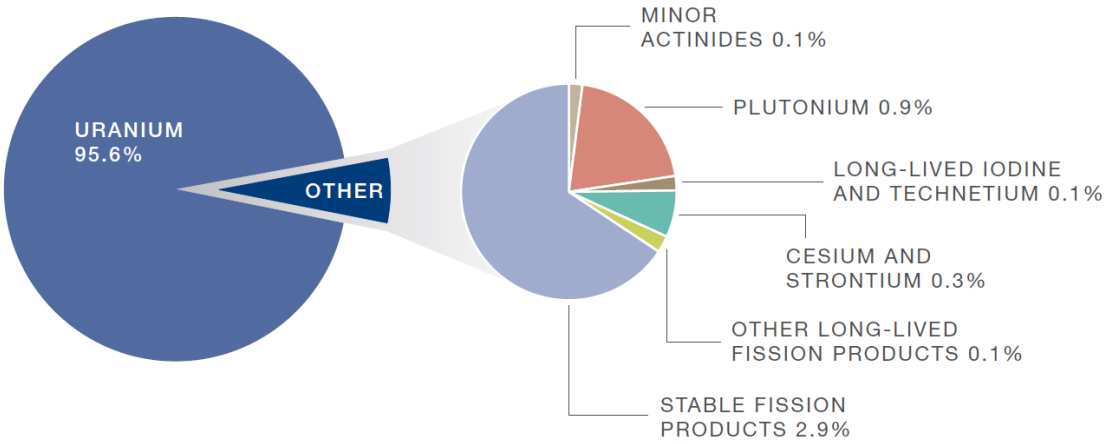

Fig. 4. Composition of spent nuclear fuel after 10 years of cooling [14]

Therefore, the first obvious reason for recycling is preserving natural resources. Used nuclear fuel is also very rich in rare earth elements (REE), about 40% of the mass of fission products in the fuel. [16]These elements, due to their distinct chemical and physical properties, have vital applications in medicine, renewable energy, defense, etc. [17]China being almost the only supplier of REE in the world can pose a national threat to the US. Recycling UNF can be a great way of recovering REE to meet local demand. [18] Also, due to their high neutron capture cross sections, REEs become problematic in processes such as transmutation, a proposed method of reducing the long-lived and most radiotoxic elements in used nuclear fuel. Last, but not least, recycling is essential in minimizing the long-term radioactivity of UNF. The extent of radioactivity of UNF will depend on the type of reactor the fuel came from, its composition, and burnup. Although present in tiny concentrations, about 1% wt, the following radionuclides are the major source of radiation in the UNF. Transuranics consisting of ^{237}Np, $^{238, 239,240}$Pu, ^{241}Am, $^{242, 244}$ Cm and long-lived fission products such as ^{99}Tc and ^{129}I are responsible for the long term, up to a million-year, radiotoxicity of the fuel whereas short-lived fission products such as ^{90}Sr and ^{137}Cs will be

the main contributor to the radiotoxicity of the fuel for the first thousand years.[8, 14, 16, 19] Therefore, recycling of UNF provides the means for segregating and concentrating these long-lived radionuclides in a much smaller volume making their disposal process, or transmutation, easier and manageable. One of the main methods for this separation is solvent extraction, or liquid-liquid extraction.

I. Solvent Extraction

Solvent extraction is a separation method that utilizes the difference in solubility of a molecule between two immiscible liquid phases as depicted in figure 5.

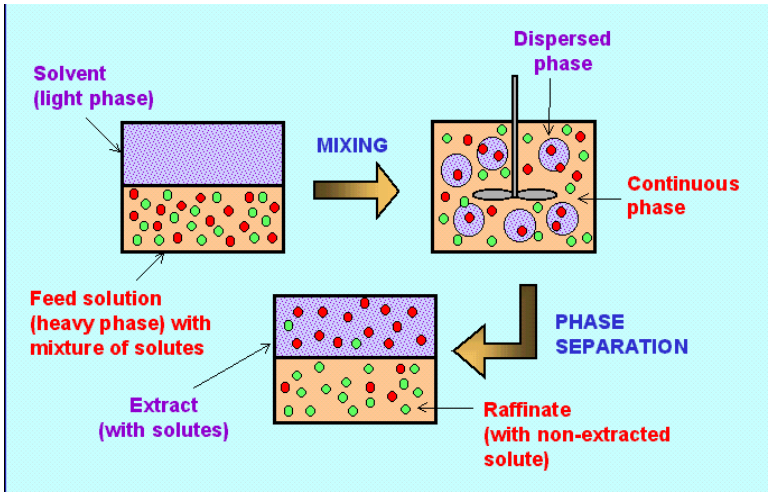

Fig. 5. A schematic representation of the process of solvent extraction [20]

The extent of extraction is measured by a parameter called the distribution ratio, D, which is a measure of the concentration of the extracted molecule in the organic phase to its remaining concentration in the aqueous phase.

$$D = \frac{C_{i,org}}{C_{i,aq}} \qquad (1)$$

All symbols for all equations are defined in the nomenclature section on page 115.

Due to the significant difference in the polarity of the two immiscible phases, which are most of the time an organic phase and an aqueous phase, the metal ions do not spontaneously partition by themselves between the two phases. Therefore, amphiphilic

reagents, molecules with both hydrophobic and hydrophilic functional groups, are needed for this separation to occur. Generally speaking, there are two mechanisms by which the metal ions interact with the amphiphilic reagents, cation exchange and solvation of metal salts.[16] These two mechanisms are explained respectively with the following reactions

$$M_{aq}^{+3} + 3HL_{org} \leftrightarrow ML_{3,org} + 3H_{aq}^{+} \qquad (2)$$

$$M_{aq}^{+3} + 3L_{aq}^{-} + 2HL_{org} \leftrightarrow ML_3(HL)_{2,org} \qquad (3)$$

One of the first solvent extraction processes developed for recycling UNF was the PUREX process. [21] It was developed in 1949 and has been implemented on the industrial scale for reprocessing UNF since 1954. In this process, which implements solvation of metal salts as in equation 3, molecules of tri-butyl phosphate in an organic diluent selectively coordinate with uranium and plutonium ions dissolved in nitric acid in the aqueous phase and transfer them into the organic phase. Over the years, with the growing interest in recycling UNF for civilian purposes, different extracting reagents were developed for the selective extraction of elements of interest. In parallel to research on the molecular and chemistry level of recycling UNF, a lot of effort was also put in designing and developing the necessary equipment that would be capable of maintaining a safe and an efficient reprocessing scheme. Some extracting reagents, such as the bis-triazine-bipyridine, BTBPs, used in separating the trivalent actinides from lanthanides, though they have high separation factors and are insusceptible to effects of radiolysis and hydrolysis, suffer from slow extraction kinetics. [22] On the other hand, Cyanex 301 is an efficient extractant; however, it will undergo radiolysis and break down to different undesirable molecules. Therefore,

depending on the chemistry of the extraction system used, some processes will require rapid operational conditions to minimize the effects of radiolysis whereas others will require batch operations to maximize efficiencies. Consequently, a variety of reprocessing equipment was designed to accommodate these needs at different stages of reprocessing UNF. Figure 6 depicts a typical solvent extraction system needed for a successful and an optimized process.

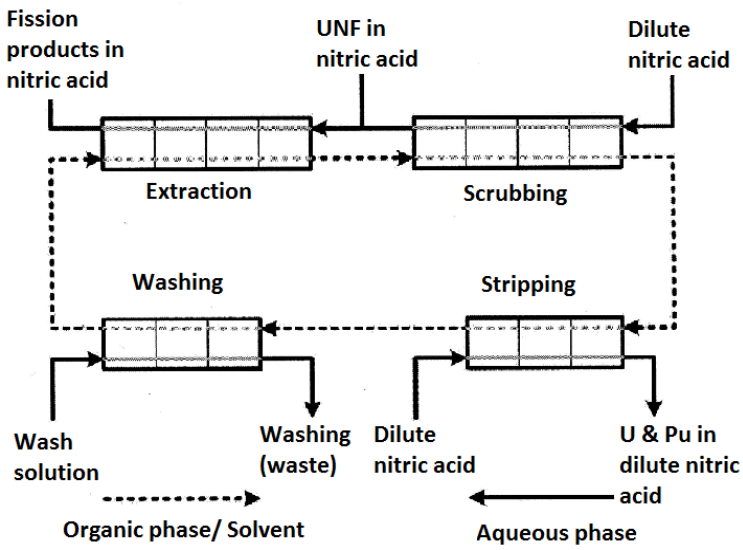

Fig. 6. A schematic representation for a typical extraction flowsheet. [16] Flow of aqueous phases depicted as solid lines and flow of organic phases as dashed lines.

Each square represents a contacting stage between the two phases and multiple stages will be required to achieve a certain extraction value. Scrubbing, washing, and stripping are important to eliminate undesired extracted species and also to recycle the organic phase. For efficient and safe operations, extraction equipment used in these stages should satisfy the following.

- Maximize interfacial area between the two phases to enhance the flux of solute between the phases.
- Minimize the contact time of the phases to reduce the effects of radiolytic degradation of the extracting reagents.
- Allow a wide range of both flowrates and also phase ratios to accommodate chemicals with different physical properties, such as viscosity and density.
- Have the ability to rapidly reach steady-state conditions.
- Have high tolerance to unexpected operational disturbances.
- Avoid the accumulation or the orientation of a critical mass of fissile nuclides to prevent the initiation of a self-sustained nuclear reaction.
- Have the potential to operate complex multi-cycle processes

Three major types of equipment have been used in the nuclear reprocessing industry. The first is called mixers-settlers. As its name indicates they are comprised of two stages. In the mixing stage the two phases are mixed with a propeller until a chemical equilibrium is achieved. Then the solution is moved to the settling stage where under gravity the two phases are separated and then moved to the next stage for further extraction. The advantage of this design is its allowance for reactions with slow kinetics to reach equilibrium in the process. Its disadvantage, however, is that it maximizes radiolysis of the extracting ligands due to the extended time needed for the two phases to separate under the gravitational acceleration. The second type of contacting equipment is called pulsed

columns. In this design, the organic and the aqueous phases are fed in a counter current manner into a column that has perforated plates along its length. As the two phases pass through the plates, droplets are created, and extraction is achieved. The third type of equipment is called centrifugal contactors. These were first developed at Savannah River National Laboratory as two stage contactors. [23] Similar to mixer-settlers, the two phases were mixed together in a stage that also acted as a pump to transfer the solution over to a centrifuge where they were separated under centrifugal forces. Centrifugal contactors however have a major advantage over mixers-settlers owing to their rapid phase separation under high centrifugal forces, up to 900G for the Costner Industries Nevada Corporation, CINC, model with 50 mm rotor diameter. This significantly minimizes the radiolysis of the organic phase. Argonne National Laboratory around 1970 modified the original design of centrifugal contactors to combine the mixing and the settling stages into one, as shown in figure 7

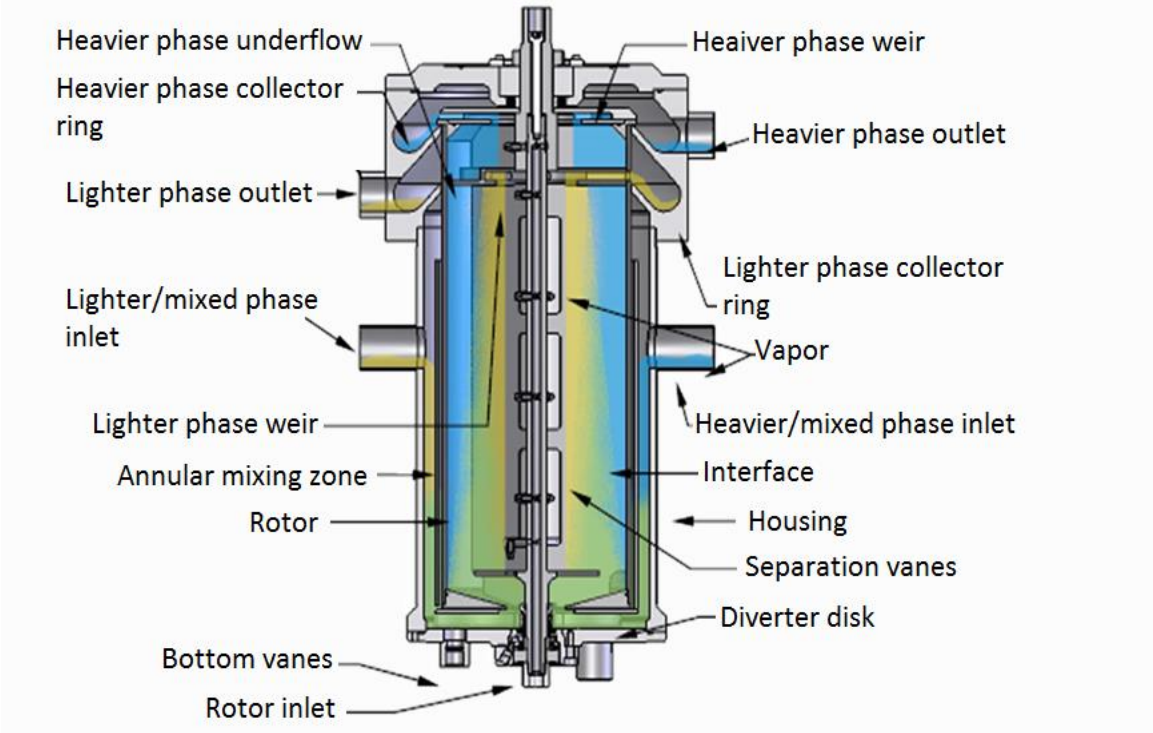

Fig. 7. Schematic cross-section representation of the CINC centrifugal Contactor [24]

and named the equipment annular centrifugal contactors (ACC) due to its annular gap. The reason for this change in design was primarily to avoid criticality during reprocessing of plutonium. Lower operational and maintenance cost due to the integration of two stages into one, and easier use in hot cells were also possible with the new design. [23, 25-27]ACCs can be divided into three distinct zones in terms of functionality and flow characteristics. These are the mixing zone or the annulus, the separating zone, and the discharge zone. The mixing zone consists of the gap between the stationary housing and the spinning rotor. The two phases enter the mixing zone trough the inlets and mix under the action of the rotor to react. As the mixture flows down the length of the annulus, vanes located at its bottom break the angular velocity of the flow and redirect it into the separating zone, which is the inside of the spinning rotor. In the separating zone, the two immiscible phases separate

under the centrifugal force based on their densities and move upwards to the discharge zone, which consist of weirs utilized in adjusting the interface of the emulsion. The throughput of ACCs is defined as its capability of completely separating the two phases with zero cross contamination. The separating zone having this functionality determines the throughput of a particular ACC. Due to the dual functionality of the rotor as a mixer and a separator, higher RPM will cause higher centrifugal acceleration of the flow particles resulting in faster separation; however, it will also result in smaller droplets of the dispersed phase, which enhances mass transfer but slows the separation process. Therefore, phase separation as can be approximated by Stokes' law, equation 4, for the terminal velocity of solid spheres moving in a viscous media, [28] and mass transfer efficiency as given by equation 5 are competing processes.

$$u_\infty = \frac{d_p^2(\rho_c - \rho_p)}{18\mu} r_{in}\Omega^2 \qquad (4)$$

$$\eta_M = \frac{C_{i,f} - C_{i,r}}{C_{i,f} - C_{i,r\,eq}} \qquad (5)$$

In 1981 R. A. Leonard came up with a non-dimensional number called the dispersion number, N_D, to assess the throughput of centrifugal contactors. N_D is defined as the ratio of the residence time of the dispersion band in the separating zone to the time it takes for a droplet to travel the thickness of the band. [29] In its general form N_D is given in equation 6.

$$N_D = \frac{1}{\tau}\sqrt{\frac{\Delta Z}{a}} \qquad (6)$$

It has been experimentally determined over a wide range of annular gaps and rotor-to-housing radius ratios that the value of N_D does not change with the mixer type. Rather, the dispersion number depends on the specific system used in terms of the relative densities of the phases and their interaction properties. Therefore, N_D can be determined from a batch test with gravitational acceleration to determine the maximum throughput of a contactor, using equation 7, given that both the volume of the separating zone and the thickness of the dispersion band are known.

$$N_D = \frac{\bar{V}}{V}\sqrt{\frac{\Delta Z}{\bar{r}\Omega^2}} \qquad (7)$$

Another factor that affects the throughput of ACCs is the annular liquid height (ALH), which is the liquid level in the annular region. Since there are no physical boundaries restricting the ALH, if it rises too high it could spill into the organic collector ring flooding the reactor. The organic to aqueous flow rate ratio, O/A, also plays a major role in limiting the throughput of ACCs. Difficulties in phase inversion caused by changes in operational conditions during a run could result in the formation of a high structural viscosity solution inside the annual gap upsetting normal operations. [23]

In order to evaluate the performance of ACCs, it is necessary to understand the characteristics of both flow and mass transfer that take place in its different sections. Over the past century, numerous experimental and theoretical studies have been conducted to characterize the flow between two rotating concentric cylinders, which is similar to the geometry of the annular zone in ACC. G.I. Taylor, building on the work of Couette, in 1923, discovered that disturbances caused by increasing the rotational velocity of a viscous fluid

confined between two independently rotating concentric cylinders will cause a transition from a Circular-Couette flow characterized with having only azimuthal velocity to the formation of oppositely spinning vortices. Taylor characterized this type of flow by a non-dimensional number that describes the ratio of centrifugal forces to viscous forces. One mathematical expression of the Taylor number for the case of a rotating inner cylinder and a stationary outer cylinder as in the ACCs is given in equation 8. Also, the Reynolds number, which compares inertial forces to viscous forces in a flow, for this case is given in equation 9.

$$\mathrm{Ta} = \frac{\mathrm{r_{in}}(\mathrm{r_{out}} - \mathrm{r_{in}})^3 \Omega^2}{\nu^2} \qquad (8)$$

$$\mathrm{Re} = \frac{\mathrm{r_{in}} \Omega (\mathrm{r_{out}} - \mathrm{r_{in}})}{\nu} \qquad (9)$$

A great deal of research in this area followed the work of Taylor. Numerical analysis for determining the onset of instabilities responsible for Taylor vortices was done by Stuart.[30] Koschemider studied the fate of these vortices as the Ta number was substantially increased over its critical value, the onset of instability, to demonstrate that turbulent Taylor vortices exist and are larger than the laminar ones.[31] Andereck and Swinney conducted numerous experiments varying the rotational velocities of both the inner and the outer cylinders in addition to their heights to discover a handful of different flow regimes characterized with vortices and spirals.[32] Lueptow investigated the effects of adding an axial Poiseuille flow to the Couette flow on formation of Taylor vortices. He concluded that axial flows will cause the formation of Taylor vortices to occur at higher Ta numbers than if the axial flow did not exist. He also investigated a wide range of flow

regimes over varying Ta and axial Re numbers. [33] All these flow regimes are not true representations of the flow in the annulus of ACCs for the following reasons. The apparatus in these studies consisted of two concentric cylinders of the same height with annular gaps that were completely full of one phase liquid fluid. The geometry of the annular gap in ACCs is different since the rotor, the inner rotating cylinder, does not extend all the way to the bottom level of the outer cylinder. Therefore, the flow in the lower section of the annulus is not truly of a Couette type. Another geometrical difference is in the existence of vanes at the bottom of the annulus responsible for redirecting the flow into the rotor for separation. In addition, the fluid in ACCs is multi-phase being aqueous, organic and a top layer of air forming a liquid-gas interface as the upper boundary of the system. Davis and Weber studied using TBP in ultrasene and uranium in nitric acid the effects of having two phases on a Couette type flow and also investigated phase continuity effects on mass transfer efficiency. [34] They observed that while having an additional phase did not interfere with the formation of Taylor vortices, higher RPMs were needed to blend the otherwise segregated vortices of different phases. They also observed that increasing the RPM resulted into better mass transfer in the case of organic continuous due to increasing holdup and interfacial area. Watanabe and Toya studied the effects of having a free surface in Couette flow with an inner rotating cylinder and an outer and a lower stationary cylinder and a wall. They used both a computational method and experiments to observe the formation of different modes of Taylor vortices based on the rate of the acceleration of the inner cylinder. [35, 36]Even though these studies somewhat reflect the flow in ACCs, none of them describe the flow field of a reactive, multiphase, turbulent, free surface, and Couette-Poiseuille flow in a geometry similar to the one in the annular gap of ACCs.

Project Aim

The objective of this research project is to study the mass transfer and stage efficiency in a miniature, lab-scale centrifugal contactor to allow studying the effects of scaling on the performance of ACCs as compared to bench-scale contactors. The Robatel BXP012, figure 8, is a French made lab-scale ACC with a rotor diameter of 12 mm. The small size of this contactor makes it more proper for studying the chemistry of processes rather than being used in industrial applications. The CINC contactor on the other hand has a rotor diameter of 50 mm allowing it to have a much higher throughput and making it suitable for use in industrial processes. The CINC contactor has already been extensively studied and hence this project will focus on characterizing the Robatel BXP012. A 20 mm and a 10 mm 3D printed contactor made by Argonne National Laboratory were also tested to aid with the study.

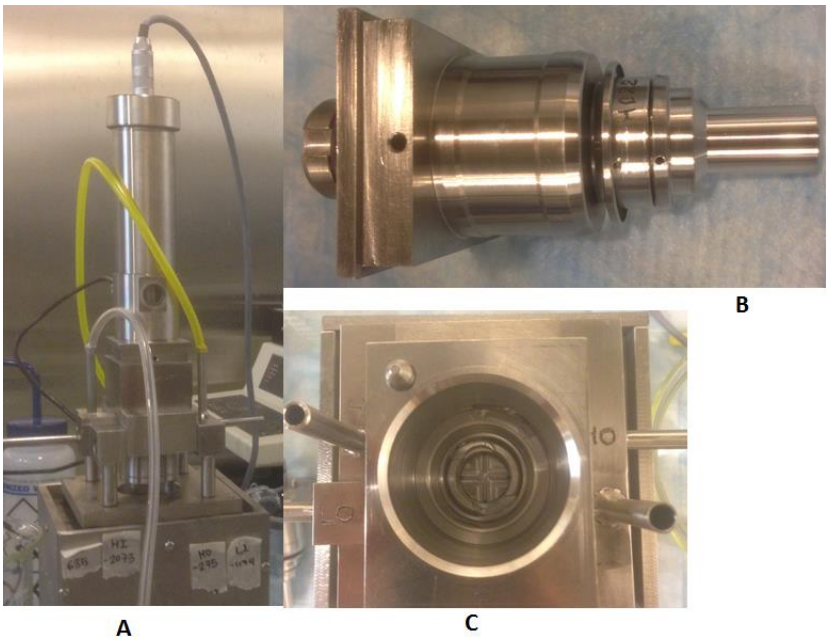

Fig. 8. Robatel BXP012. Entire assembly with the motor (A), the rotor (B), the housing and collector ring (C)

Process Efficiency

In chemical processes involving multiple liquid-liquid contacting stages, the individual stage efficiency is usually defined in term of the concentration of the species of interest as shown in equation 5 and is referred to as the Murphree efficiency η_M [37]. This is different than the overall cascade efficiency which is defined as the ratio of theoretical to needed stages for a given efficiency.

$$\eta_0 = \frac{n}{N} \tag{10}$$

The overall processes efficiency for a countercurrent process can be related to the individual stage efficacies where the distribution ratio is assumed to be constant by [38]

$$\eta_0 = \frac{\ln[1 + \eta_M \left({}^{1}/_{E_f} - 1\right)]}{\ln({}^{1}/_{E_f})} \tag{11}$$

Where E_f is the extraction factor defined as [39]

$$E_f = \frac{\overline{V_{org}}}{\overline{V_{aq}}} * D \tag{12}$$

Therefore, the greater the value of the extraction factor, which can be adjusted by changing the flow rate ratio of the two phases, the greater the separation is and hence the higher the overall separation efficiency of the process. If $E_f \gg 1$, then the process is extraction meanwhile, if $E \ll 1$ then the process is stripping. The single stage Murphree efficiency can be related to mass transfer parameters using a molar balance on the stage

$$\frac{dN_i(t)}{dt} = \overline{V_{in}} C_{i,in}(t) - \overline{V_{out}} C_{i,out}(t) + \int r_i \, dV \tag{13}$$

When the stage is operating at steady-state, equation 13 reduces to

$$0 = \overline{V_{in}} C_{i,in} - \overline{V_{out}} C_{i,out} + \int r_i \, dV \qquad (14)$$

In case of plug flow reactors PFRs, the Lagrangian term will vary across the reactor volume while for well mixed reactors, such as a CSTR, it could be assumed to be constant over the entire reactor volume. [40]

In homogenous well-mixed reactors where both the reactants and the products are in the same phase, molecular diffusion is negligible, and the reaction rate would be representative for the rate of generation or consumption of the species of interest. In heterogenous processes however, even in well-mixed systems, molecular diffusion can still have an influence on the rate of generation or consumption of the species of interest. The extent of this effect will depend on the hydrodynamics of the flow and therefore, it is more customary to represent the transfer rate in terms of mass transfer coefficient. This will be covered in more details in the kinetics chapter.

Therefore, the source term can also be written in terms of a mass transfer coefficient and the interfacial area of the droplet on which the reaction, and hence the transfer, occurs. Assuming the mass transfer coefficient is the same everywhere in the contactor

$$\int r_i \, dV = \int J_i \, dA = k\left(C_{i,eq} - C_i\right) A_{total} \qquad (15)$$

Substituting equation 15 into 14, and taking the organic phase to be the dispersed phase

$$\overline{V_{in}} C_{i,in} - \overline{V_{out}} C_{i,out} = k\left(C_{i,eq} - C_i\right) A_{total} \qquad (16)$$

Equation 16 can be further broken down into

$$\overline{V_{in}}C_{i,in} - \overline{V_{out}}C_{i,out} = k\left(C_{i,eq} - C_i\right)aV_{tot} \qquad (17)$$

And in general, the Murphree efficiency based on the dispersed phase can be expressed as

$$\eta_M = \frac{kaV_{tot}/\overline{V_D}}{1 + kaV_{tot}/\overline{V_D}} \qquad (18)$$

From equation 18, if the surface area of the dispersed phase per unit volume of mixture is known, and the mass transfer coefficient of the extraction process is also known, then the efficiency of the stage can be calculated. Overall, the efficiency of a stage will depend on two physical parameters, the extent of mixing which is responsible for maximizing the interfacial area, and also the residence time of the phases in the stage.

Approach

In this study, the following approach was implemented to study the holdup volume of the dispersed phase in mixing zone of the miniature Robatel ACC.

1- The extent of the extraction was studies as a function of flow rate, rotor speed, and phase continuity
2- Using the method of residence time distribution with a pulse input, the hold-up volume of the phases was measured. The 20 mm Argonne contactor had a drain allowing for the physical measurement of the holdup in both the annular and separation zones.
3- Using a Nitsch cell, the rate constant and the reaction order of the extraction reaction was studied. This setup also allowed for the calculation of the overall mass transfer coefficient at varying conditions.
4- Using correlations based on the rate of kinetic energy dissipation, the Sauter mean diameter of the organic droplets and the average surface area per unit volume of total holdup was calculated.
5- A molar balance was used with the above measured and calculated quantities to estimate the holdup volume of the dispersed organic phase in the mixing zone

II. Equilibrium Studies

Before performing experiments on the contactors, the extraction chemistry of the systems used was studied in a batch mode through equilibrium studies. The effects of acid, metal ion, and extractant concentration on the distribution coefficient were studied and based on slope analysis, a suggestion about the structure of the extracted species was given. The organic phase diluent consisted of Isopar L purchased from ExxonMobile. Isopar L is a mixture of C11-C13 aliphatic chains and was chosen for its lower content of aromatic compounds, less than 0.01 wt%, as compared to other commonly used industrial diluents such as kerosene, and also for being more affordable compared to much purer diluents such as dodecane. The extracting reagent was Cyanex 572 (C572) supplied by its manufacturer Cytec. C572 is a mixture of phosphinic acid and phosphonic acid esters, unspecified by the manufacturer, that is selective to trivalent lanthanides, specifically the heavier ones, through the ion exchange mechanism as shown in equation 19 [41]. C572 was chosen over other extracting reagents such as HDEHP since it could readily be used without the need for further purification. In addition, C572 has been shown to have higher selectivity for the heavier lanthanides and also better stripping efficiency requiring much lower acid concentration compared to the traditional phosphonic acids used in solvent extraction [42-44]. A general form of the C572 molecule is shown in figure. 9.

$$M_{aq}^{+3} + x(HL)_{2,org} \leftrightarrow ML_3(HL)_{2x-3_{org}} + 3H_{aq}^{+} \qquad (19)$$

The aqueous phase consisted of dysprosium nitrate made in the lab from high purity 99.999 wt% dysprosium oxide. Although zero initial concentration of hydronium ions in the aqueous phase should not affect the reaction and shift the equilibrium further to the

right, this resulted in the formation of a third phase consisting of a thick emulsion between the organic and the aqueous phases. Therefore, nitric acid was added to the aqueous phase to avoid the formation of the unwanted third phase. Aside from being one of the heavier rare earth elements found in UNF, dysprosium was chosen as the metal ion to be extracted for its high cross section for thermal neutrons, 2400 barns, suitable for neutron activation analysis.

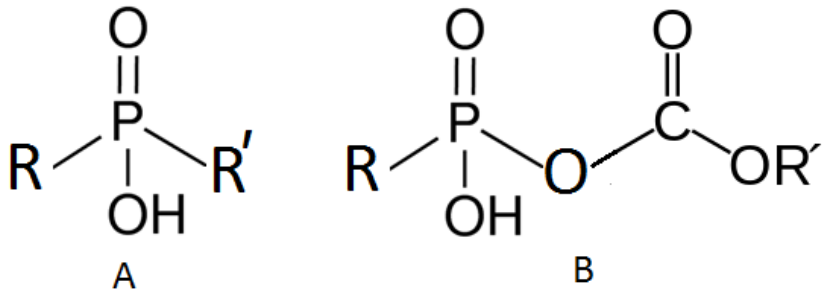

Fig. 9. A generic example of a phosphinic acid (A) and a Phosphonic acid ester (B). The R-groups represent variations of hydrocarbon chains

During the kinetics studies, the need for a simpler system with known composition was realized and therefore, the organic diluent was replaced with reagent grade, > 99%, n-dodecane and the ligand was replaced with 2-ethylhexylphosphonic acid mono-2-ethylhexyl ester HEH[EHP]. HEH[EHP] is also an acidic extractant and its structure is shown in figure 10.

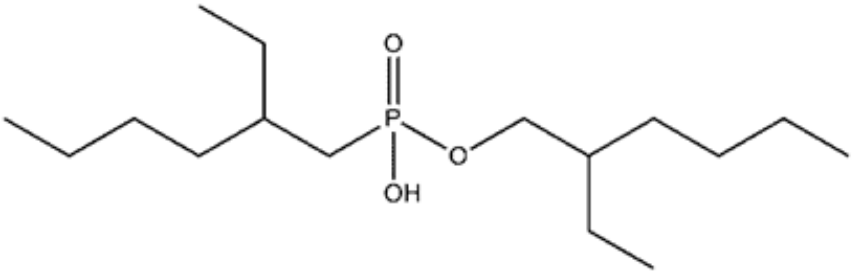

Fig. 10. A schematic representation of the HEH[EHP] molecule

In all experiments throughout this study, neutron activation analysis (NAA) was used to measure the concentration of metal ions in the two phases. These analyses were performed at the UCI TRIGA nuclear facility. NAA uses the ability of a nuclide to capture a neutron and turn into an unstable, i.e. radioactive, nuclide. Due to this instability, the nuclide decays into a more stable form by emitting beta or alpha particles. Accompanied with this decay, gamma radiation with energy specific to the nuclide is also released to lower the energy state of the nucleus. [45] The intensity of the gamma radiation is directly proportional to the number of metal ions present in a sample according to equation 20 and therefore can be used as a measure of concentration.

$$A_{rad} = \Phi\sigma N_i \left(1 - e^{-0.693^{t_{irr}}/_{t_{hlf}}}\right) e^{-0.693^{t_{cool}}/_{t_{hlf}}} \qquad (20)$$

Therefore, by choosing a metal ion with high probability of capturing neutrons and a suitable half-life, such as dysprosium, the concentration used in the experiments can be significantly lowered eliminating changes between the inlet and outlet flowrates to and out of the contactor. The rate of a reaction is expressed in terms of its reactants as

$$r = k[A]^a[B]^b \qquad (21)$$

Where a and be are the reaction rate order in the reacting components

A reversible chemical reaction at equilibrium can be explained as one having equal forward and backward rates. Therefore, at equilibrium, the reaction rate given in 21 can be expressed as

$$r_f = r_b \Rightarrow \frac{k_f}{k_b} = k_{eq} = \frac{[ML_3(HL)_{2x-3_{org}}][H^+_{aq,eq}]^3}{[M^{+3}_{aq}][(HL)_{2,org}]^x} \frac{(\gamma_{ML,org})(\gamma_{H,aq})}{(\gamma_{M,aq})(\gamma_{HL,org})} \qquad (22)$$

Since the concentration of the metal ion in the aqueous phase is very low, its activity coefficient in the aqueous phase can be taken to be 1, i.e. a dilute system. Substituting equation 1 into 22 and taking the logarithm of both sides we get

$$\log D = 3\log\left[H^{+}_{aq,eq}\right] - x\log\left[(HL)_{2,org}\right] + \log\frac{(\gamma_{ML,org})}{(\gamma_{HL,org})} + \log k_{eq} \qquad (23)$$

If the last three terms on the right-hand side of the equation can be kept constant, plotting the acid concentration at equilibrium against the distribution ratio on a log-log scale should yield a straight line with a slope of 3 given that the stoichiometry of the reaction is correct. The value of k_{eq} is a function of the ionic strength of the system and can be kept constant by maintaining a constant ionic strength throughout the runs. This was done by using ammonium nitrate to compensate for the changes in acid concentration. In addition, the large excess of C572, about three orders of magnitude, insures a relatively constant concentration of C572 during the experiments. With the same argument it could also be assumed that the magnitude of the activity coefficient does not significantly change. Therefore, the three terms in equation 23 can be assumed to be relatively constant and lumped together as in equation 24

$$\log D = 3\log\left[H^{+}_{aq,eq}\right] + C_1 \qquad (24)$$

Experiments and Discussion

1 ml of each phase was added to a vial and shaken for 15 minutes on a vortex mixer. Then, the vials were centrifuged for 3 minutes at 3000 RPM. 150 µl of each phase was pipetted out and subjected to NAA. All dilutions throughout the studies were done by serial dilution and the acidity of the aqueous phase was confirmed by auto-titration. The results of this experiment are shown in figure 11.

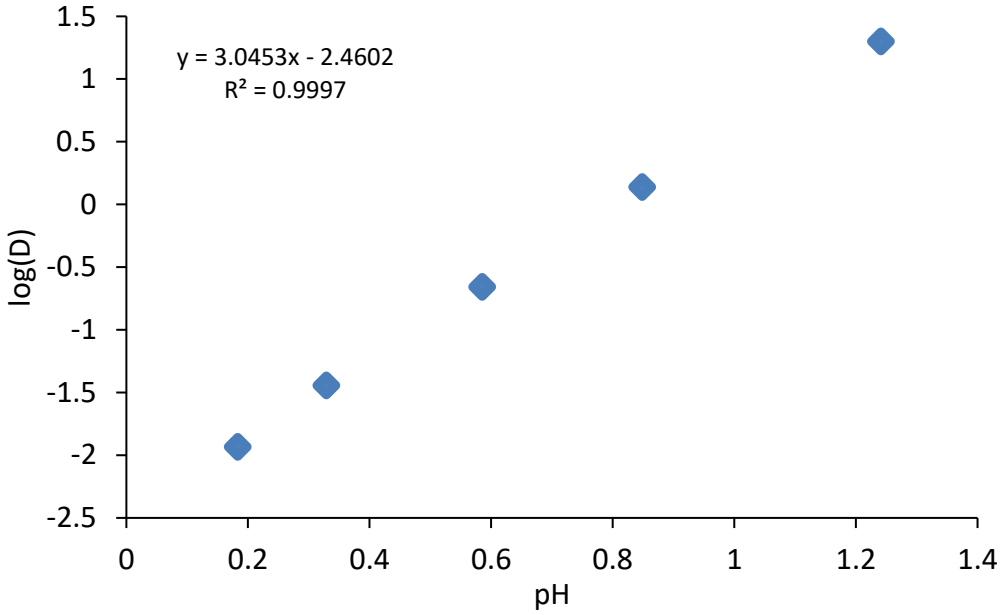

Fig. 11. Average logarithm of distribution ratios vs equilibrium concentration of hydronium ions at 0.1 mM dysprosium nitrate and 0.2 M C572 at 20.0 C

The results of this study, the slope value of 3.0, confirms that three C572 molecules are deprotonated per one dysprosium molecule extracted into the organic phase. The slight discrepancy is attributed to experimental errors and some deviation due to the assumptions made. Each point in the plot is the average of three experiments. The extraction dependence on the initial metal concentration was also studied and plotted in figure 12.

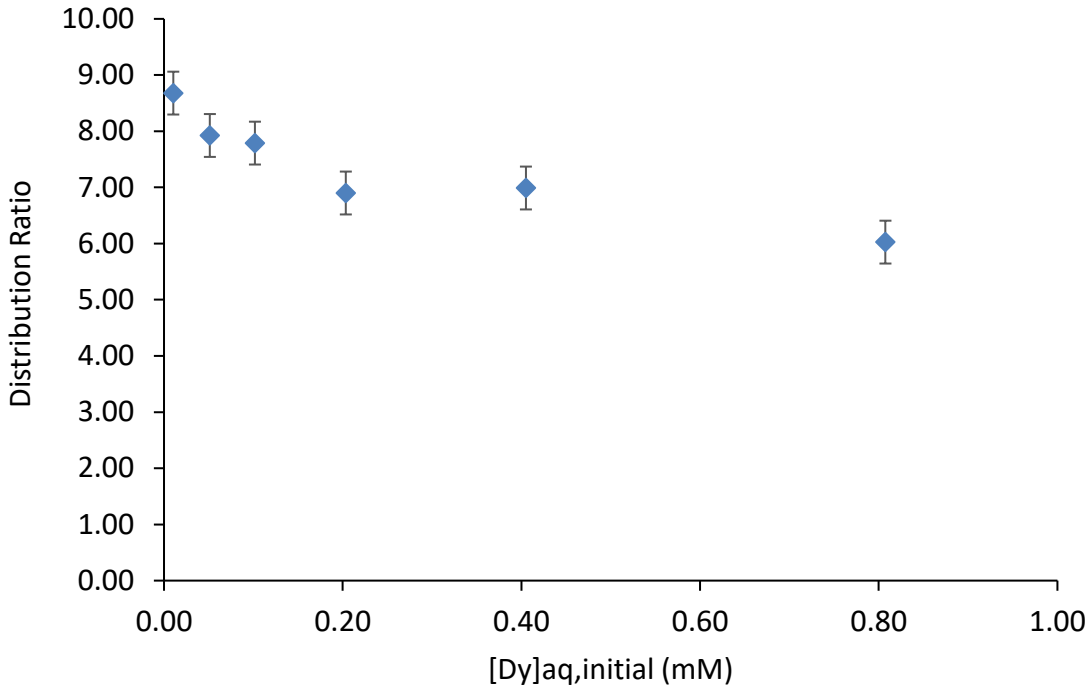

Fig. 12. Average distribution ratios vs initial concentration of dysprosium metal ions at 0.2 M C572 and 0.1 M nitric acid at 20.0 C

It seems the increase in metal concentration causes a decrease in the distribution ratio. This is expected as there is a high excess of ligand before the organic phase becomes saturated.

HEH[EHP] Equilibrium Studies

The HEH[EHP] equilibrium studies were performed at the end of each kinetics study by first pouring the entire content of the Nitsch cell, explained in detail in the kinetics chapter, into a bottle. This solution was stirred for 15 minutes on a stir plate and allowed for gravitational separation of the two phases. Then, a few milliliters from each phase was collected and centrifuged for 3 minutes at 3000 RPM. A 150 µl of each phase was pipetted for NAA. An acid dependence extraction study with HEH[EHP] was not performed since

both extractants have the same reaction mechanism. Also, this was shown to be the case by other researchers [46]. Equation 23 can be rearranged in the following form

$$\log D = x\log\left[(HL)_{2,org}\right] + C_2 \qquad (25)$$

Figure 13 shows the plots of the distribution coefficient as a function of the equilibrium concentration of unreacted HEH[EHP] at different metal ion concentrations.

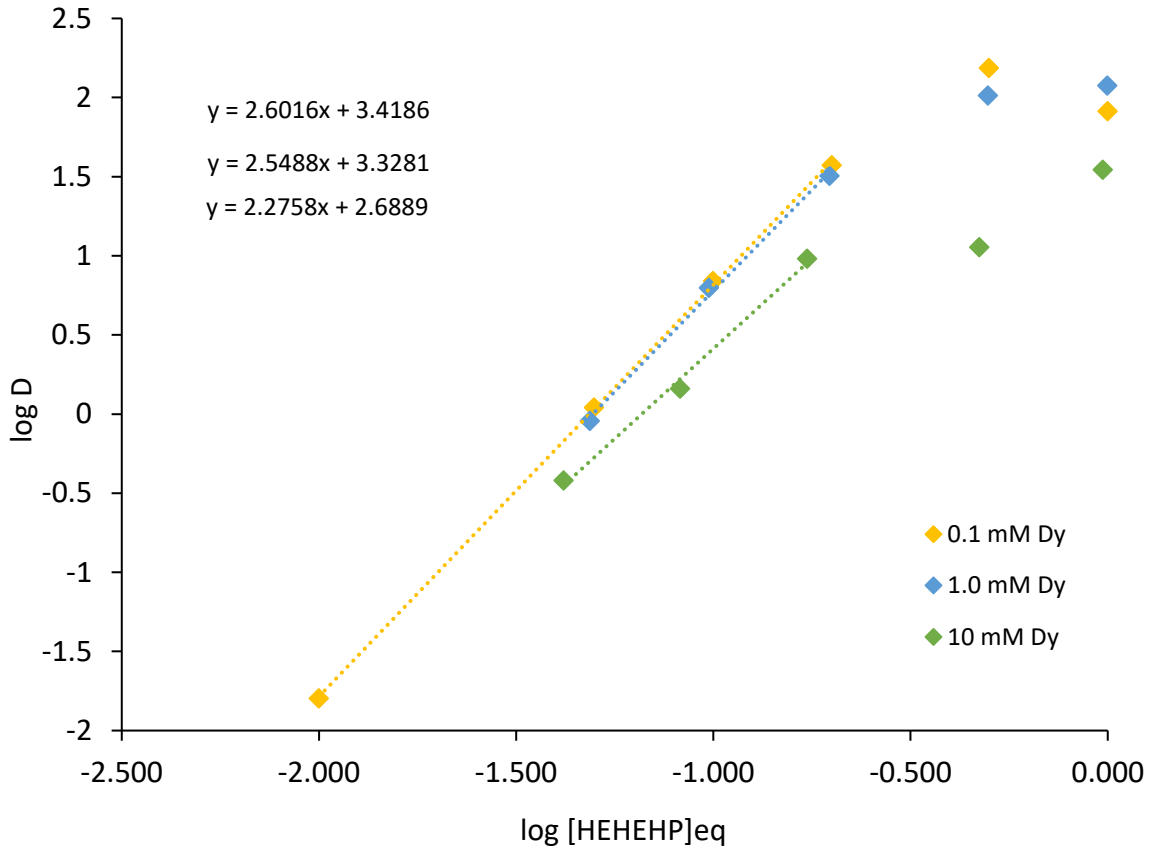

Fig. 13. Average logarithm distribution ratios vs equilibrium concentration of unreacted HEH[EHP] at 0.1 M nitric acid at 20.0 C

From figure 13 it is apparent the linear relationship derived in equation 25 breaks as the concentration of the organic ligand increases and deviates from the ideal behavior. It also appears as if the slope decreases as the concentration of the metal ion increases.

Equilibrium studies on the extraction of lanthanides with Di-(2-ethylhexyl) phosphoric acid (HDEHP), a molecule that closely resembles HEH[EHP] with the one difference of having an extra oxygen atom connecting the hexyl group to the phosphor, have yielded slope values between 2 and 3. Kneißl et al. [41] extracted europium with HDEHP and found the slope of the log D vs log [HDEHP] to be 2. They suggest the extraction stoichiometry to have the following form

$$\mathrm{Eu_{aq}}^{+3} + 2(\mathrm{HL})_{2_{org}} \leftrightarrow EuL_3(HL)_o + 3\mathrm{H^+_{aq}} \qquad (26)$$

Choppin and Nash [47] suggest two mechanisms of the extraction of trivalent americium by HDEHP. The first, shown in equations 27, is one where the organic ligand dissolves into the aqueous phase to form a complex and the other is one where the complexation happens on the interface, equations 28.

$$Am^{+3}_{\mathrm{aq}} + \mathrm{HL}_{aq} \leftrightarrow \mathrm{AmL_{aq}}^{+2} + \mathrm{H^+_{aq}} \qquad (27.\mathrm{a})$$

$$\mathrm{AmL_{aq}}^{+2} + 5/2(\mathrm{HL})_{2_{org}} \rightarrow Am((\mathrm{HL})_2)_{3,o} + 2\mathrm{H^+_{aq}} \qquad (27.\mathrm{b})$$

and

$$Am^{+3}_{\mathrm{aq}} + (\mathrm{HL})_{2,int} \leftrightarrow Am(\mathrm{HL})_{2,int}{}^{+2} + \mathrm{H^+_{aq}} \qquad (28.\mathrm{a})$$

$$Am(\mathrm{HL})_{2,int}{}^{+2} + 2(\mathrm{HL})_{2_{org}} \rightarrow Am((\mathrm{HL})_2)_{3,org} + 2\mathrm{H^+_{aq}} \qquad (28.\mathrm{b})$$

Therefore, with the slopes of 2.2-2.6 obtained in this study, we suspect that the most probable mechanisms of reaction have the forms

$$\mathrm{Dy_{aq}}^{+3} + 3(\mathrm{HL})_{2_{org}} \leftrightarrow DyL_3(HL)_{3,org} + 3\mathrm{H^+_{aq}} \qquad (29.a)$$

$$\mathrm{Dy_{aq}}^{+3} + 2(\mathrm{HL})_{2_{org}} \leftrightarrow DyL_3(HL)_{org} + 3\mathrm{H^+_{aq}} \qquad (29.b)$$

Contactor Characterization

Table 1: Physical dimensions of the Robatel BXP012

Rotor Section	Dimension (mm)
Rotor Inner Diameter	12
Annular Gap	2.25
Gap Under Rotor	4.1
Vanes	6.8x1.1x0.93
Hight of Rotor	21.2

According to the manufacturer's specifications, the Robatel BXP012 has a throughput limit of 33 ml/min with a top rotor spin speed of 10000 RPM. To test the operating limits of the system in consideration, the two phases were fed into the contactor at flow rates ranging from 0.5 ml/min to 10 ml/min keeping the aqueous to organic ratio constant at 1. Cross contamination of phases was observed at around 3000 RPM for the entire range of flow rates. Cross phase contamination will occur when centrifugal force is not high enough to separate the two phases by the time they exit the contactor separating zone. Also, unexpectedly both phases would discharge from the organic outlet when the RPM exceeded 5000. This was explained by the flooding of the mixture in the mixing zone into the organic collecting rings due to the excessive turbulence at such high RPMs. Based on these observations, the extraction efficiency was tested at 3500, 4000, and 4500 RPMs over a range of flowrates. For these experiments, the total flowrate was kept constant and aqueous to organic flowrate ratios of 0.5, 1, and 2 were tested. [23] In centrifugal contactors, depending on both the operational conditions and the physiochemical properties of the two liquid phases, one phase called the dispersed phase will form droplets within the other continuous phase. A few studies concerning phase continuity and well as phase inversion

have been conducted in stirred tanks. Selker and Sleicher using electrical resistance measurements for detection, studied the effects of density, viscosity, interfacial tension, stirring speed, shape of stirrer and starting conditions on the determination of the dispersed phase in a batch setting [48]. They detected three regions in terms of phase continuity. Two regions where only one of the phases can form the dispersed phase and a third region called the ambivalent region where either of the two phases can become dispersed. Based on their results, it is largely, if not only, the kinematic viscosity that would determine the dispersed phase. The phase with the larger kinematic viscosity has the higher likelihood of forming the dispersed phase. Also, the larger the kinematic viscosity ratio of the two phases, the wider the ambivalent region is. In the ambivalent region, the starting conditions of the operation will determine the dispersed phase. When one phase is slowly added after missing of the other phase has started, the added phase will become dispersed up to a critical holdup ratio and then phase inversion will occur. This ambivalent region was not observed in liquid-liquid flows in pipes however [49]. Luhning, also studied phase dispersion in liquid-liquid stirred batch systems and observed that the lower the surface tension between the two phases, the wider the ambivalent region is [50]. He also observed that the interfacial area of the dispersed phase linearly increases with holdup volume. The effects of impeller type and vessel inner diameter on the width of the ambivalent region were studied by Norato et. al and the ratio of these two parameters was found not to have a significant effect [51]. Unlike the type of flow in the studies mentioned, centrifugal contactors operate in a continuous mode. Comprehensive studies on phase continuity in centrifugal contactors have not been done. Though it has been observed inversion from organic to aqueous are favored[23, 52]. The conclusions from the studies

above were taken into consideration in this work. The kinematic viscosity of the organic phase was about twice that of the aqueous phase. Cyanex 572 and HEH[EHP] are surfactants and therefore lower the interfacial tension between the two phases. These are conditions that would result in the system having a wide ambivalence region.

Experiments and Discussion

Fifty milliliter syringes were used to pump the solutions into the contactor using continuous syringe type pumps made by KD Scientific. The aqueous phase pump was first started in order to prime the Robatel BXP012. After the aqueous phase started discharging, the organic pump was started. This would assure the formation of organic dispersed phase. At each experimental condition, about four residence times based on the slow phase flow rate were allowed to lapse before the first sample was collected. Three samples at each point were collected with at least one residence time difference in between. Error bars on the plots represent the standard deviation of the distribution ratio among the runs. Figures 13-15 show the variation in the distribution ratio as a function of flow rate ratio of aqueous to organic when the total flowrate was kept constant at different rotor speeds. Unless otherwise stated, 0.2 M C572, 0.1 mM $Dy(NO_3)_3$, and 0.1 M HNO_3 was used throughout this study. Aqueous to organic ratios of 0.5, 1, and 2 were tested at rotor speeds of 3500, 4000, and 4500 RPM. The hydrodynamics of the Robatel BXP012 was unstable specially for aqueous to organic ratios of 0.5, and 1. At fixed operating conditions, flooding would occur during the run. Flooding refers to the condition where cross contamination of the outgoing phases occurs. This could be attributed to sudden inversion in the continuous phase. Under higher aqueous phase flow rate, the inversion is less probable. Comparing figures 14 and

15, the distribution ratio is higher when the rotor speed is increased from 4000 to 4500 RPM. This is expected due to increased mixing. Not much difference is observed in the distribution values when the flow rate ratio is varied, however. Operationally, the contactor was most stable when the aqueous phase had a higher flow rate. It appears under these conditions the residence time and the holdup volume of the contactor is not affected by the flow rate ratio.

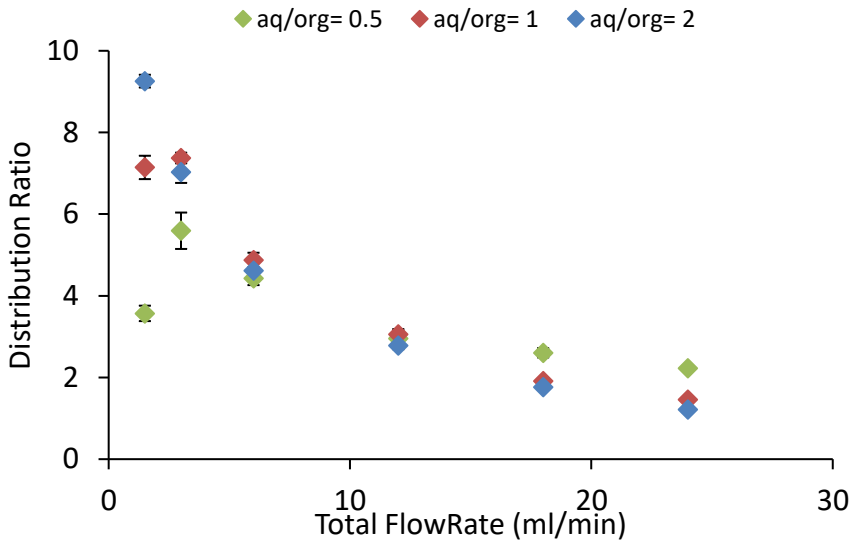

Fig. 14. Average distribution ratio vs total flowrate of aqueous and organic phases in Robatel BXP012 at 4500 RPM and room temperature

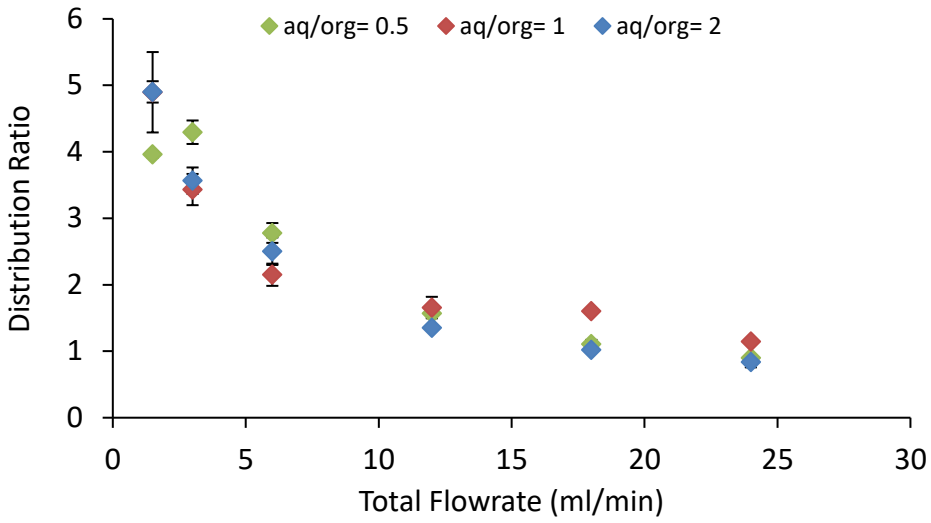

Fig. 15. Average distribution ratio vs total flowrate of aqueous and organic phases in Robatel BXP012 at 4000 RPM and room temperature

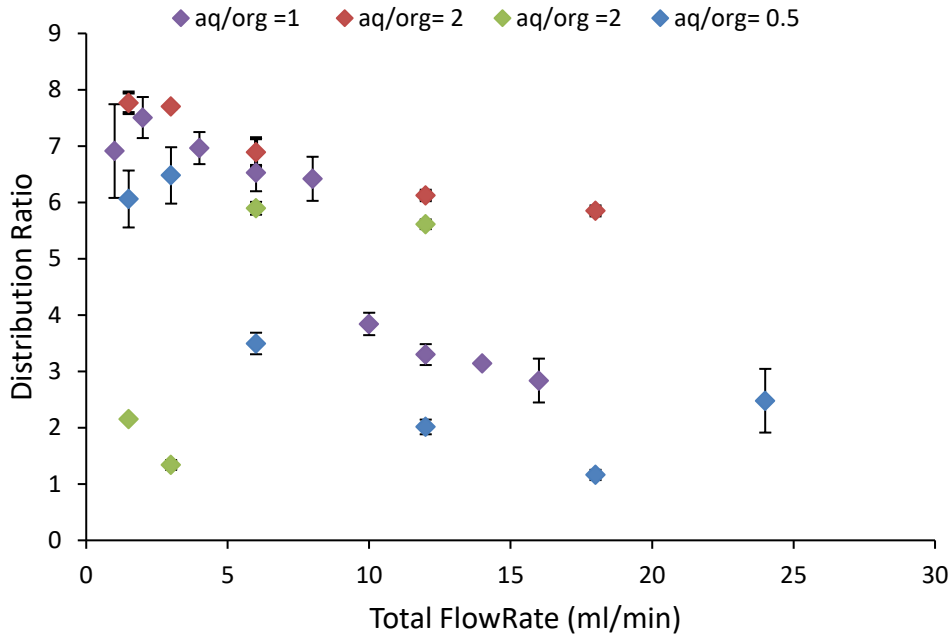

Fig. 16. Average distribution ratio vs total flowrate of aqueous and organic phases in Robatel BXP012 at 3500 RPM and room temperature

At 3500 RPM however, the hydrodynamics of the Robatel BXP012 are very unstable. From figure 16 it can be seen that the extent of extraction is unpredictable and also becomes very

dependent on the starting conditions. At aqueous to organic ratio of 2, the experiment was repeated twice. The first time the experiment was conducted as described above, these are the points in red. The second time, the aqueous phase flow rate was doubled at the end of the one to one experiment. These are the points in green. In some cases, a switch allowing multiple syringes to be connected to the contactor was used to avoid stopping the experiment when running out of solution. Although three to four residence times were allowed when switching between syringes, the contactor seems not to have recovered from the disturbances. To gain some insight into the causes of this anomaly, a contactor housing was 3D printed from poly methyl methacrylate (PMMA) and was polished using sand papers and liquid diamond polishing solutions until it was optically clear.

Fig. 17. 3D printed Robatel BXP012 housing.

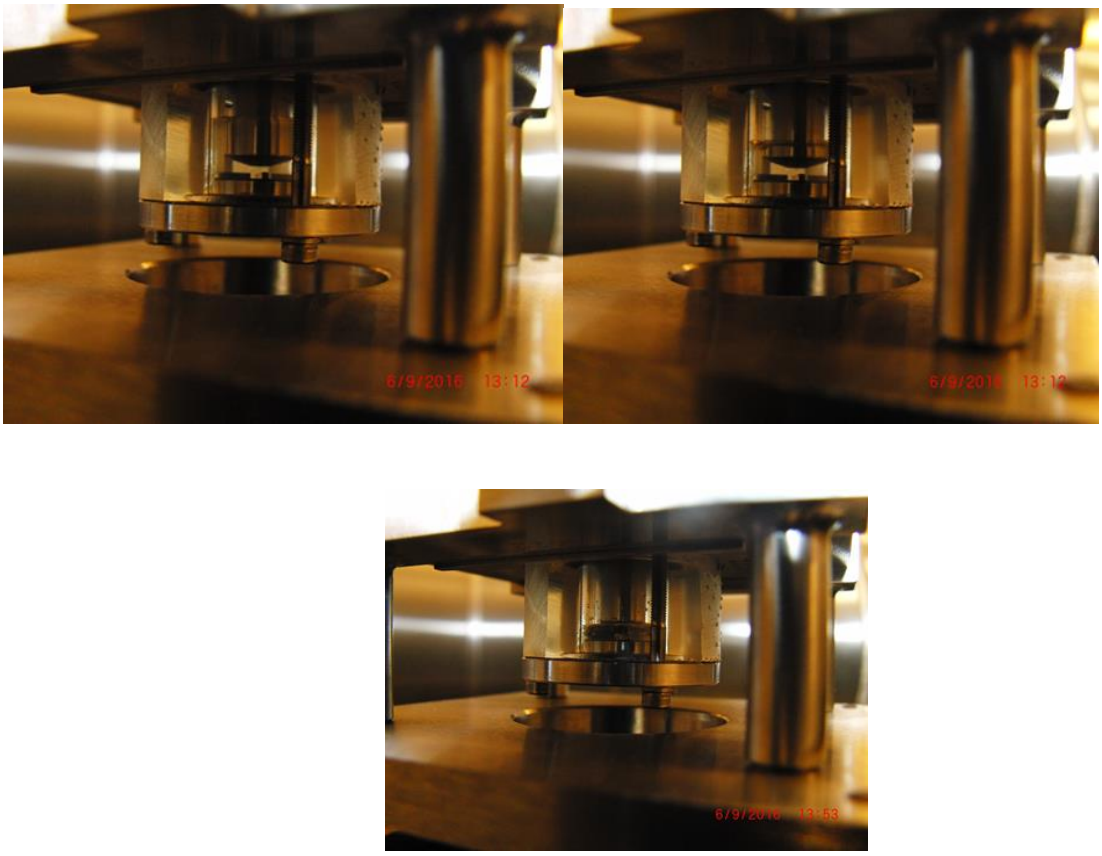

Fig. 18. Height of the aquoues phase liquid column in the mixing zone in absence of organic phase. The fluid height reduces over time.

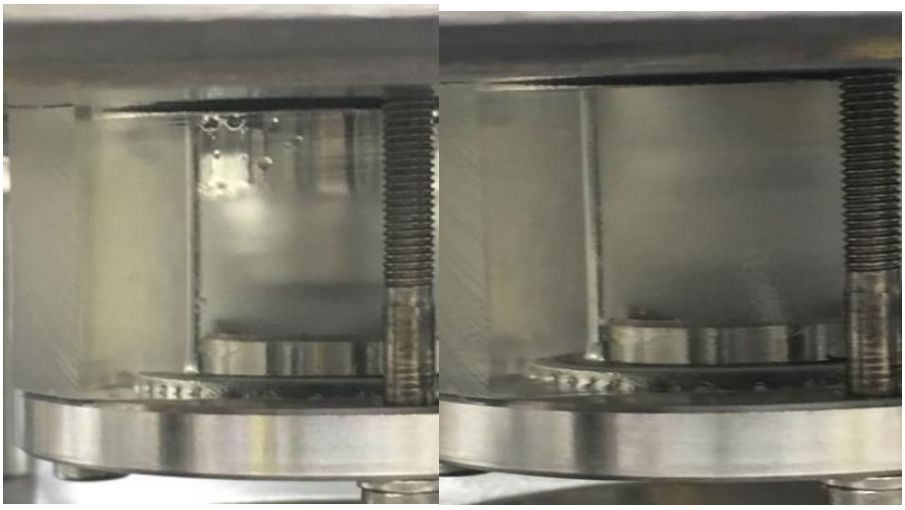

Fig. 19. Height of fluid column in the mixing zone at 3500 RPM on the left and 4500 RPM on the right

When only the aquous solution was pumped, the hight of the liquid column in the mixing zone was not stable, the liquid column would oscillate, and get completley siphoned out at random times. Figure 18 shows how the height of the liquid decreases over time at 3500 RPM. Therefore, if no aquoues phase was present in the mixing zone when the organic phase pump was started, then the assumption of aquoues continuous would not neccesarly be valid. This is another probable cause for the flooding of the contactor midruns as dispersed organic is favored. The organic phase had a lower holdup volume in the mixing zone when no aqeuous phase was present and did not seem to be oscillating. When the two phases were present, both pumps were started together, the oscillation was minimal and siphoning was not observed. Figure 19 compares the height of the fluid column in the mixing zone at 3500 and 4000 RPM. The holdup volume in the reaction zone of the contactor increases as the rotor speed increases. This increase in the hold up was also observed by Wardle et. al. when using 4 straight vanes in the CINC 50 mm ACC[53]. The increase in the fluid column height can also explain the flooding observed at 5000 RPM.

The hydrodyanmics and extraction efficiency of the Robatel BXP012 were compared to three ACCs, shown in figure20, designed and 3D printed by Argonne National Laboratory. The contactor on the left (Fig 20a) has a rotor diameter of 10 mm, and the two contactors on the right (Fig 20b) both have rotor diameters of 20 mm. The difference between the two 20 mm contactors is that the one on the left in figure 20b has an extended mixing zone to increase the residence time of the reacting solutions. Both contactors have a fixed rotor speed at 3600 RPM. A camparison of extraction at both aqueous to organic flow rates of 1 and 2 for the extraction of dysprosium with C572 is shown in figures 21 and 22.

Fig. 20. ANL contactors. a) 10 mm. b) 20 mm (extended mixing zone to the left).

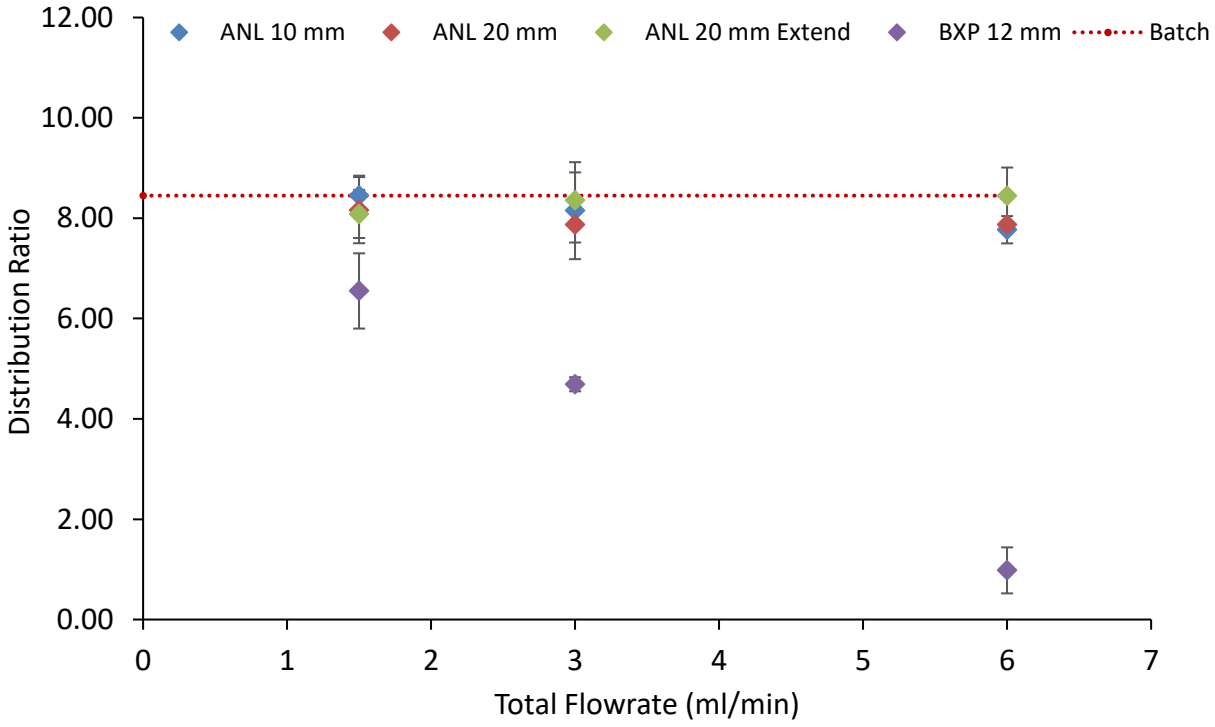

Fig. 21. Average distribution ratio vs total flowrate 3600 RPM and room temperature. Comparison of varies sizes of contactors at a/o =1

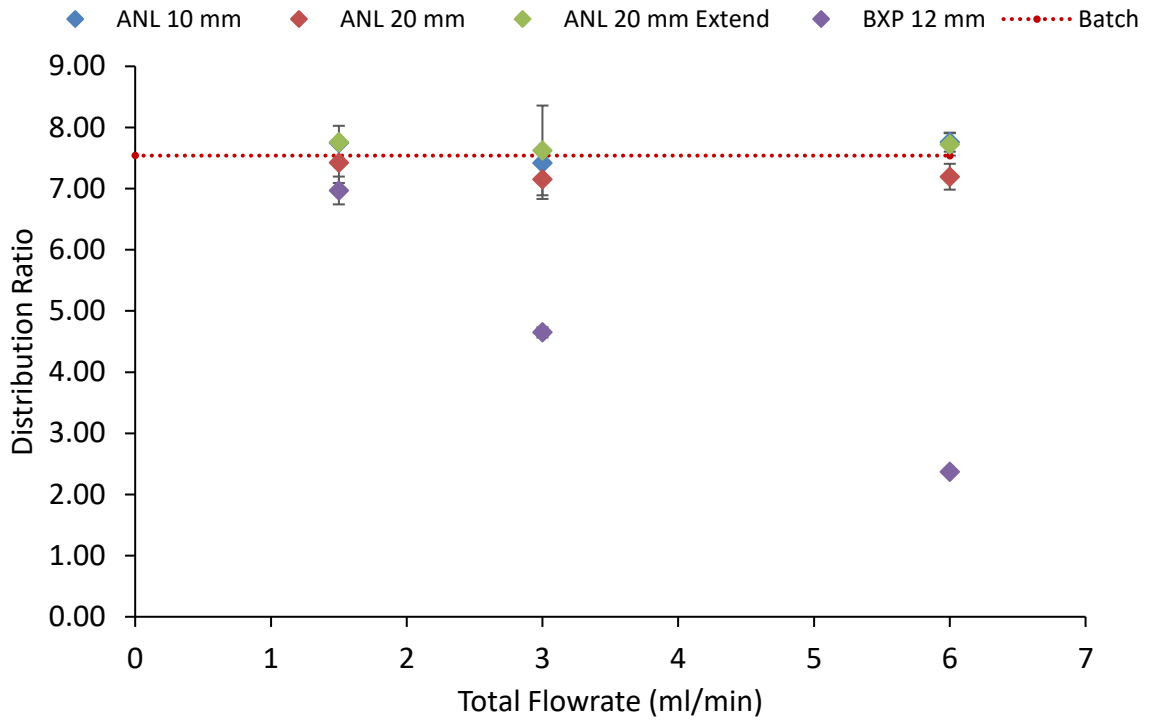

Fig. 22. Average distribution ratio vs total flowrate 3600 RPM and room temperature Comparison of varies sizes of contactors at a/o =2

At both flow rate ratios and total flow rates, the three Argonne contactors have maximum efficiency relative to the equilibrium extraction value obtained in a batch extraction for 15 min. This is not to say that the three contactors will always have the same efficiency. Since the extraction reaction is fast and perhaps instantaneous, equilibrium is reached fairly quickly, and the additional volume provided by the larger contactors is not needed for this system. At the lowest flow rate, the Robatel is also able to achieve equilibrium, however, its efficiency reduces as flow rate increases, due to decreased residence time. The increase in flow rate resulted in an increase in the holdup volume of the Robatel contactor. The increase however does not compensate for the increase in the flow rate. i.e. residence time decreases. Wardle et. al. experimentally and through computational fluid dynamics simulations was able to show that in the CINC contactor, a continuous contact between the

rotor and the fluid in the mixing zone only existed in the lower end of the rotor and up to a distance of about the length of the annular gap [54, 55]. If this also applies to the miniature contactor in consideration, then in the additional volume obtained by increasing the flow rate, the intensity of mixing will be less than that of the smaller volume.

Next, the extraction efficiency of uranyl nitrate with tributyl phosphate (TBP) was examined using all four contactors. This reaction follows the solvation mechanism explained in the introduction section. 0.01 M uranium was prepared in 3.5 M nitric acid to constitute the aqueous phase. The organic phase consisted of 1.0 M TBP in dodecane. Dodecane and isopar L have comparable kinematic viscosities of 1.78 and 1.59 mm^2/sec at 25 C respectively. The thermal neutron capture cross section of Uranium 238 is 2.68 barns compared to dysprosium 164, which is 2700 barns. Therefore, higher concentration of metal and ligand was used to allow for good statistics when counting the radionuclides after irradiation. Aqueous to organic flow rate ratios of 2 and 3 were tested with the organic flow rate being 1 ml/min for all experiments.

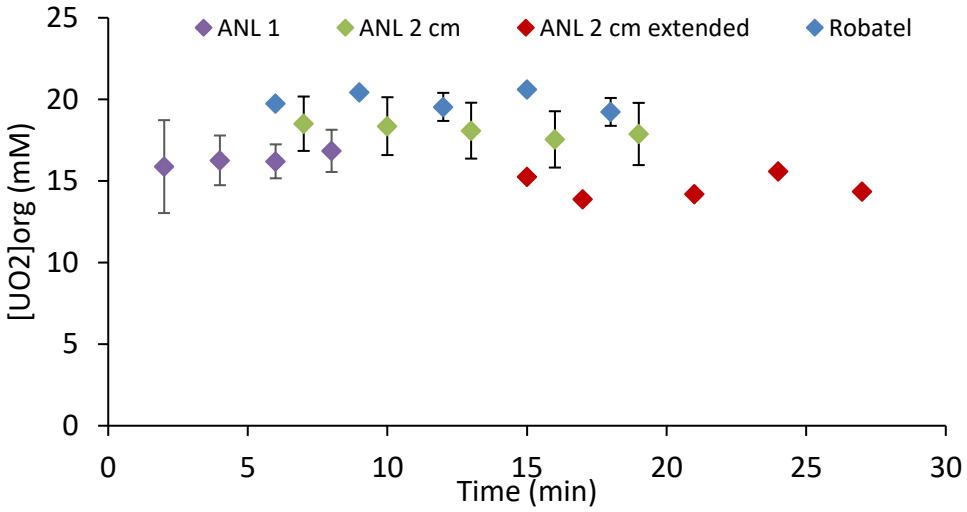

Fig. 23. Concentration of UO_2^{2+} in the organic effluent as a function of operation time at a/o =2. The first point was collected when both phases start exiting the contactor.

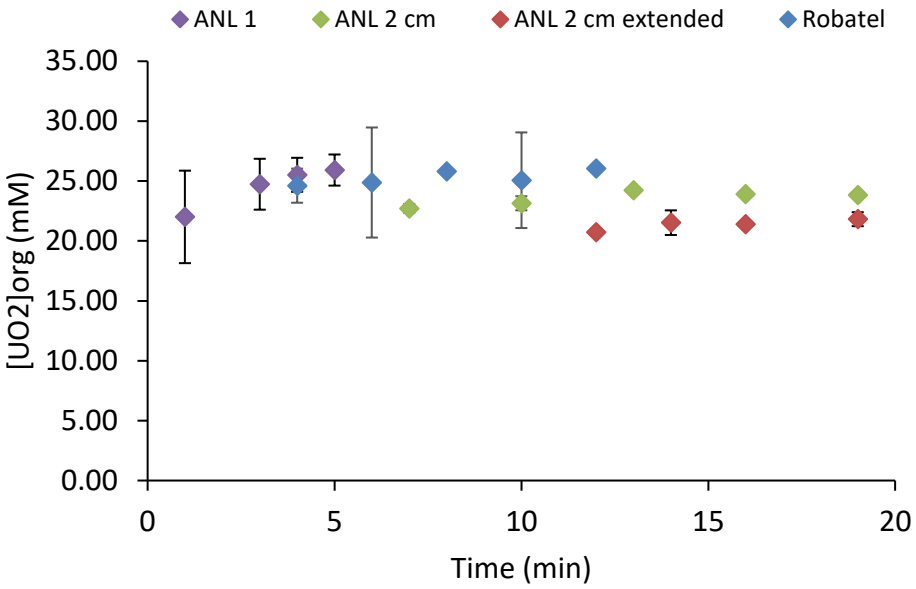

Fig. 24. Concentration of UO_2^{2+} in the organic effluent as a function of operation time at a/o =3. The first point was collected when both phases start exiting the contactor.

The error bars represent the standard deviation for repeated experiments. The total flow rate for the two cases are 3 ml/min and 4 ml/min respectively. At this total flow rate for the case of aqueous to organic flowrate ratio of two, the Robatel had lower efficiency in the extraction of dysprosium with cyanex 572. In this case of uranyl extraction, within error, the contactors seem to have about the same efficiency. The 20 mm contactor with the extended zone appears to have a slightly lower efficiency. Though this seems counter intuitive since this contactor would have a longer residence time, the extent of mixing in terms of droplet diameter might be less relative to the other contactors. According to one of the models explained in the droplet diameter section, the Sauter mean diameter is proportional to the annular gap. The 1 M TBP have probably lowered in the interfacial tension between the phases further than the 0.2 M C572. This will allow for the formation of smaller droplets, increased interfacial area, and would lower the rate of droplet

coalescence. Since the 20 mm contactors have a valve allowing for the draining of their content, the concentration of the metal ions in the mixing and separating zones where tested.

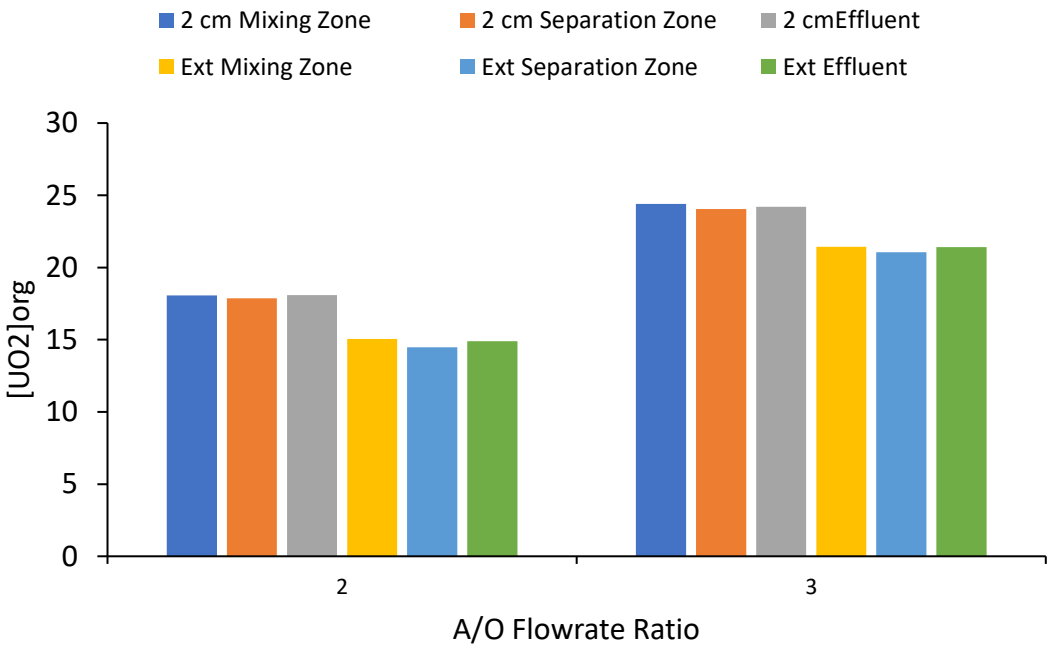

Fig. 25. Uranyl concentration of the organic phase in the mixing, separating zones of the 20 mm ANL contactors relative to the effluent concentration.

Figure 24 shows that the concentration of uranyl in the organic phase is constant over the mixing and the separating zones and equal to the concentration of the exit effluent. This is an indication that the extraction reaches its maximum extent in the mixing zone and there is no further, or negligible, extraction in the separating zone.

III. **Residence Time Distribution Analysis**:

Residence time distribution (RTD) analysis is an analytical method for determining the deviation in the behavior of a reactor from ideality.[40] In an ideal reactor, the residence time as given in equation 30 is a measure of how long a fluid element spends in the reactor before exiting.

$$\tau = \frac{V}{\overline{V}} \qquad (30)$$

A fluid element is defined as the smallest volume of a phase where continuous properties such as concentration and temperature can still be defined. In real reactors however, dead zones, described as a part of the physical volume of the reactor, exist where the fluid is stagnant and therefore cause a decrease in the residence time. Also, regions of circulating flow within the reactor cause the fluid element to spend a longer time in the reactor and therefore increase the residence time. Therefore, RTDs are characteristic of the extent of mixing in a reactor. There are two methods of performing RTD analysis: the pulse method and the step method. In this study the pulse method was performed for its relative simplicity in terms of experimental setup and availability of equipment. When a small amount of a material, a tracer, is instantaneously injected, represented as a Dirac delta function, into a well-mixed reactor such as a CSTR, in an ideal situation the exit concentration would follow the profile shown in figure 26.

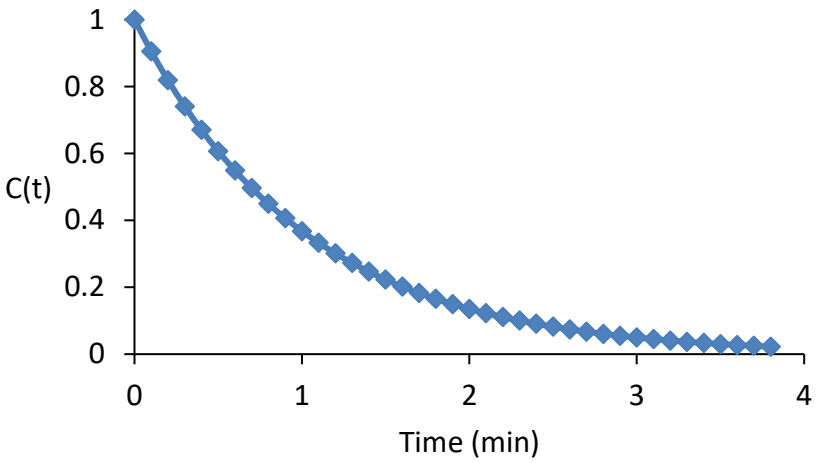

Fig. 26. The change in concentration vs time following an injection of a tracer in a perfectly-mixed ideal CSTR.

A differential number of the injected tracer leaves the reactor in a differential amount of time as in equation 31

$$\mathrm{d}N_i = \bar{\mathrm{V}} C_i(\mathrm{t})\mathrm{dt} \qquad (31)$$

The fraction of this differential volume of elements leaving the reactor between times t_1 and t_2 can be obtained by integration of equation 31 and dividing by equation 32, which is the total number of elements, N_0, present in the tracer.

$$\mathrm{N}_{0,\mathrm{i}} = \int_0^{\infty} \bar{\mathrm{V}} C_i(\mathrm{t})\mathrm{dt} \qquad (32)$$

Equation 32 makes the assumption that the tracer is chemically inert, and that transport only happens through advection. For an incompressible fluid, this ratio is given in equation 24 where the function E (t) is called the residence time distribution function (RTDF) and it describes how much time different fluid elements have spent in the reactor.

$$\frac{N_i}{\mathrm{N_{0,i}}} = \frac{\int_{t_1}^{t_2} \overline{V} C_i(t)\mathrm{d}t}{\int_0^{\infty} \overline{V} C_i(t)\mathrm{d}t} = \int_{t_1}^{t_2} \mathrm{E}(t)\mathrm{d}t \qquad (34)$$

Therefore, integration of the RTDF between the time of injection and infinity should give a value of one indicating that all of the tracer has exited the contactor. This was used to verify the mass balance in these experiments.

$$\int_0^{\infty} \mathrm{E}(t)\mathrm{d}t = 1 \qquad (35)$$

The average residence time is then given by taking the moment of the RTDF function. If this value matches the value in equation 30, then the reactor is said to be ideal.

$$\tau_{\mathrm{avg}} = \frac{\int_0^{\infty} t\mathrm{E}(t)\mathrm{d}t}{\int_0^{\infty} \mathrm{E}(t)\mathrm{d}t} = \int_0^{\infty} t\mathrm{E}(t)\mathrm{d}t \qquad (36)$$

The second moment of the residence time distribution function is the variance, which is a measure of the spread of distribution around the mean.

$$ß^2 = \int_0^{\infty} (t-\tau)^2 E(t)dt \qquad (37)$$

The tracer used must be inert, meaning it must not react with any of the constituents in the processes. It must also have negligible solubility in the opposite phase and no affinity to be adsorbed on the different reactor components. These are required to assure all the input mass is recovered, otherwise the data would be false. It is also desired to use a type of

tracer that could be detected with a probe over real time rather than sampling. This would prevent disturbing and changing the hydrodynamics of the flow.

Experiments and Discussion

RTD analyses for the Robatel BXP012 ACC were performed both on the aqueous and the organic phases. As was explained earlier, ACCs consist of the mixing region, followed by the separating region and then the collector rings where the phases accumulate to some extent before being discharged out of the contactor. Therefore, RTD experiments would reflect the total residence time in the contactor rather than just the mixing zone. Physical separation of these different sections is not possible. Unlike other types of contactors studied in the literature such as the CINC contactor, the Robatel BXP012 does not have a drain to allow the insertion of a probe. Another uncertainty arises from the collector rings. The collector rings would always contain some liquid effecting the concentration of the exit stream. These problems were obvious beforehand; however, the experiments were still performed to give an approximate idea of the size of the collector rings relative to the working volume of the contactor and also more importantly to see variations in the holdup volume of the contactor with changes in flow rate and rotor speed assuming these parameters would only affect the characteristics of the mixing zone. In both organic and aqueous RTD experiments, the rotor was set to the desired speed, the contactor was first primed with the aqueous phase and then the pump for the organic phase was started. The pumps used were of the continuous syringe type made by KD Scientific. After the organic phase started exiting the contactor, a few minutes were allowed to pass to insure steady-state operation before the tracer was injected straight inside the mixing zone of the contactor using a needle and a

syringe. The clock was started immediately with the injection and samples were collected over time and analyzed using NAA. For the aqueous phase RTD experiments, the organic phase consisted of only isopar L, to avoid extraction of dysprosium into the organic phase. The aqueous phase consisted of 0.1 M nitric acid and the pulse of tracer was 1.0 M $Dy(NO_3)_3$. In the organic RTD experiments, the organic phase consisted of 0.2 M C572 in isopar L, the aqueous phase consisted of ammonium nitrate instead of nitric acid to avoid any stripping of $Dy(NO_3)_3$ from the organic into the aqueous phase. The tracer was prepared by extracting dysprosium ions into a 0.2 M C572 in a batch equilibrium extraction. The pKa of ammonium is about ten orders of magnitude higher than that of nitric acid therefore the use of ammonium nitrate insured essentially zero stripping of dysprosium. This was experimentally verified prior to conducting the RTD experiment. Figures 27-29 show the concentration of the tracer in the aqueous phase in the exit stream at varying rotor speeds and figures 230-32 show to ones for the organic phase. The results are summarized in tables 2 and 3.

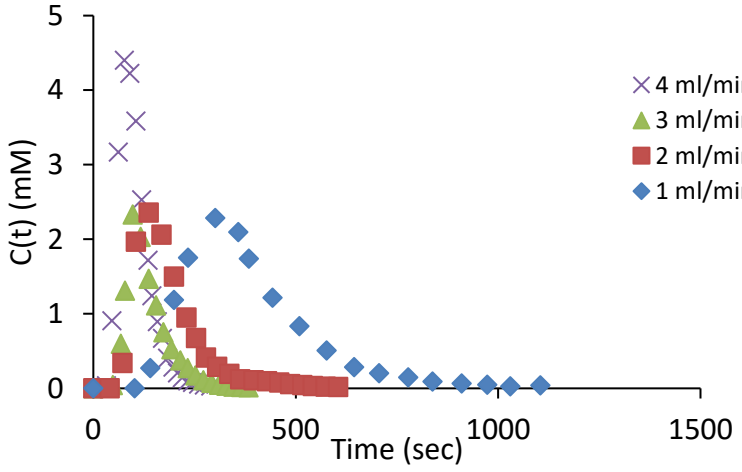

Fig. 27. Concentration of the tracer in the aqueous phase leaving the Robatel BXP012 contactor as a function of time for A/O=1 and 3500 RPM

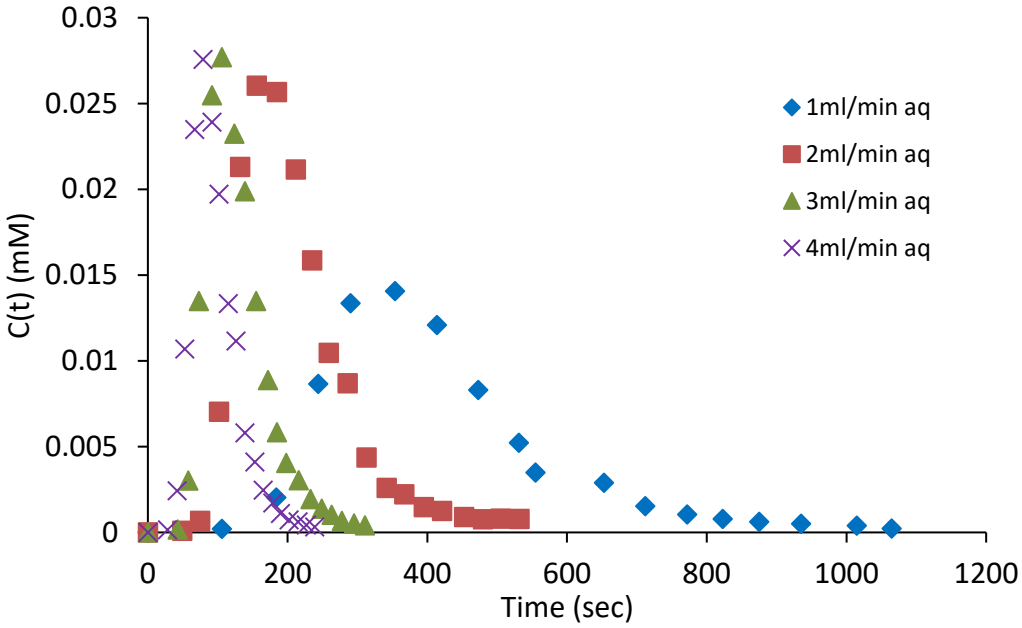

Fig. 28. Concentration of the tracer in the aqueous phase leaving the Robatel BXP012 contactor as a function of time for A/O=1 and 4000 RPM

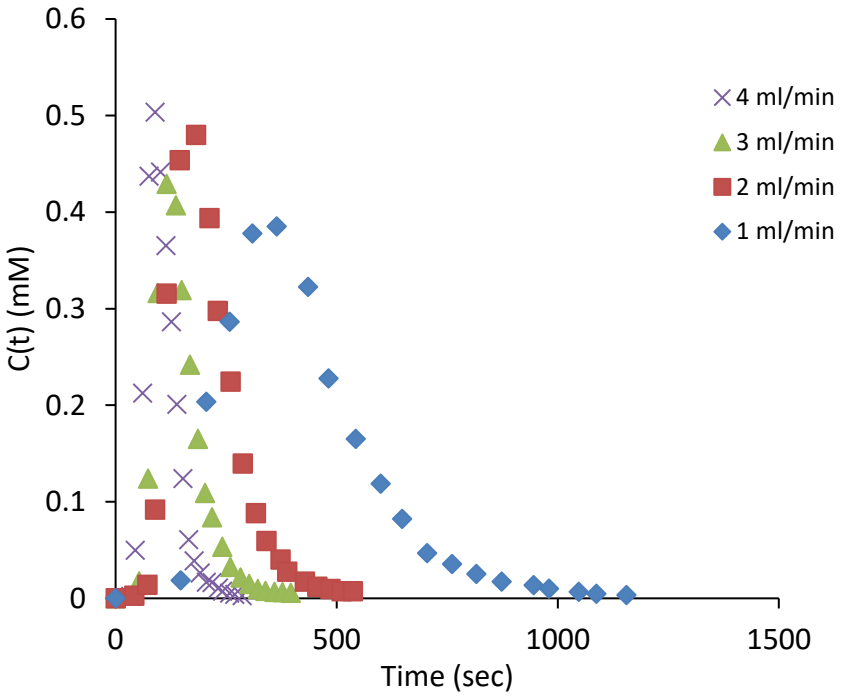

Fig. 29. Concentration of the tracer in the aqueous phase leaving the Robatel BXP012 contactor as a function of time for A/O=1 and 4500 RPM.

Table 2. Summary of the aqueous phase RTD results at 4000 RPM

Rotor Speed (RPM)	Flow Rate (ml/min/pump)	Average Holdup Time (sec)	Aqueous Holdup Volume (ml)
3500	1	388.0 ± 6.5	6.5 ± 0.1
	2	188.6 ± 6.5	6.3 ± 0.2
	3	137.3 ± 4.1	6.9 ± 0.2
	4	102.2 ± 0.4	6.8 ± 0.03
4000	1	402.1 ± 9.1	6.7 ± 0.2
	2	196.5 ± 7.0	6.5 ± 0.2
	3	133.4 ± 5.9	6.7 ± 0.3
	4	101.1 ± 5.4	6.7 ± 0.4
4500	1	415.2 ± 3.7	6.9 ±0.1
	2	206.6 ± 7.3	6.9 ± 0.2
	3	141.0 ± 5.5	7.0 ± 0.3
	4	105.3 ± 0.4	7.0 ± 0.03

Tables 2 and 3 show that the holdup volume of the contactor is relatively constant at different flowrates. Since for these experiments the flowrates of both phases were identical, the difference in their holdup volume is explained by a larger aqueous collector ring, which is visually noticeably larger. In laminar flows, the holdup volume of dissimilar phases is independent of their relative flowrates and is determined by their relative dynamic viscosities with the more

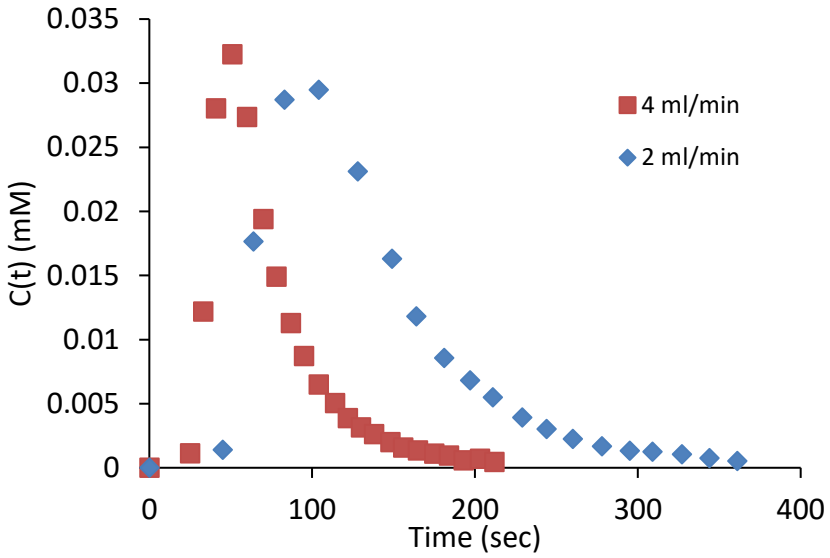

Fig. 30. Concentration of the tracer in the organic phase leaving the Robatel BXP012 contactor as a function of time for A/O=1 and 3500 RPM.

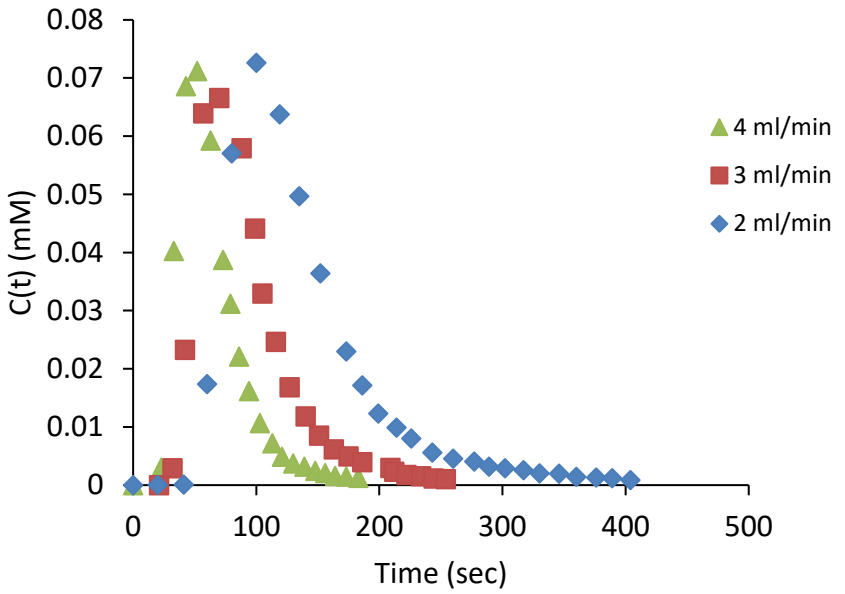

Fig. 31. Concentration of the tracer in the organic phase leaving the Robatel BXP012 contactor as a function of time for A/O=1 and 4000 RPM.

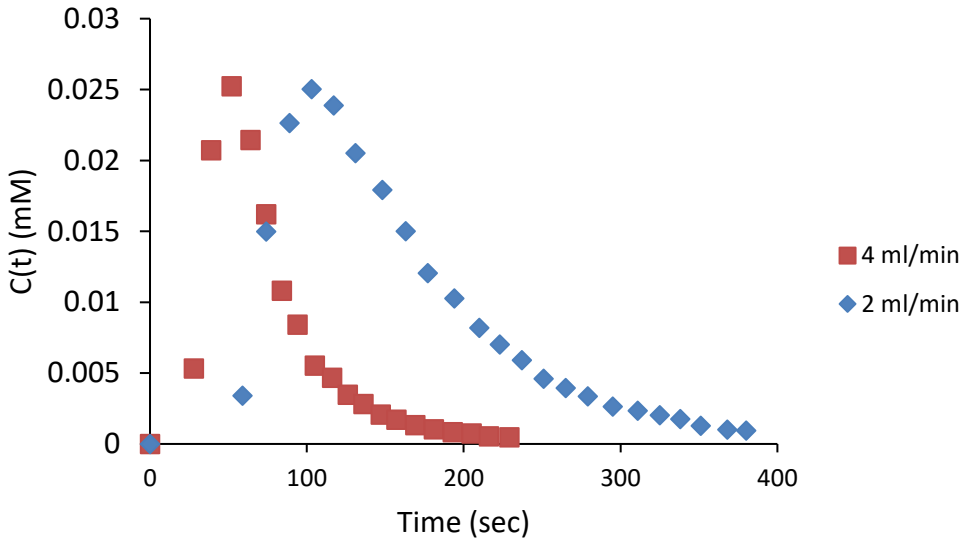

Fig. 32. Concentration of the tracer in the organic phase leaving the Robatel BXP012 contactor as a function of time for A/O=1 and 4500 RPM.

Table 3. Summary of the organic phase RTD results

Rotor Speed (RPM)	Flow Rate (ml/min/pump)	Average Holdup Time (sec)	Organic Holdup Volume (ml)
3500	2	133.4 ± 5.3	4.4 ± 0.2
	4	69.7 ± 1.1	4.6 ± 0.07
4000	2	133.5	4.45
	3	89.6	4.48
	4	62.8	4.19
4500	2	150.7	5.0
	4	72.2	4.8

Sampling was the most challenging aspect of these experiments due to the unpredictability of the time intervals at which the exit aqueous stream leaves the reactor. Unlike the organic phase, the aqueous phase does not exit the collector ring until enough volume has accumulated. This not only caused the samples collected to represent more of an averaged concentration over some time, it also restricted the frequency and the time intervals at which sampling could be done. On the other hand, the organic phase had a much more stable and consistent exit flow allowing for more frequent sampling and accurate representation of the mixing zone concentration. The organic collector ring is also

narrower than the aqueous phase preventing accumulation. The Robatel BXP012 is made of Hastelloy. Its wettability was probably the reason why the aqueous phase would build up and not easily flow out. Conducting time dependent studies on this contactor was quite challenging. Due to unexpected flooding of the contactor mid-runs, and the excessive accumulation of the aqueous phase in the collector ring in some runs before exiting, these experiments were repeated multiple times at each experimental condition until a reasonably smooth plot was obtained. The aqueous phase holdup seems to be relatively constant over the range of flow rates and rotor speeds studied. A slight increase seems to occur at 4500 RPM. A slightly more pronounced increase in the holdup volume of the organic phase seems to occur at 4500 RPM relative to the lower RPMs. A few RTD experiments were conducted after replacing the original housing of the contactor with the PMMA one. It was confirmed that the holdup was not affected by this change and that the slight increase in the holdup volume happens in the mixing zone of the contactor, as was expected. The total holdup volume of the Robatel BXP012 looks to be about 11-12 ml. The volume was attempted to physically be measured by stopping the pumps and the rotor and collecting the content of the contactor in a volumetric flask. This method did not really work because as soon as the rotor is stopped, its pumping action stops causing the content of the separation zone to be drained in the mixing zone. This total volume is greater than the maximum capacity of the mixing zone and the additional volume would spill over in the organic collecting ring. Therefore, it was not possible to segregate the content of the different section of the contactor.

Since the 20 mm Argonne centrifugal contactor has a drain allowing for the physical measurement of its holdup volume, RTD was attempted to look at its deviation from the

ideal behavior. As shown in figure 33, the concentration of the tracer never reached zero after extended times of running, the experiment was stopped after running out of solution in the syringe, suggesting either a large holdup volume and/or the channeling of some of the feed flow straight to the outlet.

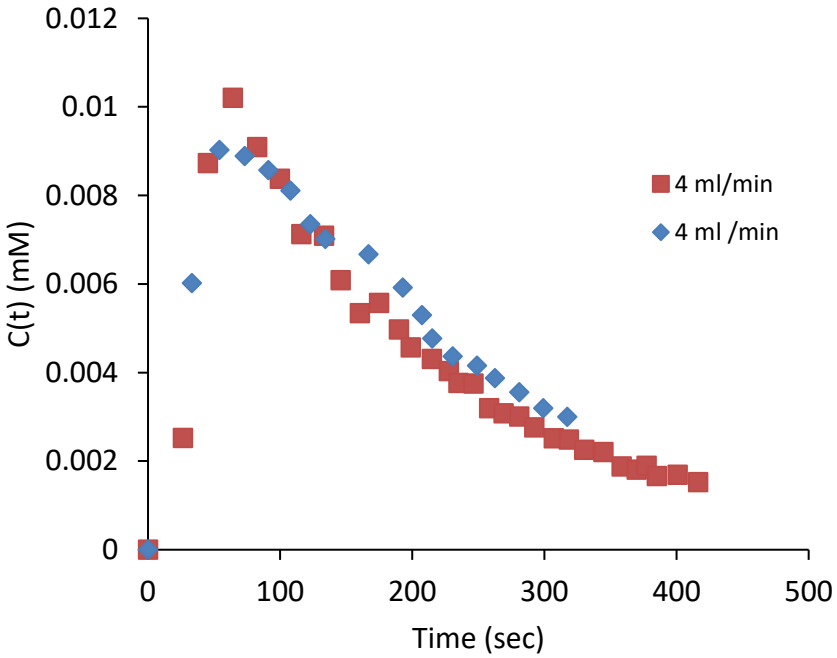

Fig. 33. Concentration of the tracer in the aqueous phase leaving the ANL 20 mm ACC with non-extended mixing zone as a function of time for A/O=1 at 3600 RPM.

The holdup volume of the mixing zone and the separating zone of both 20 mm Argonne contactors was measured. Both pumps containing the neat isopar L and the 0.1 M nitric acid were started simultaneously. The time it took for the phases to start exiting the reactor was taken as a residence time. After the contactor was determined to be operating under steady-state conditions, the pumps were stopped, and the draining valve was opened to

collect the content of the mixing zone of the contactor. Then, the rotor was stopped to collect the content of the separating zone of the contactor. The experiments were repeated three times and for each of the subsequent experiment additional time equal to an extra residence time was allowed to pass before draining the contactor. It should be noted however that stopping the pumps did not result in an instant stopping of the exit streams. As mentioned in the earlier chapter, the rotor also acts as a pump allowing the solution in the mixing zone to enter the separation zone. When the feed pumps were stopped, the rotor was still able to pump a slight amount of the mixture in the mixing zone into the separation zone. The alignment of the rotor also had some effect on the holdup volume. The rotor on these contactors does not have a tight grip on the housing. A slight misalignment caused the rotor to come in contact with the inner wall of the housing. This was also frequently caused after draining the content of the mixing zone. Any misalignment would alter the symmetry of the mixing zone affecting the hydrodynamics and therefor the holdup. Those same measurements were also performed at the end of the extraction experiments, in the presence of C572 and dysprosium. The results are summarized in tables 4 and 5 below.

Table 4: Holdup volume of the organic phase in the mixing zone of the 20 mm ANL contactors under varying parameters. The error represents the standard deviation of multiple runs.

Type	Flowrate Ratio	Total Flowrate (ml/min)	With Mass Transfer (Y/N)*	Total Volume (ml)	Organic Volume (ml)
Non-Extended	2	3	N	5 ± 1.1	1.3 ± 0.1
		6	N	3.7	1.4
Non-Extended	2	1.5	Y	3.2 ± 0.4	1.7 ± 0.2
		3	Y	2.8 ± 0.1	1.0 ± 0.3
		6	Y	3.2 ± 0.2	0.9 ± 0.1
Non-Extended	1	2	N	5.2 ± 0.5	3.7 ± 0.6
		4	N	4.6 ± 0.6	3.3 ± 0.4
		6	N	4.8 ± 0.7	2.5 ± 1.0
		8	N	4.2	2.8
Extended	2	1.5	N	14	5
		6	N	16	5
Extended	2	1.5	Y	15 ± 0.1	4.5 ± 0.7
		3	Y	14.8 ± 1.1	3.5 ± 0.7
		6	Y	13.5 ± 1.7	3.2 ± 0.3
Extended	1	2	N	17.3 ± 0.6	12 ± 1.7
		4	N	17.0 ± 0.1	10.7 ± 0.6
		6	N	16	10
Extended	1	1.5	Y	18.5 ± 1.4	12.5 ± 0.7
		2	Y	15.5	11.5
		3	Y	16.8 ± 1.1	10.8 ± 1.1

		4	Y	16.5	11
		6	Y	16.3 ± 0.4	9.3 ± 0.4

Note: The * refers to extraction during the RTD experiment as opposed to only having the two phases without the presence of metal ions.

Table 5: Holdup volume of the organic phase in the separating zone of the 20 mm ANL contactors under varying parameters. The error represents the standard deviation of multiple runs.

Type	Flowrate Ratio	Total Flowrate (ml/min)	Reaction (Y/N)?	Total Volume (ml)	Organic Volume (ml)
Non-Extended	2	3	N	8.4	0.9
		6	N	8.6	1.2
Non-Extended	2	1.5	Y	8.1 ± 0.7	1.5 ± 0.1
		3	Y	8.2 ± 0.1	0.9 ± 0.1
		6	Y	8.5 ± 0.2	0.9 ± 0.1
Non-Extended	1	2	N	7.9	3.0
		4	N	7.9	0.9
		6	N	8.3	1.2
		8	N	8.6	1.1
Extended	2	1.5	N	7.4	0.8
		6	N	8.8	1.2
Extended	2	1.5	Y	6.5 ± 0.7	0.7 ± 0.1
		3	Y	7.0 ± 0.8	1.0 ± 0.8
		6	Y	8.0 ± 0.1	1.0 ± 0.1
Extended	1	2	N	7.0	1

		4	N	7.4	0.9
		6	N	7.9	1.1
Extended	1	1.5	Y	6.1 ± 0.7	0.6 ± 0
		2	Y	7.0 ± 0.1	1.0 ± 0.1
		3	Y	7.3 ± 0.4	0.9 ± 0.1
		4	Y	7.4 ± 0.1	0.9 ± 0.1
		6	Y	7.9	1.1

To conclude the results above, at both aqueous to organic ratios of 2 and 1, both reactive and non-reactive conditions, and for both the 20 mm ANL contactors of normal and extended mixing zones, the separation zone always has a total volume of around 8 ml regardless of flow rate. The organic phase always has less holdup than the aqueous phase. The mixing zone holdup however is more sensitive to the operating conditions especially in the contactor with the smaller annular gap. When the aqueous to organic flow rate ratio is 1, the organic phase appears to always have a higher holdup volume in the mixing zone under all conditions. The hydrodynamics of the flow in the mixing zone of these contactors was not clear although they are made of partially transparent material. The mixing zone results suggest the fluid has an oscillating height similar to the findings in the CINC contactor. This suggests the narrow annular gap in the Robatel BXP012 stabilizes those oscillatory movements.

IV. Extraction Kinetics

Knowledge of interfacial kinetics of mass transfer across two phases is a key step in developing both safe and economical separation processes. Distillation, absorption, extraction, etc. are common examples of interfacial processes having wide applications in many chemical industries including but not limited to biochemical, petrochemical, and nuclear. Many researchers have investigated the phenomena of interfacial mass transfer in liquid-liquid extraction using different equipment. Listed below are some of the common equipment with a brief explanation.

1- Rising or Falling Drop Method

In this method, either rising organic droplets or falling aqueous droplets are introduced in a column containing the opposite phase. The droplets are collected for analysis on the opposite side of where they were initially introduced. A schematic representation of the apparatus and the droplet is shown in figure 34.

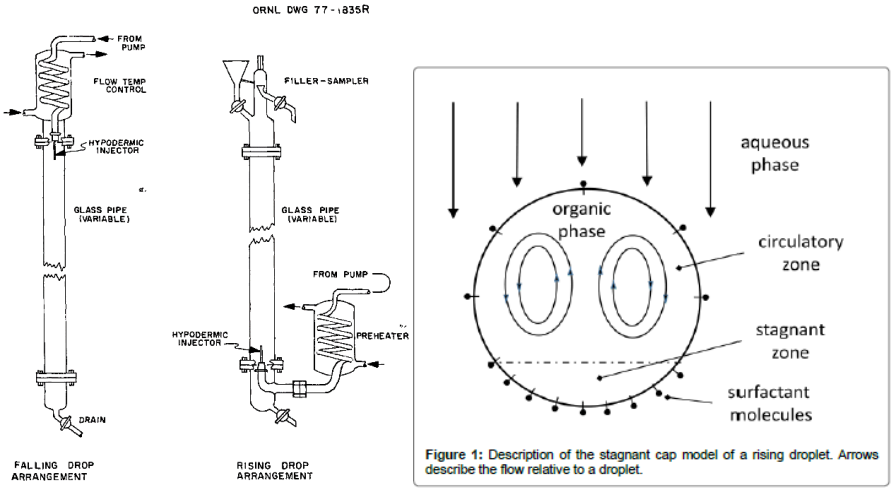

Fig. 34. A schematic representation of a rising-falling bubble apparatus, left, and an organic droplet, right. [56]

One of the advantages of this method lies in its simplicity in terms of not having moving parts. A major disadvantage however is its limitation in the droplet residence time determined by the height of the column.

2- Highly agitated mixers

In this type of equipment, the two phases are highly agitated to create a large interfacial area followed by quick separation and analysis. An example of this type of equipment is the Kenics centrifugal contactor-centrifuge shown in figure 35 which was used to study the kinetics of uranium interphase transfer by Horner and others at Oak Ridge National Laboratory [56]. A major drawback with this type of equipment is the unknown interfacial area of the two phases during the mixing prosses. This interfacial area being large also limits the use of this type of equipment for systems having reaction rates significantly slower than the mixing time. Otherwise equilibrium would be achieved during mixing and kinetics and collected data would be meaningless.

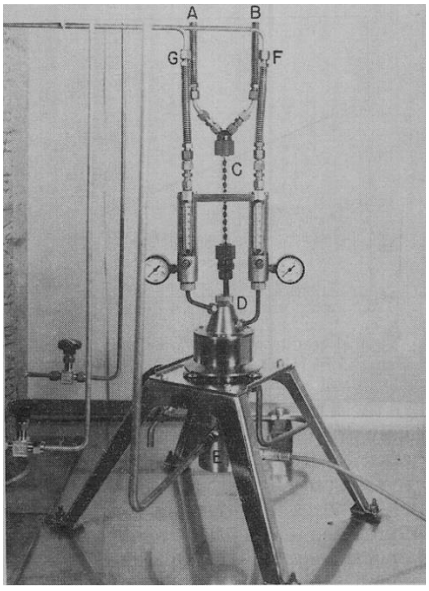

Fig. 35. The Kenics centrifugal contactor-centrifuge [56]. A and B are the inlets to the contactor, C is the Kenics mixer and D is the centrifugal separator

3- Microfluidic devices

A major advantage that this device has, schematically shown in figure 36, over all others is the small volume, a few microliters, of liquids needed to perform kinetic studies. This becomes especially advantageous in minimizing waste and dose exposure to the experimenter when radioactive nuclides are used. Researchers working on microfluid devices claim molecular diffusion is almost negligible in the formed droplets because of its highly internal mixing due to chaotic advection [57]. Although these devices have been shown to work, the use of microfluidics for measuring interfacial kinetics is a new concept and the design and fabrication of these cells are still in developing stages [58].

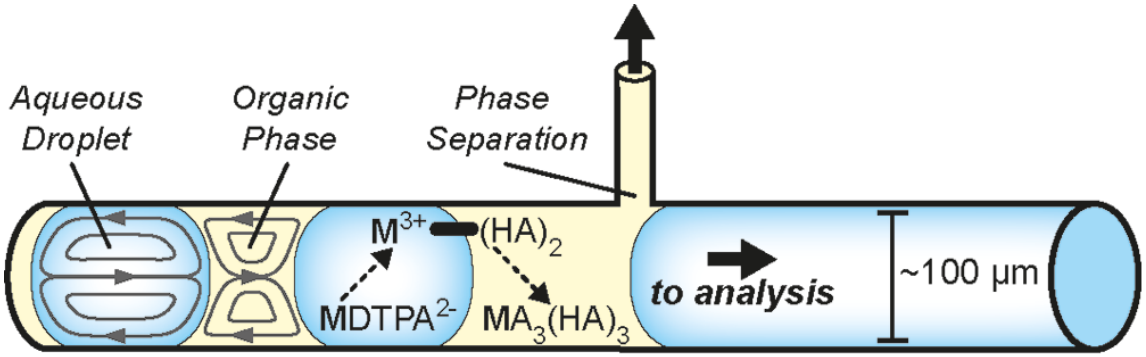

Fig. 36. A schematic representation of a microfluidic device[58]

4- Stirred cells

Another common method has been the use of the so-called constant-interface stirred cells first introduced and designed by Lewis in 1954 and schematically shown in figure 37.

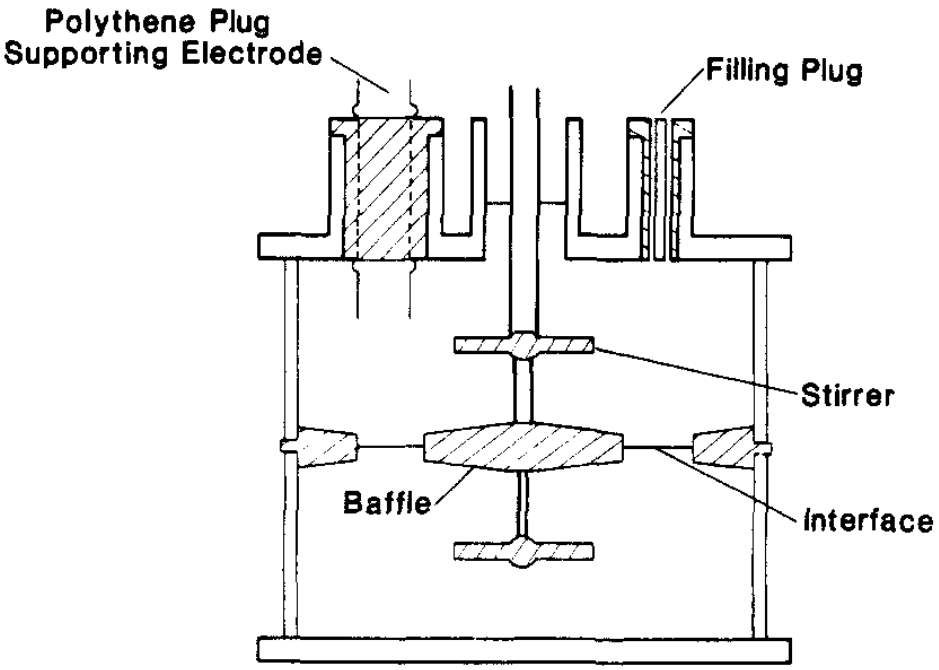

Fig. 37. A schematic representation of the Lewis stirred cell [59].

The main feature of this equipment is its design to maintain a constant and a measurable interface while stirring the two phases. The two partially or fully immiscible phases are placed on top of each other, individually stirred, and their composition is monitored over time. Modifications to the original design of the Lewis cell to improve its performance were done by many researchers. The first major modifications were by Nitsch and Hillekamp in 1980. Screens were installed on top and the bottom of the interface allowing for higher stirring rates while maintaining a laminar interface. The two stirrers were also decoupled allowing for independent stirring speed of the two phases and the original flat stirrers were replaced with pitched ones promoting turbulence in the bulk. Later in 1982 Danesi and others at Argonne National Laboratory modified the design again to include continuous sampling of the phases through a loop and built a smaller size stirred cell named the ARMOLLEX.

Although these improvements have helped stabilize the performance of the constant interface stirred cells, nevertheless, the main challenge remains the ability of determining the limiting step in an interfacial mass transfer process. Each of molecular diffusion, turbulent eddy diffusion, interfacial and bulk chemical reactions can be the limiting step depending on the system and the operating conditions. The challenge of identifying this step arises from the lack of having clear hydrodynamic models fully describing the flow near the interface. In the next section a brief description of some of the hydrodynamic models used to analyze the data collected with stirred cells is provided.

Theory

a- General Transport Concepts Relevant to Lewis Type Stirred Cells

One of the fundamental parameters for transport is the molar flux, defined as the number of moles of a species that crosses a unit area in a unit time (e.g. mol/cm^{2}s). When a fixed coordinate system in space is used, the molar flux will have two contributions. The first one is from the averaged molar velocity of the stream in the direction of mass transfer and the other is from the molecular diffusive flux due to concentration gradients.

Molecular diffusion is the process by which species move from regions of high to low chemical potential until an equilibrium throughout the system is reached. A mathematical formulation for the molecular diffusion of species i was first provided by Fick in 1855.

$$j_{i,y} = -D_{ci}\nabla C_i \qquad (38)$$

Therefore, the total molar flux of species A in the y direction for a fixed coordinate system is:

$$N_{i,y} = -D_{ci}\frac{\partial C_i}{\partial y} + C_i u_y \qquad (39)$$

In the case where the medium is stagnant, v_y is zero and the molar flux relative to a fixed coordinate system becomes:

$$N_{i,y} = -D_{ci}\frac{\partial C_i}{\partial y} = j_{i,y} \qquad (40)$$

A molar balance around a control volume with no chemical reactions present or convective mass transfer gives Fick's second law of transient diffusion shown in equation (41)

$$\frac{\partial C_i}{\partial t} = D_{ci}\frac{\partial^2 C_i}{\partial y^2} \qquad (41)$$

Another engineering representation of mass transfer is given through the idea of mass transfer coefficient. The mass transfer coefficient, k, is defined as

$$k = \frac{N_{i,y}}{(C_{i,1} - C_{i,2})} \qquad (42)$$

Thus, the mass transfer coefficient is the proportionality constant between the number of moles of species crossing a plane in response in to a concentration difference, a driving force, on both sides of the plane. The concept of the overall mass transfer coefficient becomes useful when multiple resistances to mass transfer are present such as diffusion in one medium followed by a boundary crossing resistance into a different phase, either by means of a chemical reaction or pure diffusion, and then diffusion into the bulk of the second phase.

In liquid-liquid extraction, if $C_{i1}, C_{i,2}$ represent the concentration of solute i in the bulk and the interface of the organic phase, respectively, then k_o would be the mass transfer coefficient of i in the organic phase. If, however $C_{A,2}$ is taken to be the equilibrium concentration instead, then the overall mass transfer coefficient is called k_{Oo} and the two are related as:

$$\frac{1}{k_{Oo}} = \frac{1}{k_o} + \frac{D_i}{k_a} = \frac{D_i}{k_{Oa}} \qquad (43)$$

b- Molar balance

A general molar balance on each of the phases in the Lewis cell can be written as

$$\frac{dVC_i}{dt} = \mathrm{A}j_i + Vr_i \qquad (44)$$

Depending on what system is being studied in a Lewis cell, if only an interfacial chemical reaction is responsible for the transfer of solute i across the boundaries of the control volume then the reaction term vanishes since the reaction becomes a boundary condition. Also, for dilute systems, the transfer of i across the interface can be assumed to have negligible effect on the volume and therefore equation 44 becomes

$$j_i = \frac{V}{A}\frac{dC_i}{dt} \qquad (45)$$

c- Hydrodynamic Models

1- Whitman's Two-Film Theory (1923)

Whitman's two-film theory for mass transfer at gas-liquid interface has frequently been applied to liquid-liquid interfacial mass transfer. This theory assumes a steady-state mass transfer and equilibrium to be established at the interface. In the context of stirred cells, the assumptions leading to the use of this theory are:

a- The bulk organic and aqueous phases are in a turbulent state where there is no resistance to mass transfer.

b- The turbulent eddies die out near the interface resulting in the formation of two thin stagnant layers containing all the resistance to mass transfer across the interface.

A schematic representation of the hydrodynamics in a Lewis cell reflecting the two-film theory is given in figure 38

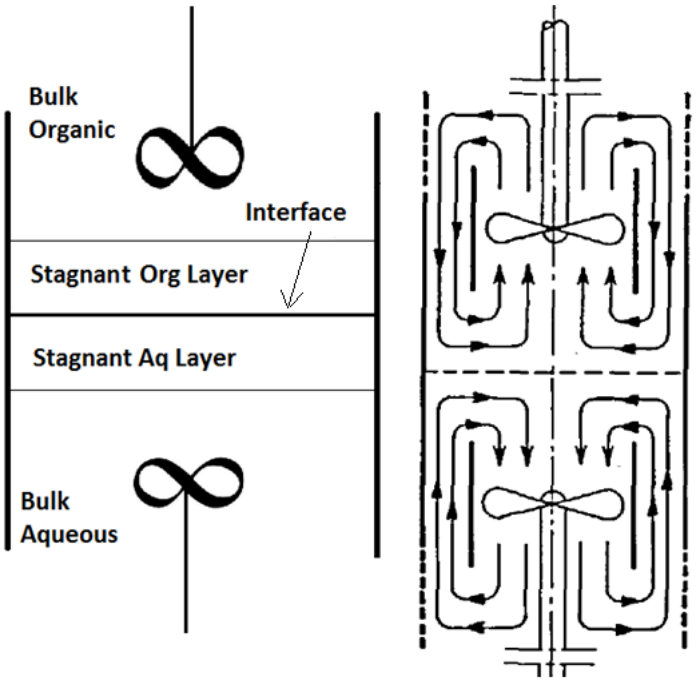

Fig. 38. A schematic representation of the hydrodynamics in a Lewis cell, right, the stagnant layers, left.

Making use of equations 42 and 45 for one-dimensional mass transfer with $C_{i,1} = C_{i,b}$ and $C_{i,2} = C_{i,int}$ being the concentration of i in the bulk and the interface respectively we get

$$N_{i,y} = k\left(C_{i,b} - C_{i,int}\right) = D_{ci}\frac{dC_i}{dy} = \frac{D_{ci}}{D_L}\left(C_{i,b} - C_{i,int}\right) \qquad (46)$$

Therefore, the mass transfer coefficient becomes

$$k = \frac{D_{ci}}{D_L} \qquad (47)$$

If both D_i and L are known, then the applicability of this theory in the Lewis cell can be validated.

Since the Lewis cell operates in a batch setting, the assumption of steady-state is obviously not valid as the concentration of solute i changes over time. However, for short periods of time, the concentration at the boundaries could be assumed to be constant.

2- Surface Renewal Theory

This is a more realistic model in which the films forming around the interface are not stagnant in time but rather renewed by turbulent eddies from the bulk phases. The interface is considered to be composed of fluid elements with a semi-infinite domain. The solution to Fick's second law with the following boundary conditions is:

$$t = 0\ ;\ 0 < y < \infty \qquad C = C_b$$

$$t > 0\ ;\ y = 0 \quad C = C_{int}$$

$$t > 0\ ; y = \infty \quad C = C_b$$

$$\frac{C_i - C_{i,b}}{C_{i,int} - C_{i,b}} = erfc\frac{y}{\sqrt{4D_{ci}\tau}} \qquad (48)$$

Where erfc is the complimentary error function. From equations 42 and 48 we get

$$k = \sqrt{\frac{D_{ci}}{\pi t}} \qquad (49)$$

In this model $k \propto D_{ci}^{0.5}$

Two postulations have been proposed to account for the renewal rate of the interfacial elements.

A- The Higbie Postulation: States that all surface elements spend the same amount of time at the interface before being replaced. In this formulation the mass transfer coefficient becomes

$$k = \sqrt{\frac{D_{ci}}{\pi t_b}} \qquad (50)$$

B- The Danckwert's postulation: States that different elements spend different amount of time at the interface and therefore a mean surface renewal rate is used instead

$$k = \sqrt{D_{ci}S} \qquad (51)$$

3- The Film-Penetration Model

This model postulated by Toor and Marchello is a modification to Highbie's penetration where there is the additional assumption that fluid elements residing at the interface not only have a finite residence time but also a finite depth.

$$t > 0 \; ; y = D_L \quad C = C_b$$

The mathematical results of this theory can be presented in two ways

$$N_{i,y} = \sqrt{D_{ci}s}\left[1 + 2\sum_{n=1}^{\infty} \exp(-2nD_L\sqrt{{}^{s}/_{Dc_i}}\right]\left(C_{i,b} - C_{i,int}\right) \qquad (52)$$

and

$$N_{i,y} = \frac{D_{ci}}{D_L}\left[1 + {}^{1}/_{3}\left(\frac{sD_L{}^{2}}{D_{ci}}\right) + {}^{1}/_{45}\left(\frac{sD_L{}^{2}}{D_{ci}}\right)^{2} + \cdots\right]\left(C_{i,b} - C_{i,int}\right) \qquad (53)$$

For high surface renewal rates equation 52 reduces to Danckwert's model and for low surface renewal rates equation 53 reduces to the film theory.

Other models have been developed by many researchers including Perlmutter's multiple capacitance model which sets the Higbie and Danckwert's models as the limiting cases for interfacial renewal, Ruckenstein's model in which surface elements are not taken to have discrete volumes but rather be mixing with neighboring elements, etc.

Although these theories set the upper and lower limits of mass transfer coefficients obtained in a stir cell under a given condition, they have multiple unknown parameters such as diffusion film length, surface renewal rate, velocity profiles, number of

capacitances, and other physiochemical parameters making it difficult to experimentally validate.

Another source of complexity comes from the Marangoni effect at the interface. Local instabilities due to surface tension caused by concentration and temperature gradients at the interface prompt mixing. In systems where the interfacial tension is high, measured mass transfer coefficients will have higher values than the ones theoretically calculated due to Marangoni instabilities.

Therefore, given the complexity of the hydrodynamics, empirical correlations have been developed to obtain mass transfer coefficients rather than seeking analytical solutions to the transport equation.

Lewis in 1954 was the first to design a transfer cell to measure individual mass transfer coefficients of partially miscible liquids [59, 60]. His conclusion was that turbulent eddies from either phase approach the interface and therefore molecular diffusivity had no role in moving the transferred molecules to the interface. Based on his interpretation of the data, Lewis formed the first correlation of mass transfer coefficient in the Lewis cell. Following Lewis's work, other researchers including Sherwood, Gordon, McManamey, etc. carried out more stirred cell studies on other binary systems and arrived with correlations incorporating diffusion coefficient values for the transferred species. It is worth noting that all of these studies and correlations were formed for partially miscible binary systems not exhibiting interfacial chemical reactions. Therefore, interfacial diffusion and mixing are the two mechanisms responsible for the transfer of one phase into the other. It should also be noted that these correlations are device specific. Stirred cells with different designs were

used in the various studies resulting in hydrodynamics that differ from one cell to the other. [61-63]

Stirred cells for the use of studying chemical reaction kinetics

When an interfacial chemical reaction is required to transfer a solute from a raffinate phase into an extract phase, three consecutive steps are needed to achieve the process. First, the solute molecules would have to reach the interface by means of diffusion, then react with some of the extract phase components, which would also need to reach the interface, and then diffuse into the bulk of the extract phase. Therefore, both processes would have an effect on the overall mass transfer rate. If the chemical reaction is fast, then diffusion time scales would determine the rate of mass transfer. A general correlation for diffusion-controlled mass transfer is given by

$$rate = kr^p \qquad (54)$$

However, if the interfacial chemical reaction rate is slow relative to diffusion timescales, then the process of mass transfer would be dictated by the rate of the chemical reaction. It also is possible that both processes have comparable timescales with both reflecting the overall mass transfer rate. Figure 39 shows the predicted plot shape of flux vs. stirring speed in a Lewis type stirred cell. At low stirring speeds, large stagnant regions near the interface exist, and therefore diffusion time scales dominate. As the stirring speed increases, turbulence reaches closer to the interface thinning the stagnant layers and therefore reducing the effects of diffusion timescale. If flux keeps increasing with increasing mixing speed, it would be an indication that reaction timescales are negligible. However, if the flux seizes to increase, then one of the two explanations could be possible.

Either diffusion becomes negligible and the rate observed is due to the chemical reactions only, or a mixed regime is stablished where increasing stirring speed does not further decrease stagnant zones and the observed rate constant reflects both reaction and diffusion time scales. It should be emphasized that the only way the solutes can transfer from one phase to the other is through the interfacial reaction. It should also be noted that beyond a critical stirring speed, the interface becomes turbulent increasing the flux due to the increased surface area.

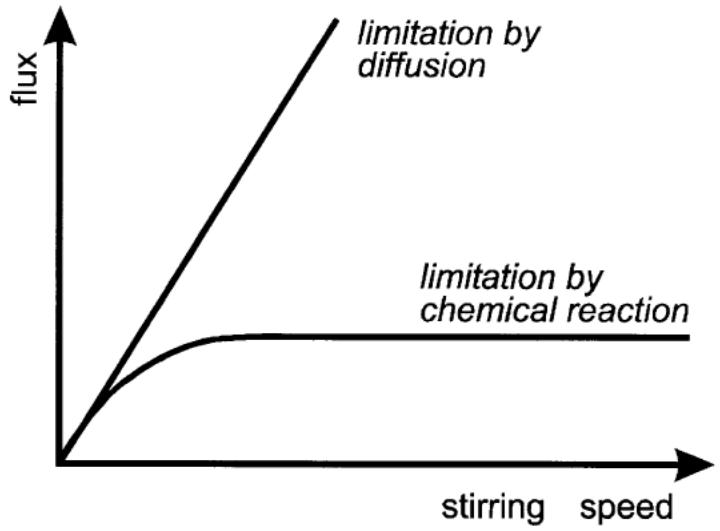

Fig. 39. Dependence of flux on stirring speed in Lewis cells [64]

One of the earliest interfacial mass transfer kinetics studies using a Lewis cell was on the extraction of uranyl nitrate with TBP at the Hanford laboratories by L. Burger [65]. The study included the effects of concentration, temperature, surfactants, and stirring speed on the extraction rate. Burger observed different effects from stirring speed based on the initial metal ion concentration in the aqueous phase in addition to different reaction rate orders depending on the initial concertation. Another observation was that while surface active impurities inhibit the initial rate of transfer, a reduction in the rate was a function of

degree of saturation of the adjacent phase and not time. Horner et al. at Oak Ridge National Laboratory also conducted extraction experiments with the uranyl-TBP system. They concluded that both the extraction and stripping processes were controlled by the interfacial reaction. This was contrary to Burger's conclusion of a diffusion-controlled stripping process [56, 62, 65]. Nitsch, using his modified stirred cell showed the extraction rate can change from being reaction limited to diffusion limited upon increasing the concentration of the extractable zinc ions [66]. Vandegrift studied the transfer of calcium with HDEHP and proposed a mechanism for the interfacial chemical reaction [67]. Danesi proposed a mechanism for the mixed regime interfacial mass transfer where he treated the diffusion of metal ions to the interface as an adsorption reaction [68]. Hughes has mathematically shown that in the case of fast reactions happening in the aqueous film a mixed regime of both diffusion and reaction control the rate of extraction [69] between the aqueous and organic phases. Geist using Di-(2-ethylhexyl)phosphoric acid (HDEHP) studied the rate of extraction of some rare earth elements including Nd using a larger version of the same Nitsch cell used in the current study and concluded that diffusion of the metal ions was the rate limiting step [64]. El-Hefny studied the kinetics of Nd extraction using a mixture of neutral extractants commercially known as Cyanex 921 to conclude the reaction rate to be the limiting step [70]. As part of his graduate studies at the Imperial College of Science and Technology, Lawrence James Austin using specialized optical lenses photographed the interface of both binary and ternary systems during mass transfer across the interface [71]. He observed that depending on the density of the transferring species relative to the solvents, the interface becomes unstable depending on the direction of transfer. His experiments also showed increased organic phase stirring had less of an

influence on the thickness of the organic stagnant film unlike the aqueous film. In addition, when the two phases were stirred at equal speeds, the hydrodynamics on the organic side of the interface changed from a single stagnant layer, Whitman's thin film theory, to the surface renewal mode as stirring was increased from 100 RPM to 200 RPM. The aqueous side however, remained laminar up to 400 RPM.

Noting the wide range of conclusions from many studies, it is clear the data obtained by a stirred cell is highly sensitive to the hydrodynamics of the interface, experimental conditions, impurities, etc. and extreme care must be taken to obtain reproducible data.

Experimental setup

A jacketed beaker with sampling ports shown in figure 40 was initially used as the stir cell. The beaker had a volume of 2x150 ml and a cross sectional area of 38.5 cm^3. A 5-cm stir bar sitting at the bottom of the beaker was used in the aqueous phase while a 4-cm narrower stirrer made of PMMA was placed half way the distance in the organic phase. The proper volume of each phase, measured by mass for consistency, was added to the cell. A stir plate was calibrated for speed using a tachometer. The independently rotating stirrers were set to their desired speeds spinning in a contra-rotating manner. It was noted that having the stirrers spin in a co-rotating manner caused the interface to spin adding more degree of uncertainty to its stability. The water bath was turned on and sufficient time was allowed for thermal equilibration at the desired temperature. At time zero, 1 ml of $Dy(NO_3)_3$ solution with the proper concentration was injected into the aqueous phase through the sampling port, the clock was started and 200 µL samples from each phase were collected at the same instance using needles. This setup had a few deviations from a proper

Lewis cell. First, the stirrers were not identical in shape and were not symmetrically placed with respect to the interface. The beaker did not have any vertical or horizontal baffles and also had a free surface. The organic phase was open to the atmosphere. These were the reasons for this stir cell to have a very limited operating range before disturbing the otherwise laminar interface. The highest possible stirring speed was 80 RPM in the aqueous phase. For similar studies, values of up to 500 RPM are reported in the literature with comparable interfacial areas. The limited range of operation prompted the need to use a more sophisticated stir cell to study the kinetics of interfacial mass transfer.

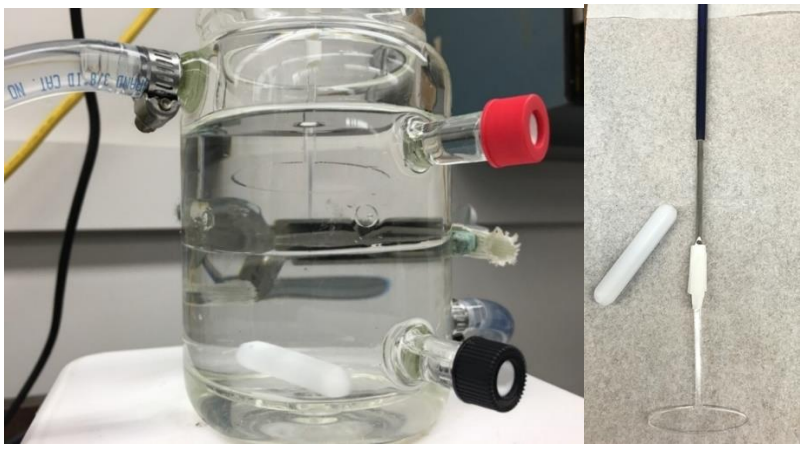

Fig. 40. Stirred beaker, left, stirrers, right.

A Nitsch cell, designed by researchers at the Karlsruhe Institute of Technology in Germany, was manufactured at the University of California Irvine, see figure 41, and used in the remaining kinetic studies. This Nitsch cell has the features of the ARMOLLEX stir cell in addition to vertical baffles placed at the top and the bottom sections of the cell as shown in figure 41. These baffles help with mixing of the bulk phases. This new design of the Nitsch cell also has two small cylindrical tubes that are placed around the stirrers. The function of these cylinders is to stabilize the interface at faster mixing. The Nitsch cell has a total volume of about 116 ml, a cross sectional area of 12.56 cm^2, and pitched stirrers with three

blades each shown in figure 42. The cell is jacketed with an external cylinder to allow for temperature control through a water bath. Initially, regular AC motors were installed. However, due to high fluctuations in their set stirring speeds over the duration of an experiment, they were later replaced with stepper motors for accurate speed control figure 43.

Fig. 41. The Nitsch cell designed at the Karlsruhe Institute of Technology

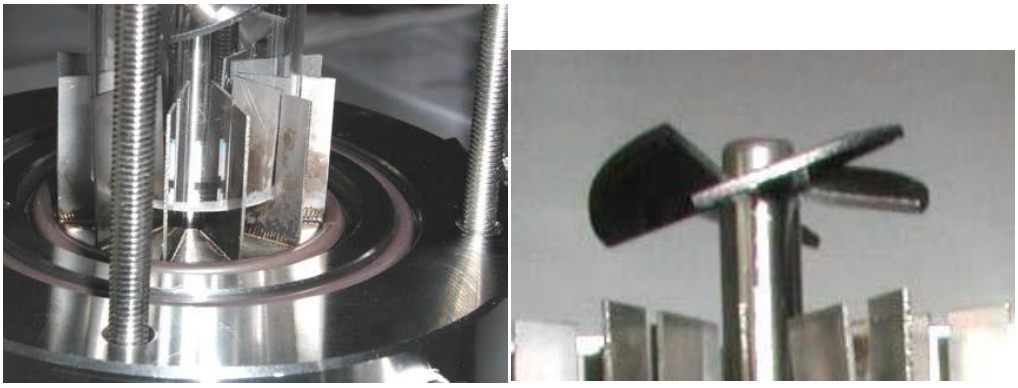

Fig. 42. On the left are the vertical baffles on which the inner cylinder is placed. On the right is the three bladed pitched stirrers

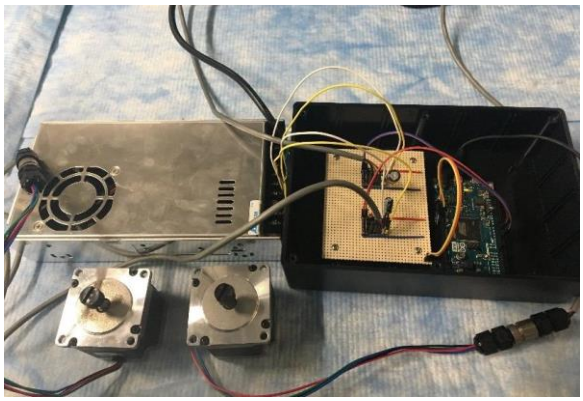

Fig. 43. The stepper motors connected to the control circuit

Similar to the experiments performed in the beaker, the aqueous phase was weighed and added to the Nitsch cell. Then, the organic phase was carefully placed on top of the aqueous phase. Entrained organic droplets can stick to the lower baffles and cylinder therefore extreme care was needed when adding the organic phase. The two stirrers were set to spin in a contra-rotating manner. The temperature control bath was started, and an hour was allowed for thermal equilibration. At time zero, a long needle entering from the top of the cell and going through the interface was used to spike the aqueous phase with 1 ml of concentrated solute to obtain the desired initial concentration. The addition of the pulse was done from above since a small tube connected to the sampling port from the inside prevented the needle to go entirely inside the solution causing some of the pulse to remain in the sampling channel. A useful feature of this Nitsch cell is it allows for continuous monitoring of the concentration in the two phases through a loop without the need for batch sampling. This feature was not used in these studies due to lack of instrumental capabilities. Two syringes, one entering from the top into the organic phase and one from the bottom into the aqueous phase, were used to collect 80 μL samples every 15 minutes.

After the end of each kinetics experiment, the entire solution was brought to equilibrium and samples of each phase were again analyzed.

Nitsch cell cleaning

As the literature points out, impurities and surface-active agents significantly alter the results and can become a major source of data irreproducibility. As the manual recommends, after each use the cell should be filled with acetone a few times to ensure all aqueous and organic matter is washed away. Unfortunately, due to machinist error, the baffles shown in figure 41 were not accurately aligned causing the glass-made internal cylinder to crack before being fully inserted. The cylinders were first replaced by ones made from Polymethyl methacrylate (PMMA). PMMA is not resistant to acetone and therefore soap was used to clean the cell. It was soon realized that soap residues would remain in the cell regardless of how many times it was flushed with water. Teflon being at least resistive to ethanol, new cylinders made of Teflon were used, however, a deflection towards the aqueous cylinder in the interface was noted. Repeated experiments gave inconsistent results when Teflon was used instead of PMMA. PMMA cylinders were used in all subsequent experiment since they were hydrodynamically favorable. After each experiment, the cell was dismantled, and cleaned with nano-pure water and dilute ethanol. In most cases, dust particulates could be seen at the interface.

Results and Discussion

Extraction of dysprosium Cyanex-572 in Isopar L in the Lewis cell

Figure 44 shows the concentration profile in the aqueous phase over time at different stirring speeds. After about ten hours, equilibrium is reached. The data for all three plots for the first two hour can be fitted well with an exponential function given in figure 45.

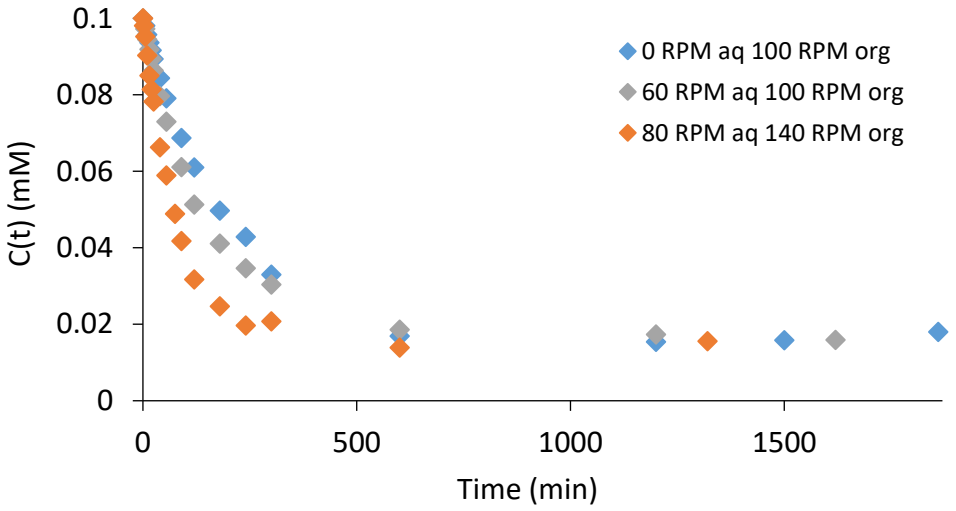

Fig. 44. Dysprosium concentration profile in the aqueous phase as a function of time

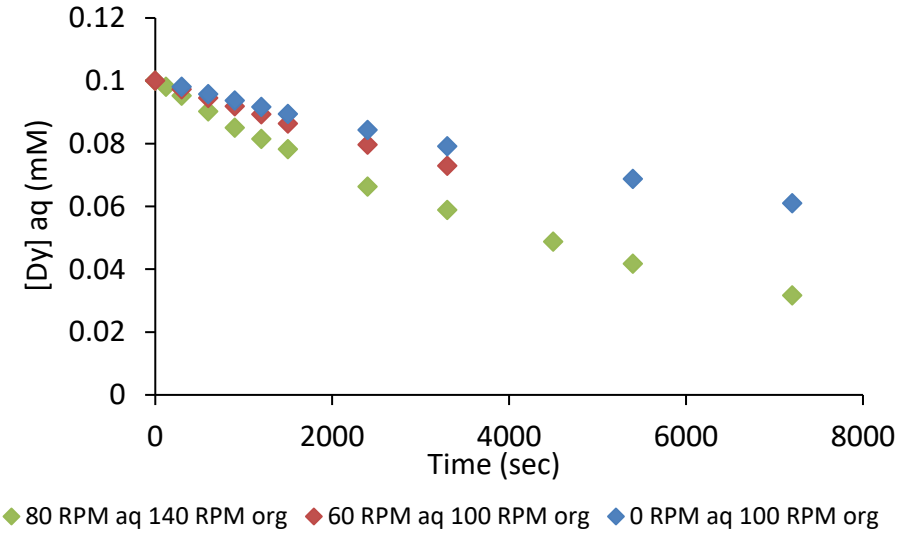

Fig. 45. Concentration of dysprosium ions in the aqueous phase as a function of time. The initial rate fits first order kinetics

The rate constant for the interfacial reaction given in equation 54

$$M_{aq}^{+3} + 3HL_{org} \leftrightarrow ML_{3,org} + 3H_{aq}^{+} \quad (54)$$

Can be written as

$$r_f = \frac{-dC_{M,aq}}{dt} = k_f\left[M_{aq}^{+3}\right]^a[HL_{org}]^b - k_b\left[H_{aq}^{+}\right]^c[ML_{3\,org}]^d \quad (55)$$

Two simplification to equation 55 are possible at the initial start of the process. Ion-exchange extraction reactions are reversible following the Le Chatelet principle. Therefore, to avoid the effects of the backward reaction on the forward reaction rate constant only the first 20 minutes of contact were considered, far away from equilibrium. The backward reaction can be assumed negligible since the concentration of $ML_{3,org}$ will be negligible relative to the concentration of HL_{org}. Also, in the case where the initial concentration of free ligands in the organic phase are significantly higher relative to the metal ion concentration in the aqueous phase, the forward rate constant can be lumped with the $[HL_{org}]^b$ term and equation 55 reduces to

$$r_f = \frac{-dC_{Dy,aq}}{dt} = k_{O,aq}\left[M_{aq}^{+3}\right]^a \quad (56)$$

Where

$$k_{O,aq} = k_f[HL_{org}]^b \quad (57)$$

When a is taken to be 1 the solution to equation 56 is

$$\ln C_{M^{+3},aq} = -k_{O,aq}t + \ln C_{M^{+3}0} \qquad (58)$$

Figure 46 shows the data form straight lines backing the above assumption. However, it is clear how the observed rate constant increases as the stirring rate increases meaning the process is diffusion controlled.

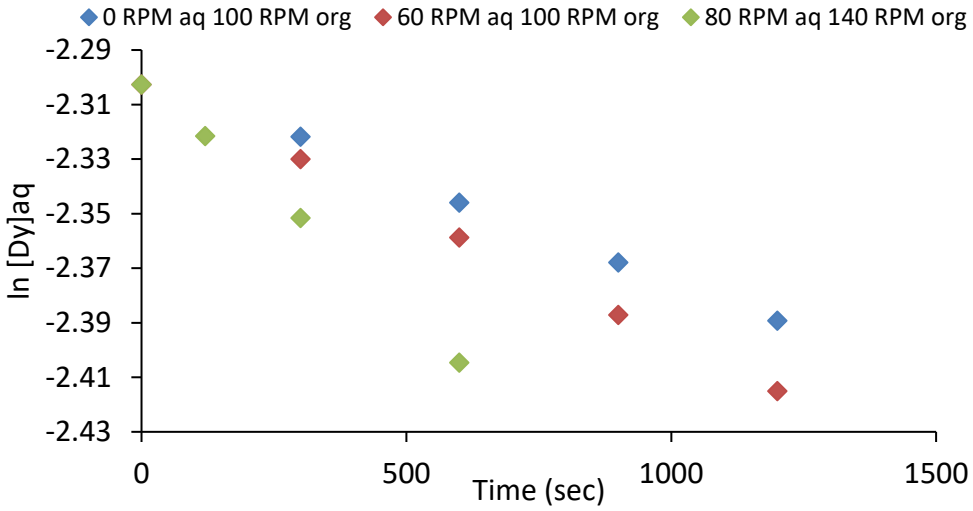

Fig. 46. Natural logarithm of the remaining concentration in the aqueous phase as function of time in the Lewis cell.

Using equation 45 the initial flux is calculated

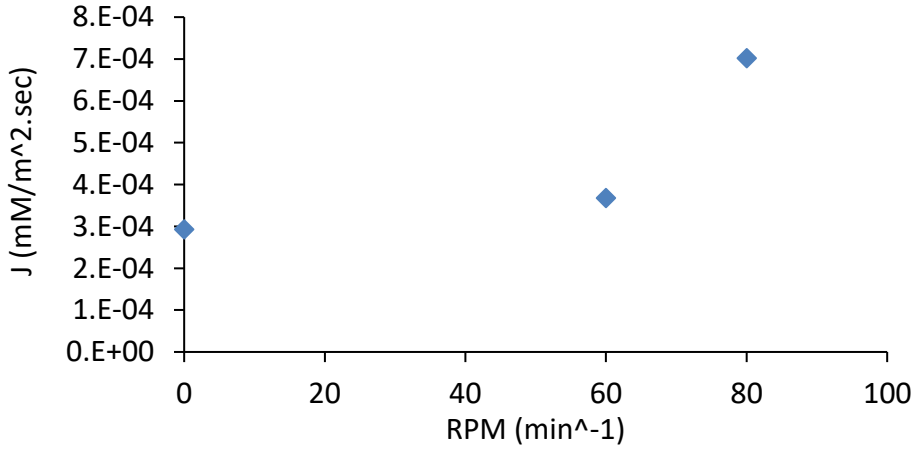

Fig. 47. The flux of dysprosium into the organic phase as a function of stirring speed

From equation 42 assuming the interfacial concentration of the metal ions is negligible relative to bulk concentration we get

$$J_{i,aq} = k\left(C_{b,aq} - 0\right) \qquad (59)$$

And therefore, we can plot K to get

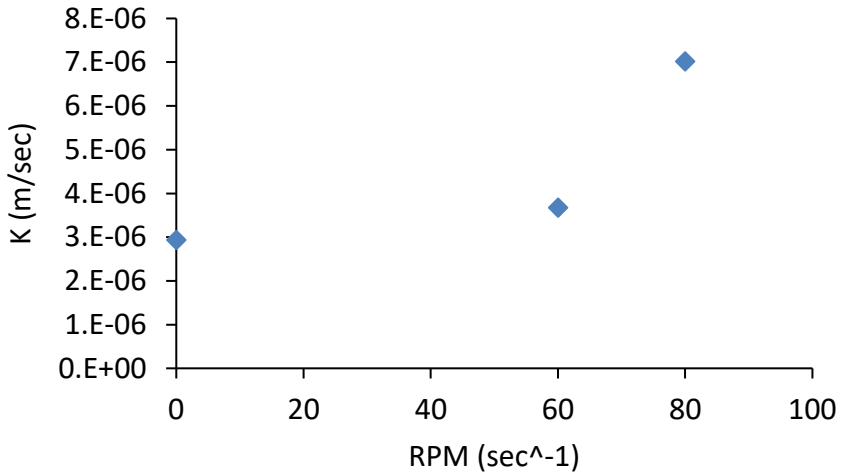

Fig. 48. The mass transfer coefficient in the aqueous phase as a function of stirring speed

Similar to Nitsch's improvement on the Lewis cell which included the installation of screens around the interface, meshes, shown in figure 49, were installed in each phase close to the interface. The purpose of these screens was to allow for faster stirring while maintaining a laminar interface. As the results in figure 50 indicate, K_{obs} at 100 RPM in the aqueous phase with meshes was much lower compared to the one at 80 RPM without the meshes. Therefore, it was evident that this modification created large stagnant layers most likely in both phases hindering the flux. Perhaps the most useful information from the stirred beaker experiments was the confirming the chemical reaction was only interfacial. The interface was decreased using a thin layer of PMMA shown in figure 57 by 75%. The

observed rate constant decreased by about a factor of four indicating the Cyanex 572 components were only surface active and did not go inside the bulk of the aqueous phase.

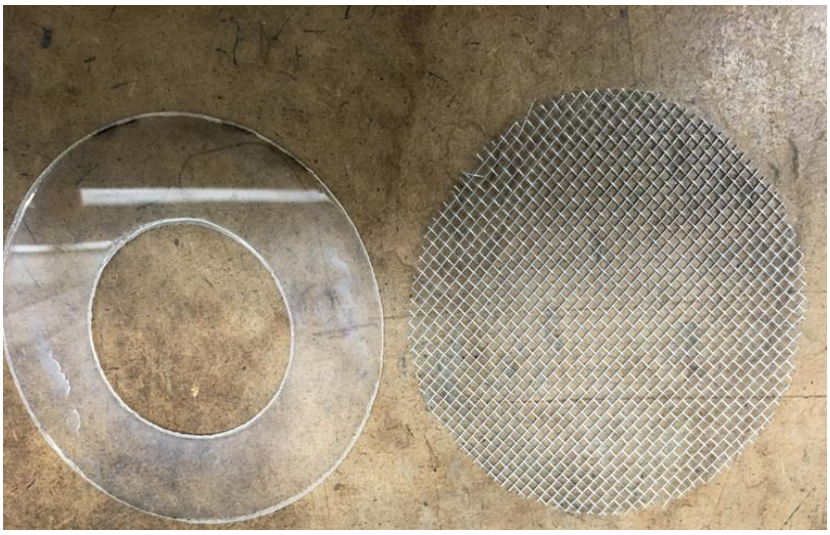

Fig. 49. Aluminum mesh, right, used in the high RPM experiment and a thin layer of PMMA, left, used in the interfacial area reduction experiment

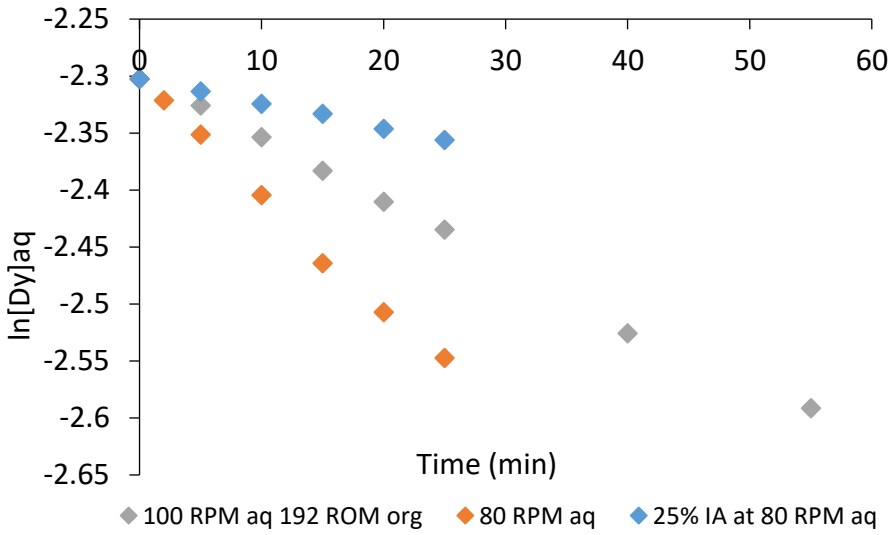

Fig. 50. Comparison of the reaction observed rate constant between the highest possible stirring without the addition of meshes and higher stirring speed with the presence of meshes

Figure 51 shows the results from the Nitsch cell for the same system. At 20 °C fixing the organic stirring speed at 300 RPM, it appears the flux reaches a plateau when the aqueous

stirring speed reaches about 300 RPM as well. However, when the organic speed is increased to 400 RPM, the flux further increases indicating either less diffusion effects on the organic side or contribution from momentum transfer from the organic to the aqueous side. This slight increase in the flux could also be contributed to the rippling of the interface as turbulence intensifies and reaches closer the interface.

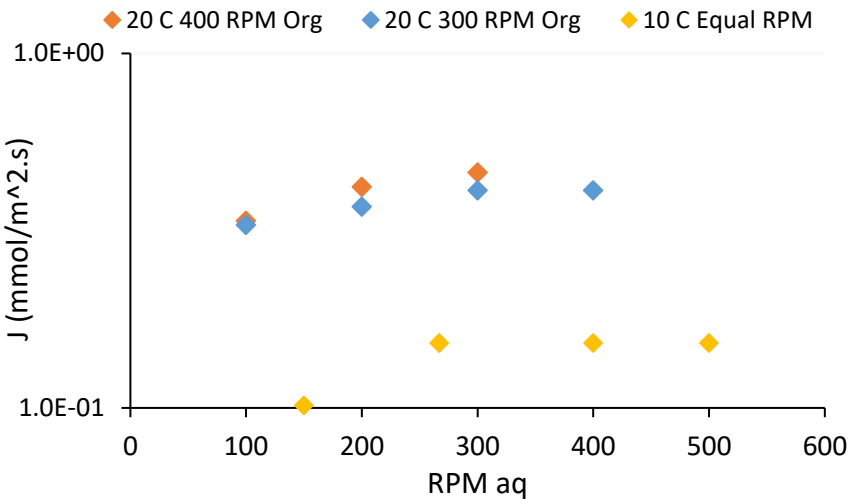

Fig. 51. 0.1 mM $Dy(NO_3)_3$ in 0.1 M HNO_3 and 0.2 M C572 in Isopar l at 20.0 °C

In the Nitsch cell, a three-order magnitude increase in the flux was observed compared to the stirred beaker. This was evidence how insufficient mixing was in the stirred beaker.

The effect of temperature on both diffusivity and extraction has been studied and it has been reported that the activation energy associated with metal ions diffusion in aqueous media does not usually surpass 20.9 kJ/mol [47]. The Nitsch cell experiments were repeated at 10.0 °C with both stirrers having the same speed, as it was observed to yield the most stable interface. Using the Arrhenius equation, the activation energy was calculated to be

77.3 kJ/mol. This could be a good indication the process was controlled by a chemical reaction.

The mass transfer coefficient at 20.0 °C in the plateau region is about 4.61E-4 m/s and the observed rate constant is about 1.25 E-4 sec^-1. To investigate both the forward rate constant and the reaction order in Cyanex 572, experiments at varying Cyanex 572 concertation are needed. However, since the components and the composition of Cyanex 572 was not clear, it was decided to replace Cyanex 572 with HEH[EHP], a single component extractant. The diluent was also replaced by n-dodecane to minimize impurities.

HEH[EHP] Experiments

HEH[EHP] is an acidic reagent used in the Actinide Lanthanide Separation (ALSEP) process and also in the Advanced Trivalent Actinide Lanthanide Separation with Phosphorus-Reagent Extraction from Aqueous Komplexes (Advanced TALSPEAK). Extraction of metal ions with HEH[EHP] occurs by the same mechanism of proton exchange as Cyanex 572. The structure of HEH[EHP] is shown in figure 10. All experiments were carried at 20.0 °C with equal stirring speed in both phases. The dependency of the initial flux on stirring speed was tested with the 0.1 mM dysprosium nitrate experiments and the plateau region was confirmed to start around 300 RPM. All subsequent experiments were conducted at 300 RPM. Some experiments, with higher HEH[EHP] concentration, were also performed at 400 RPM to see whether the increased viscosity of the organic phase affected the plateau behavior.

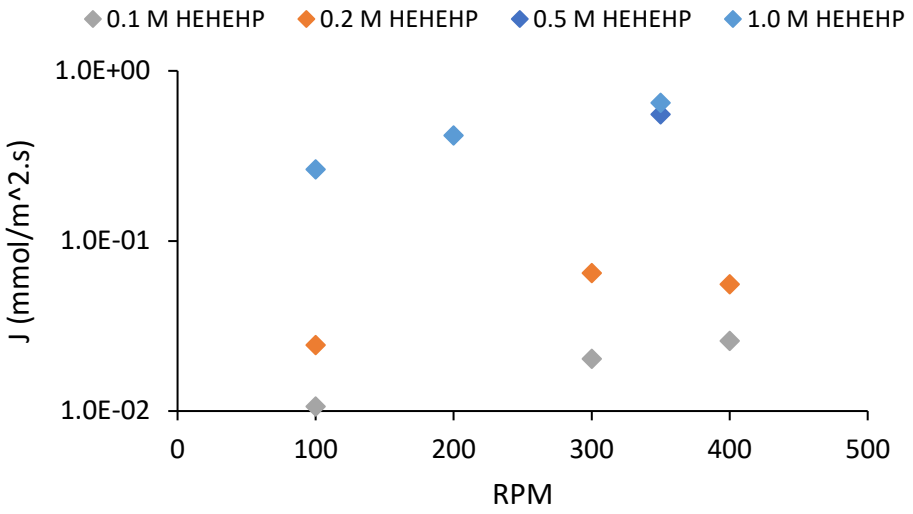

Fig. 52. 0.1 mM $Dy(NO_3)_3$ in 0.1 M HNO_3 HEH[EHP] in dodecane at 20.0 °C

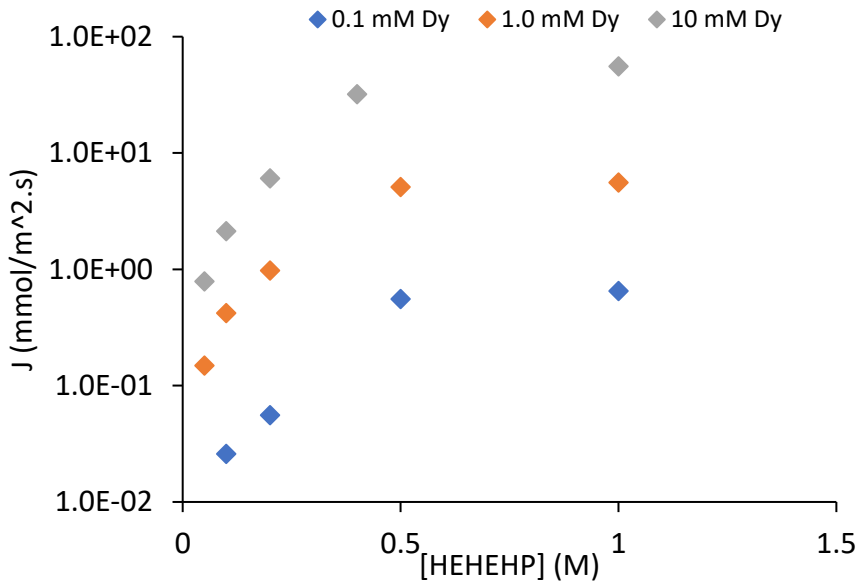

Fig. 53. The flux dependence on the HEH[EHP] concentration in the plateau region $Dy(NO_3)_3$ in 0.1 M HNO_3 HEH[EHP] in dodecane at 20.0 °C

If a true reaction-limited regime is stablished at 300-400 RPM, changes in the concentration of metal ions and changes in the concentration of the ligand would reflect changes in the flux according to their order on the reaction rate. Examining figure 53, it

appears the increase in flux at a given ligand concentration with increasing metal ion concentration is not consistent specially at the lower ligand concentrations. At 0.5 and 1.0 M HEH[EHP], the increase is more consistent and is closer to the expected value. Increasing the dysprosium ions concentration by an order of magnitude increases the flux by about an order of magnitude.

At low stirring rate, the thin film layer theory can be applicable as was discussed in the theory section. Most lanthanides have diffusion coefficients in the range of 1E-10 m^2/sec. Using equation 47 a diffusion length of about 0.3 μm is obtained at 20.0 °C. At the higher stirring speeds, the thin layer theory is not applicable, and the surface renewal theory can be applied.

An equation for the rate of surface renewal based on the rate of turbulent energy dissipation was derived by Bulicka and Prochazika [72]. In their model given in equation 60 they show the dependence of surface renewal in each phase on the dissipated turbulent energy in both phases.

$$S_{ij} = \frac{\varepsilon_{ib}\rho_i v_i^{0.5} + \varepsilon_{jb}\rho_j v_j^{0.5}}{\rho_i v_i^{1.5} + \rho_j v_j^{1.5}} \qquad (60)$$

Where

$$\varepsilon = \frac{u^3}{L_c} \qquad (61)$$

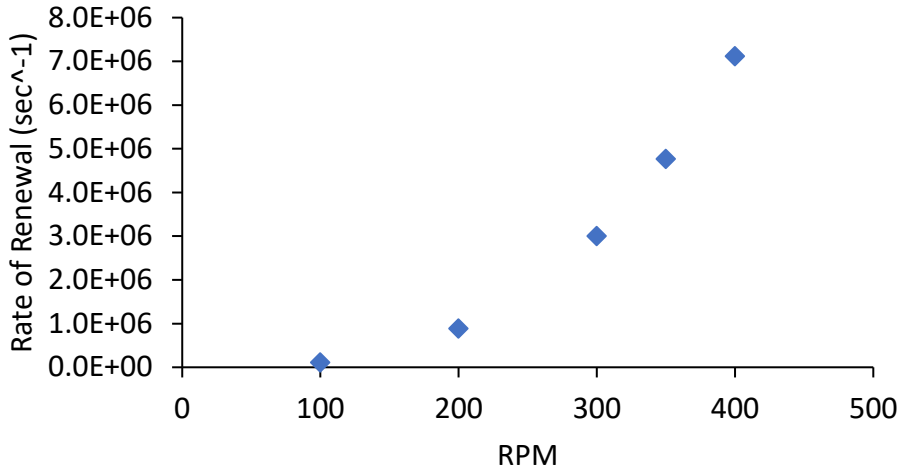

Fig. 54. shows the rate of surface renewal as a function of stirring speed.

From Danckwert's theory, equation 51, the mass transfer coefficient for the case of 400 RPM is 2.67E-02 (m/sec). This value of the mass transfer coefficient is significantly higher than all the mass transfer coefficients experimentally obtained shown in figure 55. This could be explained by the dominant reaction time when diffusion is negligible under such high rates of surface renewal.

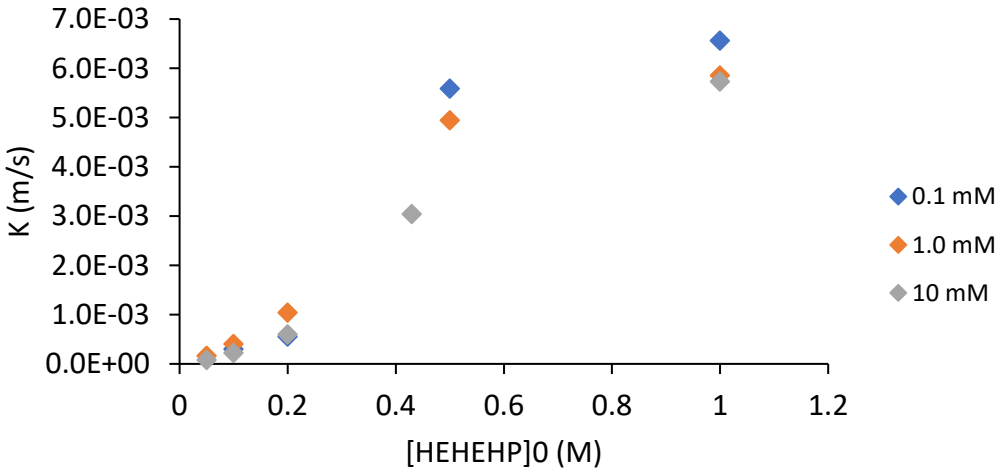

Fig. 55. Overall mass transfer coefficient of dysprosium extraction from the aqueous to organic phase as a function of ligand concentration

From figure 55, it also appears the mass transfer coefficient reaches a plateau as the concentration of the HEH[EHP] increases. The viscosity and the density of the organic phase was measured at different ligand concentration. Within error, they were both constant up to 0.4 M HEH[EHP]. Assuming the Reynolds number in the lower concentration range was not affected by the slight increase in both viscosity and density, the hydrodynamics should remain the same between these runs. Since this is the plateau region on the flux vs RPM plot, then in the case of a true chemical reaction, the increase in the concentration of the ligand should increase the flux according to its order. Since HEH[EHP] is a surfactant, its concentration at the interface will be different than the bulk phase with a logarithmic relationship between bulk and interfacial concentrations according to Gibbs adsorption isotherm. Figure 56 shows how the interfacial tension between HEH[EHP] and nitric acid changes as a function of concentration. From figure 57 it is apparent that the interface is almost saturated around 0.5 M HEH[EHP] and therefore the extraction rate becomes independent of the ligand concentration. At 1.0 M ligand, the Reynold's number is slightly lower, but the change in the rate of surface renewal is negligible. Therefore, it is unlikely that the plateau in figure 55 at 1 molar is caused by the decrease in the Reynold's number. i.e. increased diffusion effects.

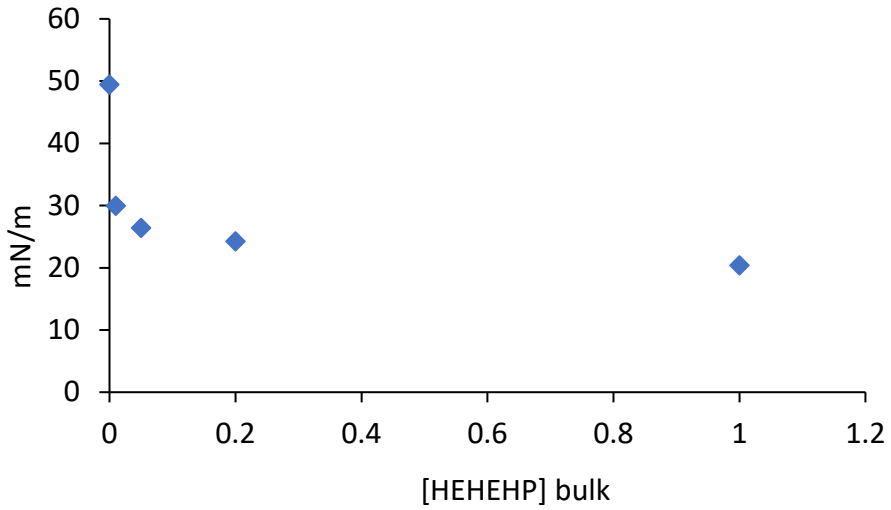

Fig. 56. Interfacial Tension of HEH[EHP] in Dodecane with 0.1 M HNO3

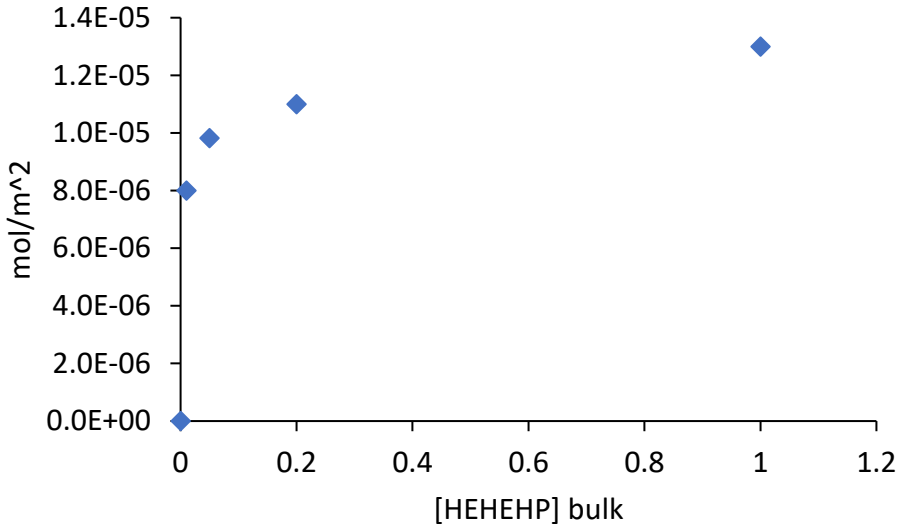

Fig. 57. Number of molecules per unit interface area calculated using the Gibbs adsorption Isotherm

Going back to equation 56, for the assumption of constant concentration of ligand to hold, a large excess of it is needed. Therefore, the case with 0.1 mM dysprosium nitrate is perhaps the most valid experimental condition. Also, to avoid the effects of interfacial saturation with the ligand molecules, the 1 M HEH[EHP] condition is most likely not a good data point. Figure 58 shows plots based on the solution of equation 57 where the slope would be the

order of the reaction rate in ligand concentration and the inverse natural logarithm of the intercept would be the forward reaction rate constant.

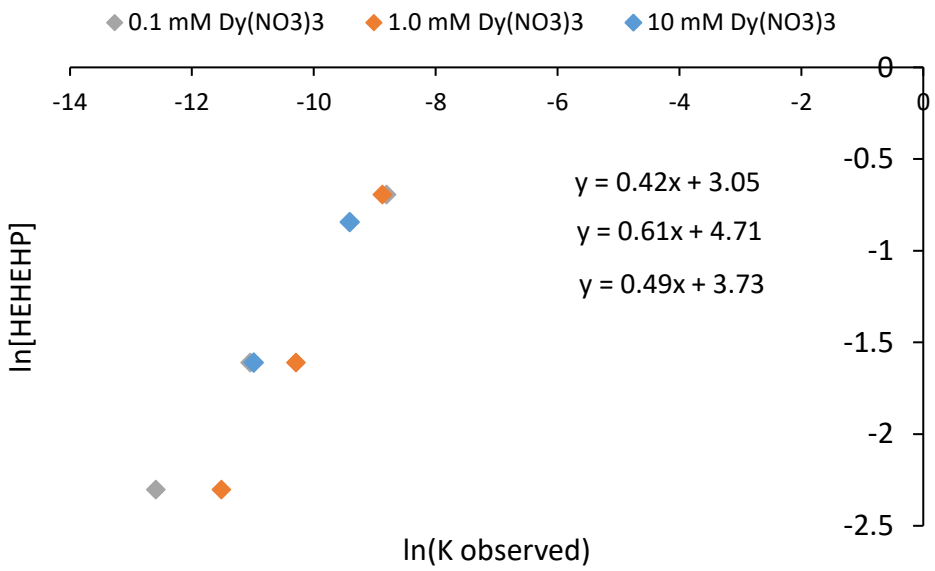

Fig. 58. Natural logarithm of the concentration of ligand as a function of observed rate constant

In the extraction of Lu3+ with 0.2–0.4 molar HEH(EHP) in a Lewis cell, a slope of 0.60 was obtained by Jinshi [73], which corresponds to our 1.0 mM dysprosium case.

From the 0.1 mM dysprosium experiments at 0.1, 0.2, and 0.5 M HEH[EHP], the reaction rate order in ligand concentration would be 0.51 and the forward rate constant would be 0.033 giving a rate equation

$$\frac{d[Dy]}{dt} = -0.033 * [Dy]^1 * [(HEHEHP)_2]^{0.51} \qquad (62)$$

Figures 59-61 compare the initial rate constants obtained experimentally to those obtained by the models for the various metal concentrations such as the one in equation 62 for 0.1 mM Dy.

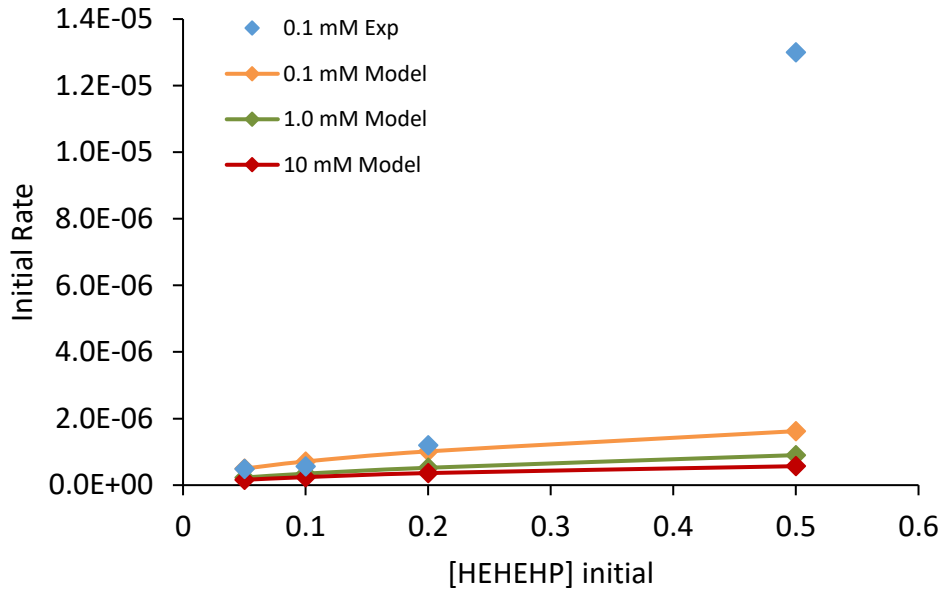

Fig. 59. Initial rate of extraction as a function of initial ligand concentration for 0.1 mM initial dysprosium concentration

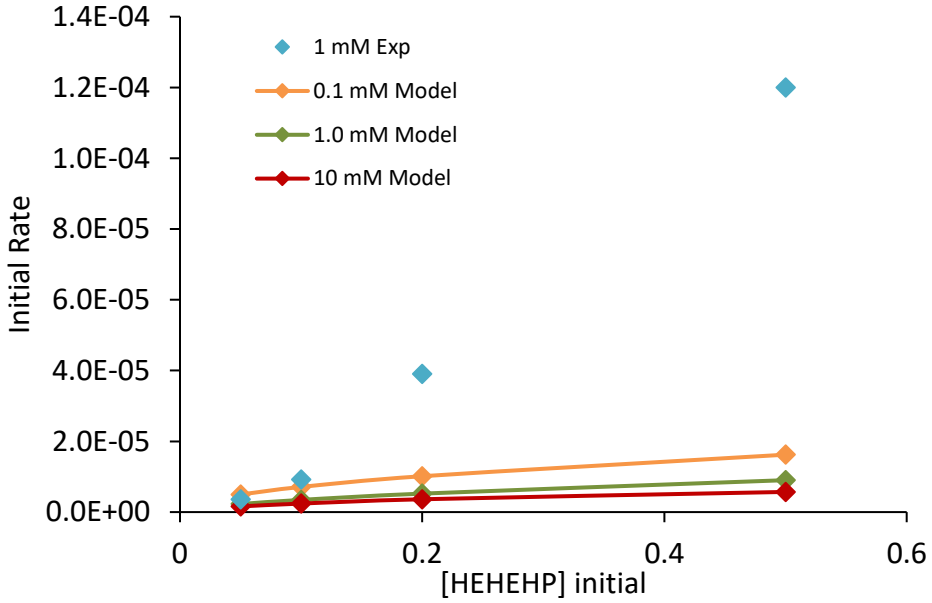

Fig. 60. Initial rate of extraction as a function of initial ligand concentration for 1.0 mM initial dysprosium concentration

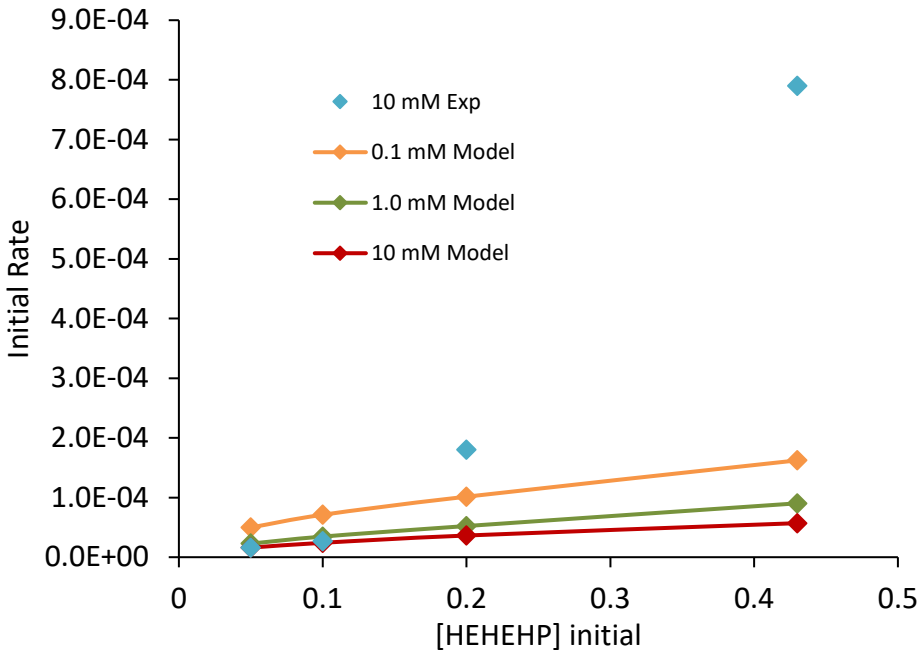

Fig. 61. Initial rate of extraction as a function of initial ligand concentration for 10 mM initial dysprosium concentration

All experimental values of the initial rate are about an order of magnitude higher than predicted by the models at the highest ligand concentration used. Also, all models for the 0.05 M and 0.1 M ligand concentrations seem to well match the experimental values. The deviation seems to start as both the metal and ligand concentrations increase. In the case of 0.1 mM initial dysprosium concentration, the model still well matches the experimental point. It seems the combination in the increase of both species changes the extraction mechanics and perhaps the hydrodynamics in the organic side. Since the model underestimates the reaction rate, ignoring the backwards reaction rate does not seem to be the affecting factor.

Choppin and Nash suggested a first order in metal ion and half order in ligand concentrations for the rate of dysprosium extraction with HDEHP in stirred cells [47]. They

used much lower, a couple orders of magnitude, concentration of both metal ions and ligand. From the data presented here, it appears the model is consistent with previous findings and breaks at much higher concentrations. The mechanisms suggested in equations 29.a and 29.b can be further broken down into the following

$$(HL)_{2,org} \leftrightarrow (HL)_{2,int} \qquad ; at\ equilibrium \qquad (63)$$

$$Dy^{+3} + 0.5(HL)_{2,int} \leftrightarrow DyL_{int}^{+2} + H^{+} \qquad slow \qquad (64)$$

$$DyL_{int}^{+2} + (HL)_{2,int} \rightarrow DyL_{3,int} + 2H^{+} \qquad fast \qquad (65)$$

$$DyL_{3,int} + (HL)_{int} \rightarrow (DyL_3)(HL)_{org} \quad fast \qquad (66)$$

Or

$$DyL_{3,int} + 3(HL)_{int} \rightarrow (DyL_3)(HL)_{3,org} \qquad fast \qquad (67)$$

V. Mixing and droplet formation

In almost all chemical processes, mixing has a significant role in determining efficiency. In the context of centrifugal contactors, where the mixing of two immiscible liquids takes place, one phase, the so-called the dispersed phase, will form droplets within the other, so-called continuous phase. The number and the size of these droplets are governed by a balance of forces acting to break and coalesce them. The smaller the size of these droplets, the larger will be their surface area to volume ratio. This in turn will increase the interfacial area, the contact area of the two phases, allowing for higher rates of mass and/or heat transport and hence a more efficient process.

Relevant theoretical background

According to Hinze [74], the two major forces responsible for breaking a droplet are the turbulent dynamic pressure fluctuations and viscous shear stresses. When the magnitude of these forces exceeds that of the restoring forces, droplet breakage occurs. Interfacial tension and internal viscous stresses are the two main counteracting forces responsible for the cohesion of the droplet. Hinze distinguished three basic types of globule deformation and splitting based on the hydrodynamics of the surrounding fluid. In the case of the ambient fluid being in a turbulent motion, the deformation is of the "bulgy" type and is caused solely by dynamic pressure. Centrifugal contactors are characterized to have such type of flow. Also, from the early works of Kolmogorov and Hinze, it has been agreed that turbulent eddies having the size of a droplet or smaller are responsible for the breakage of the droplet meanwhile those with larger dimensions will only cause translational motion. Since dynamic pressure fluctuations contribute to breakage, droplets can still form in the

case where both phases have the same or similar velocities. A correlation accounting for the dynamic pressure stresses is given by

$$\tau_s \propto \frac{\rho_c \overline{u_\lambda'^2}}{2} \qquad (68)$$

Where

$$u_i = \bar{u}_i + u_i' \qquad (69)$$

In the inertial subrange, where the turbulent energy is transferred from large energy-containing scales to the energy dissipating Kolmogorov microscales, for the case of homogenous and isotropic turbulence, the fluctuating component of velocity can be defined in terms of the rate of turbulent energy dissipation as

$$\overline{u_\lambda'^2} = C_3(\varepsilon\lambda)^{2/3} \cong 2.0((\varepsilon\lambda)^{\frac{2}{3}} \qquad (70)$$

The forces responsible for droplet breakage and coalescence can be represented with two non-dimensional numbers. The Weber number We, equation 71, gives the ratio of shear stresses to surface tension and the Ohnesorge number Oh, equation 72, relates viscous forces to inertial forces and surface tension.

$$We = \frac{\tau_s d}{\sigma_s} \qquad (71)$$

$$Oh = \frac{\mu_d}{\sqrt{\rho_d d \sigma_s}} \qquad (72)$$

At the critical Weber number, the dynamic stresses, τ, are great enough to overcome the adhesive surface tension forces, causing the droplet to break.

Substituting equations 68 and 70 into 71 and taking $\lambda = d_{max}$ we get

$$We_{critical} = \frac{\rho_c \varepsilon^{2/3} d_{max}^{5/3}}{\sigma_s} \qquad (73)$$

Assuming the internal viscous stresses in the droplets are negligible and hence neglecting the Oh number, the maximum droplet diameter can be expressed generally as

$$d_{max} = C_4 (\frac{\sigma_s}{\rho_c})^{3/5} \varepsilon^{-2/5} \qquad (74)$$

In general, the rate of turbulent energy dissipation is defined as

$$\varepsilon \equiv \nu \langle \frac{\partial u_{ij}'}{\partial x_j} \frac{\partial u_i'}{\partial x_j} + \frac{\partial u_i'}{\partial x_j} \frac{\partial u_j'}{\partial x_i} \rangle \qquad (75)$$

In the case of isotropic turbulence, the rate of dissipation simplifies and can be represented as

$$\varepsilon = 15\nu \frac{u'^2}{\lambda^2} \qquad (76)$$

From equations 75 and 76, it is apparent that knowledge on the fluctuating components of the instantaneous velocities and their gradients is required to calculate the rate of energy dissipation for the calculation of droplet diameters. Experimentally, using imaging techniques such as Laser Doppler Velocimetry LDV or Particle Image Velocimetry PIV it is

possible to get information on the velocity field. Such measurements are challenging in terms of obtaining clear images and require sophisticated equipment including ultrafast cameras, lenses, light sources, and signal synchronizing equipment. Computational fluid dynamics CFD can also be used to estimate the velocity profile in such equipment. The challenge with this approach other than the validity of the model used is the high computational power needed to obtain acceptable results. This becomes especially important when multiple phases are used, and high resolution is needed to distinguish the phases.

In stirred tanks, the rate of turbulent energy dissipation is proportional to[75]

$$\varepsilon \propto \Omega^3 {d_b}^2 \qquad (77)$$

Also, the Weber number for stirred tanks is given as

$$We_T = \frac{\rho_c \, \Omega^2 {d_b}^3}{\sigma} \qquad (78)$$

Substituting 77 and 78 into 74 we get

$$\frac{d_{max}}{d_{in}} = C_5 (We_T)^{-3/5} \qquad (79)$$

Hinze, using the results from Clay experiments of Couette flow in two coaxial cylinders with the inner one rotating, found the constant to have a value of 0.725[74].

$$\frac{d_{max}}{d_{in}} = 0.725 (We_T)^{-3/5} \qquad (80)$$

Haas performed dimensional analysis and using three different liquid extraction equipment including an Couette disperser, derived a correlation for the maximum droplet diameter [76].

$$\frac{d_{max}}{\Delta r} = 150(We)^{-0.65}Re^{-0.2}(\frac{\mu_d}{\mu_c})^{0.5}(\frac{\Delta r}{d_{in}})^{0.5} \qquad (81)$$

The Sauter mean diameter is another concept used in droplet analysis. It is defined as

$$d_{32} = \frac{\sum f_i d_i^3}{\sum f_i d_i^2} \qquad (82)$$

It represents the diameter of a sphere that would have the same volume to surface area ratio as a particle of a random shape. If one is not interested in the distribution of droplet sizes within an apparatus but rather is only interested in the overall efficiency of a unit, an average size of droplet based on an average value of turbulent energy dissipation reflecting the entire operating unit can be used. Sprow was the first to propose that Sauter mean diameter to be proportional to the maximum droplet diameter

$$d_{32}\ \alpha\ d_{max} \rightarrow \frac{d_{32}}{d_b} = C_6(We_T)^{-3/5} \qquad (83)$$

When droplet coalescence becomes significant affecting droplet dimeter, equation 83 takes the form

$$\frac{d_{32}}{L_c} = C_7(1 + C_8\phi_v){We_T}^{-3/5} \qquad (84)$$

Zhou et. al has summarized most correlations in the literature between the Sauter mean diameter and the maximum droplet diameter developed by many researches under various tank and propeller geometries as well as fluid properties.

A relationship between the average rate of turbulent energy dissipation and the Sauter mean diameter was developed by Haas

$$d_{32} = \frac{2}{3}\left(\frac{\sigma_s}{\rho_c}\right)^{3/5}\overline{\varepsilon^{-2/5}} \qquad (85)$$

Using the annular gap as the characteristic length in equation 42, Tison [77] developed equation 84 into

$$\frac{d_{32}}{\Delta r} = 74.95 * 10^{-3}(1 + 2.7\phi_v){We_T}^{-0.125} \qquad (86)$$

When the Sauter mean diameter is known, the specific interfacial area between the two phases can be calculated if the volume fraction of the dispersed phase is known according to

$$a = \frac{6\phi_v}{d_{32}} \qquad (87)$$

Review of relevant literature

Wardle et al. conducted a thorough investigation of the hydrodynamics of the flow in the V02 model centrifugal contactor built by Costner Industries Nevada Corporation (CINC). The CINC V02 is made of stainless steel, has a 5.08 cm rotor diameter, and an annular gap of 6.3 mm. Using Large Eddy Simulations LES and the Volume of Fluid VOF method for CFD analysis in addition to LDV and PIV experiments, they studied the effects of vane geometry

on both the velocity field and the height of fluid column in the mixing region of the contactor. [53] Their studies showed variations in the velocity field both axially and radially in addition to changes in the volume holdup in the mixing zone of the contactor. The spatial variations in velocity result in spatial distribution of turbulent energy dissipation and hence a distribution in droplet diameter throughout the mixing zone of the contactor. Kadam et al. using three centrifugal contactors with diameters of 30, 75, and 250 mm developed correlations for the Sauter mean droplet diameter in terms of the dispersed phase holdup volume and the effective interfacial area [78]. Housings, outer cylinders, with different diameters were used to vary the width of the annulus gap. Various organic solvents including kerosene and butanol were used as the organic phase and pure water as the aqueous phase. In their studies, samples were collected from three different locations in the annular zone of the contactors for analysis. They showed at low dispersed phase holdup, the Sauter mean diameter remains relatively constant and a rapid increase was observed at increasing holdup, which is expected as the rate of coalesces increases. Their experiments also showed a decrease in the Sauter mean diameter at increasing continuous phase viscosity, decreasing interfacial tension, and increasing power per unit volume consumption. The mean diameter of droplets in these studied varied between 8-55 μm. Schuur et al. with the aid of Focused Beam Reflectance Measurement (FBRM) and RTD studied the hydrodynamics of flow and droplet size in the CINC V02 centrifugal contactor using water as the aqueous phase and four different organic solvents including heptane and toluene. While their studies showed increasing the feed flowrates did not noticeably affect holdup volumes, increasing the flowrate of the dispersed organic phase resulted in a decrease in the Sauter mean diameter. The mean Sauter diameters reported in these

studies were in the range of 150-650 μm. Ronnie Andersson and Bengt Andersson using high-speed imaging techniques studied the dynamics of droplet and bubble deformation and breakage under turbulent flow conditions [79]. Their two major conclusions were first unlike bubbles, the daughter fragments of droplets are of equal size and that a droplet breaks into several fragments while a bubble will for the most part split into two. Tamhane et al. using the phase doppler particle analyzer method studied droplet size distribution of the Taylor-Couette flow between an inner rotating cylinder and an outer stationary cylinder [80]. Although the flow in this setup resembles that of in the mixing zone of centrifugal contactors, it differs in two major ways. First, it lacks axial flow that centrifugal contactors have. Second, similar to the previous studies mentioned, this setup lacks a free surface which prevents the entrainments of air in the mixing zone. A mean droplet size in the range of 28-206 μm was observed as a function of power consumption and holdup volume of the dispersed phase. Wyatt et al. performed droplet size distribution studies with on the CINC V02 centrifugal contactor using direct imaging of the dispersed organic phase [81]. A fluorescing dye was added to the organic phase allowing for clear distinction from air bubbles. At all mixing speeds a log-normal distribution of droplets was observed with the width of the distribution narrowing as the mixing speed increased. The droplets ranged in size between 40 μm to 1 mm in diameter with the mean shifting towards 100 μm at 3000 RPM. The smallest droplets appeared to be near the rotor inlet whereas the largest ones were near the mixing zone inlet. Another observation consistent with previous studies was the minimal effect of holdup ratio on the mean droplet diameter.

Perhaps the only two correlations developed for predicting the Sauter mean diameter of droplets formed in the mixing zone of annular centrifugal contactors with experiments

performed in these type contactors are those of Kadam and Tison with the former accounting for both volumetric flowrates and annular liquid height

$$d_{3,2} = 8.5 * 10^{-3} \left(\frac{P}{V}\right)^{-0.21} \rho_c^{-0.17} \sigma^{0.6} \left(\frac{\mu_D}{\mu_c}\right)^{0.1} (1 + 8.5\phi_D) \qquad (88)$$

The dimensions of the contactor Tison used in his studies is not clear. Some of the geometric dimensions of the ANL 20 mm ACC are outside the range of dimensions of the contactors used by Kadam, such as the annular gap and the bottom clearance. Also, some of the experimental conditions in this study are also outside of the range tested by Kadam, such as the Reynolds number. For the lack of any better correlations in the literature, all available ones were compared, and the results are plotted in the figures below. A comparison between the organic phase ratios measured experimentally and the calculated ones using Kadam's correlation yield differences between 16%-50% with the correlation over-estimating the holdup volume irrespective to whether interfacial mass transfer occurred. Some of these discrepancies can be attributed to errors in measuring the height of the dispersion column in the mixing zone.

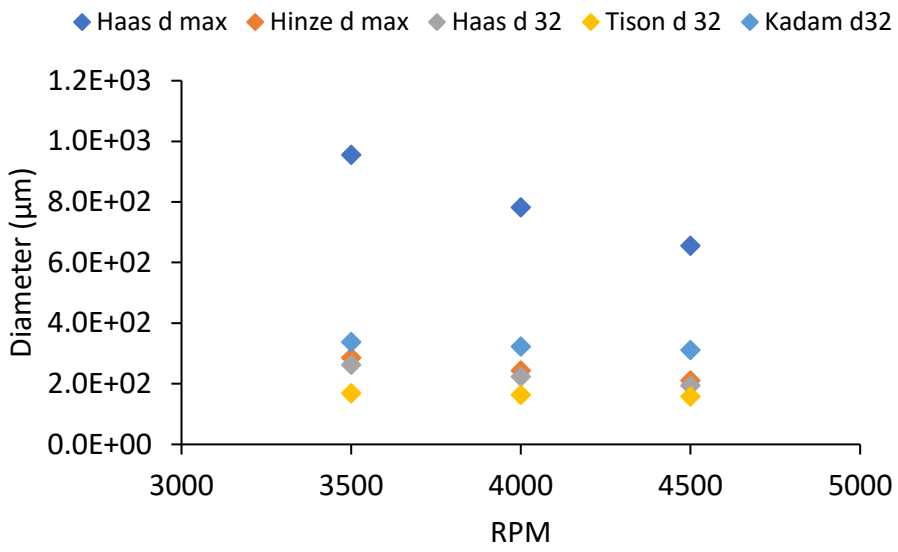

Fig. 62. Sauter and maximum droplet diameter in the mixing zone of the Robatel BXP012 at a/o =1 as a function of rotor speed

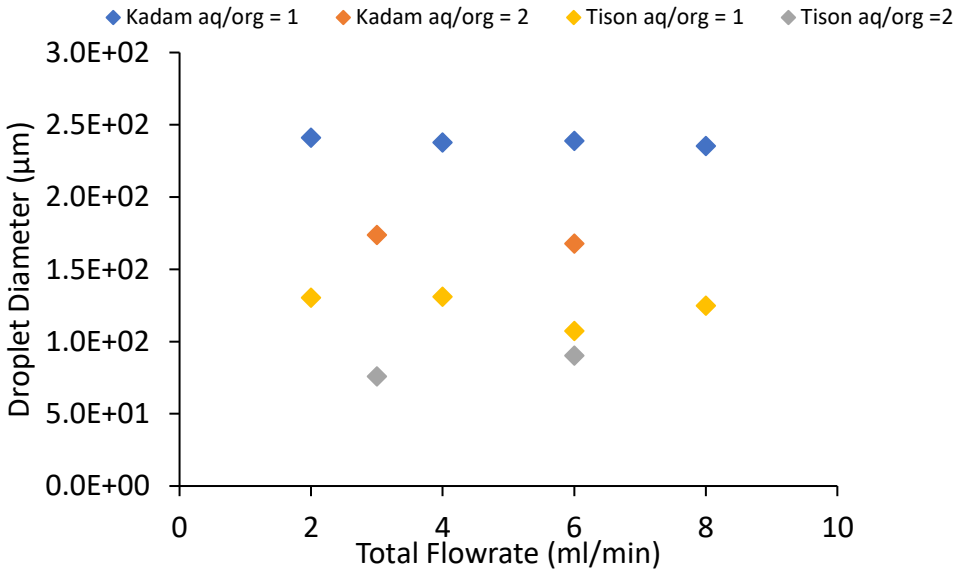

Fig. 63. Sauter and maximum droplet diameter in the mixing zone of the 20 mm ANL ACC as a function of total flow rate

Final Analysis

To have more confidence in the assumption of organic dispersed, i.e. organic phase forming droplets within the continuous aqueous phase, the case of aqueous to organic flow rates ratio of two will first be considered. In all experiments, non-recycled clean organic solution was used and therefore equations 17 and 87 upon rearrangement would give

$$V_{org} = \frac{d_{32}\overline{V_{org,out}}C_{Dy,org,out}}{6k\left(C_{Dy,eq}\right)} \qquad (89)$$

Table 6: Comparison between the Robatel and the Argonne contactors in terms of non-dimensional quantities.

Contactor Type	RPM	Re	Ta	We
Robatel BXP012	3500	918	2.71E+5	384
	3600	945	2.87E+5	406
	4000	1050	3.54E+5	501
	4500	1181	4.49E+5	635
Argonne 20 mm	3600	1000	1.35E+5	1650

In order to solve for the dispersed phase holdup volume, the Sauter mean diameter as well as the overall mass transfer coefficient in the contactor need to be known. The other quantities can be easily measured. Since the 20 mm Argonne contactor can be drained and the content of its mixing zone can be measured, it was used to compare the Sauter mean diameter correlations that do not account for phase holdup ratio with the ones that do. By comparing Tison's correlation to Haas's, no significant difference was found in the

predicted diameters, both have the same order of magnitude. Haas's correlation was used in the calculations for the sake of simplicity.

Overall Mass Transfer Coefficient obtained from the Nitsch Cell

Mass transfer coefficients are specific to each contacting equipment and usually a value obtained from one type of equipment would not be valid for another. Centrifugal contactors are characterized by having high Ta numbers making molecular diffusion negligible. In the system studied, the only way for the metal ions to transfer into the organic phase is through the interfacial chemical reaction. It was demonstrated that when the extraction is performed in the Nitsch cell, past around 300 RPM no increase in flux was observed as stirring speed increased, meaning molecular diffusion is negligible. Since the assumption of negligible molecular diffusion also applies for these types of mixers, the mass transfer coefficient obtained from the Nitsch cell was first used in equation 89 to estimate the organic holdup volume. The results are shown in figures 64-66. From the plots, it appears the organic holdup volume ranges from a minimum of 0.1 ml to a maximum of 0.9 ml. The lower end of this range seems to be unreasonably small, assuming the Sauter mean diameter correlation used hold true. Also, it appears as the organic phase has a larger holdup volume when the aqueous to organic flowrate ratio is two. Although not proved, one would expect some of the volume previously occupied by the organic phase to become replaced by the aqueous as the flow rate of the aqueous is increased. A sudden discharge of the organic phase was noticed when the aqueous phase flowrate was increased during experiments suggesting changes in holdup volume.

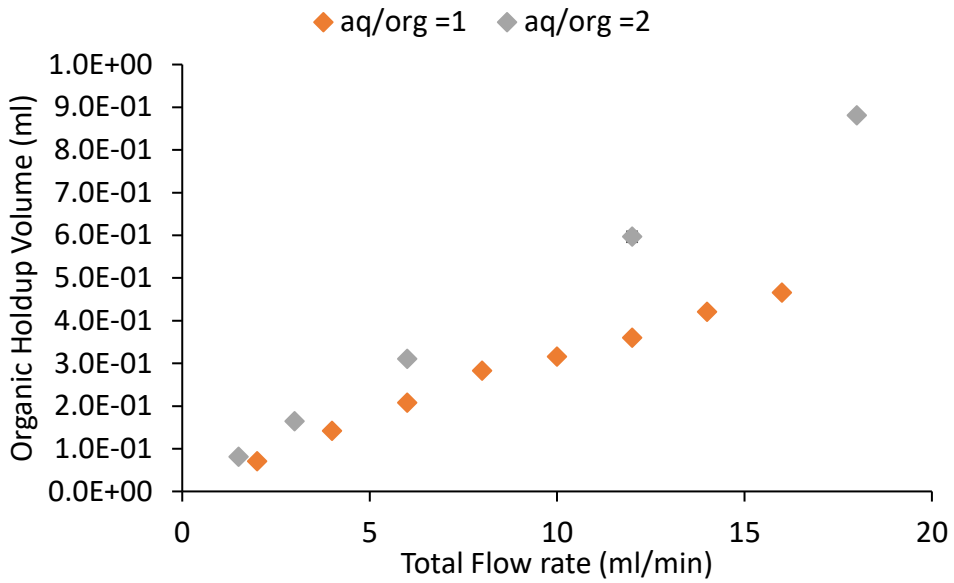

Fig.64. The organic holdup volume in the mixing zone as a function of total flowrate for the Robatel contactor at 3500 RPM using the mass transfer coefficient obtained from the Nitsch cell

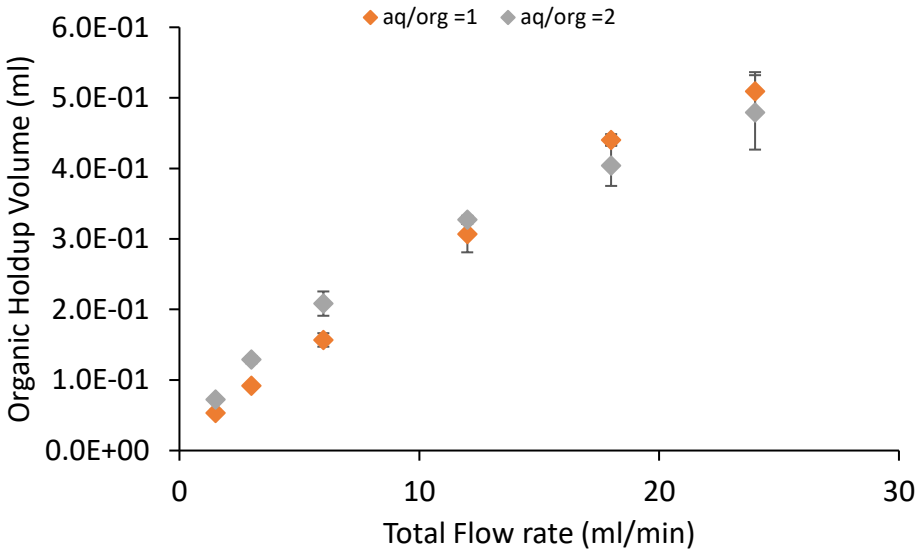

Fig.65. The organic holdup volume in the mixing zone as a function of total flowrate for the Robatel contactor at 4000 RPM using the mass transfer coefficient obtained from the Nitsch cell

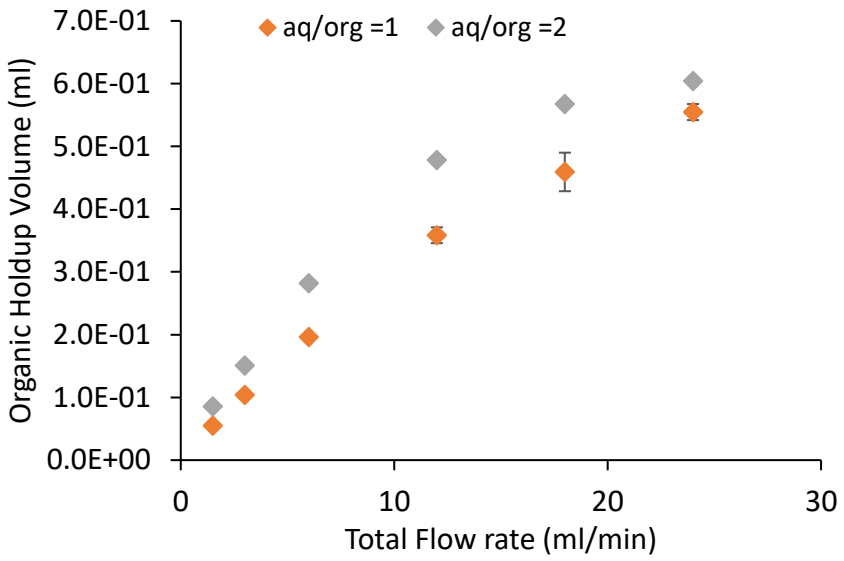

Fig.66. The organic holdup volume in the mixing zone as a function of total flowrate for the Robatel contactor at 4500 RPM using the mass transfer coefficient obtained from the Nitsch cell

Overall Mass Transfer Coefficient obtained from the 20 mm Argonne contactor

From table 1, the hydrodynamics of the two contactors seem to be similar in terms of the Reynolds and the Taylor numbers. Even though the Argonne contactor has a Weber number about three times larger compared to the Robatel at 4000 and 4500 RPMs, the Sauter mean diameters of the two contactors are almost identical meaning they both result in the same interfacial density. From equation one, using the data from the 20 mm contactor, the overall mass transfer coefficient was found to have an average value of 1.1E-06 ± 8.5E-07 m/sec and 3.1E-07 ±2.6E-07 $^{m}/_{sec}$ for aqueous to organic ratios of 2 and 1 respectively. The mass transfer coefficient slightly increases with increasing total flowrate. It is worth noticing the close value of the overall mass transfer coefficient in the centrifugal contactor relative to the Nitsch cell with a little decrease in the contactor, although one would expect the opposite as mixing is much more intense in the contactor. One major

difference however lies in the dispersed phase Reynolds number. In the Nitsch cell, both phases are highly agitated resulting in Reynolds numbers in the range of 3000-3500 in each phase. In the contactor however, the highest achievable dispersed phase Reynold number is about 350 when the droplet radius is taken as the characteristic length and the rotor linear velocity as the droplet speed. This might have a significant effect on the diffusion of the organic ligands to the interface and hence slowing the process of mass transfer. The one order drop in magnitude of the Reynolds number might be the reason for the one order drop in the mass transfer coefficient. Another possible contributor to the faster mass transfer kinetics observed in the Nitsch cell might be due to the correct size of the interfacial area. At high stirring speeds, although the interface appears to be stable, waves and some ripples are still present increasing the actual interfacial area. This would artificially increase the observed rate and hence the mass transfer coefficient. Figures 67-69 show the organic holdup volume in the Robatel using overall mass transfer coefficients obtained from the Argonne 20 mm contactor and Sauter mean diameters obtained from Tison's correlation. These results are more realistic relative to the ones obtained by using the Nitsch cell mass transfer coefficient. For all three RPMs, the holdup decreased with an increasing aqueous to organic flowrate ratio. This is reasonable as it is expected for the aqueous holdup to slightly increase when its flowrate is increased. Also, the predicted volume for the organic phase is more realistic relative to the ones obtained with the Nitsch cell mass transfer coefficient. The mass transfer coefficients for the first three points on the plots are directly calculated from the 20 mm contactor data. The mass transfer coefficients for the rest of the points were extrapolated. However, there must be a point beyond which

increasing the flowrates would not further increase the mass transfer coefficients otherwise the organic holdup would reach zero.

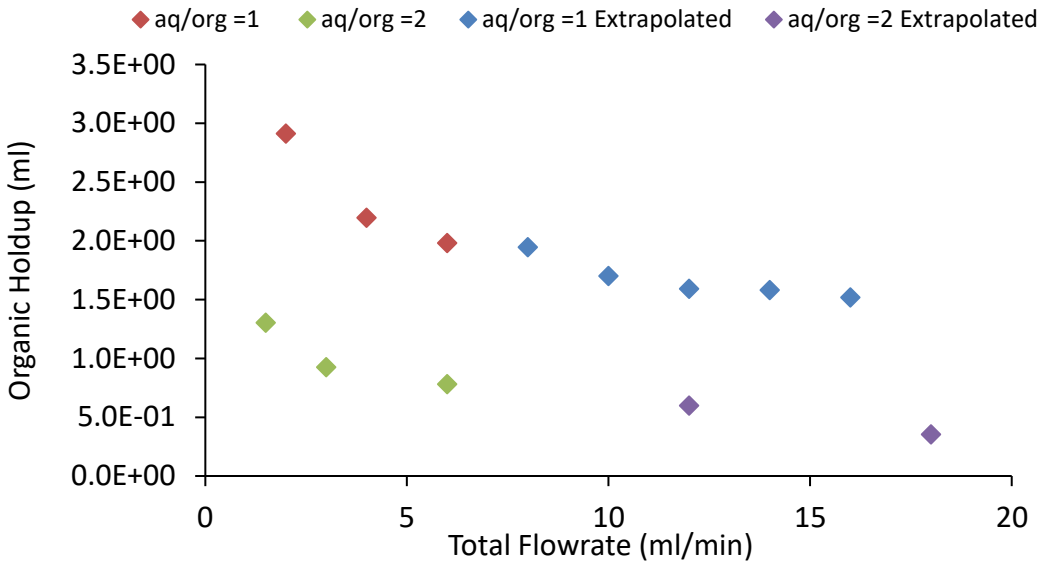

Fig.67. The organic holdup volume in the mixing zone as a function of total flowrate for the Robatel contactor at 3500 RPM

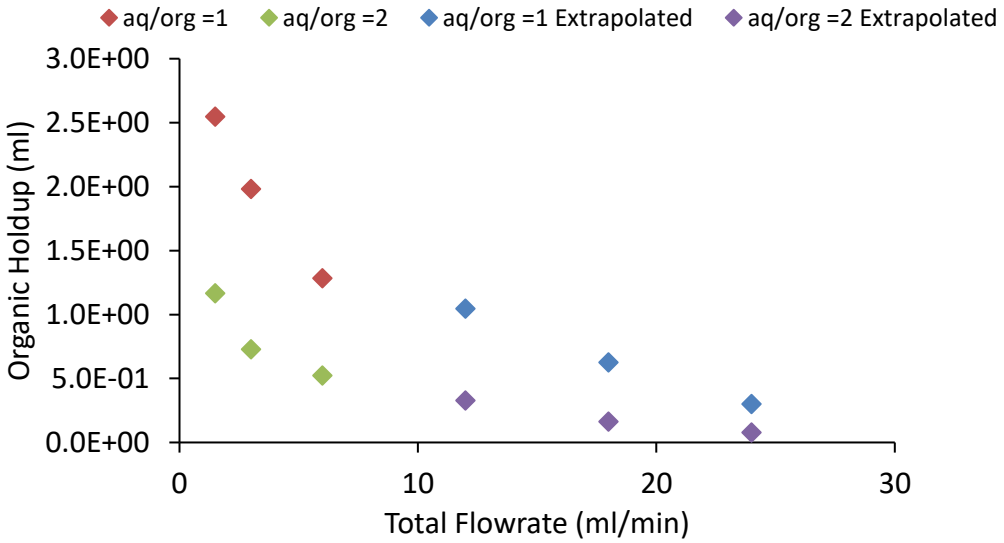

Fig.68. The organic holdup volume in the mixing zone as a function of total flowrate for the Robatel contactor at 4000 RPM

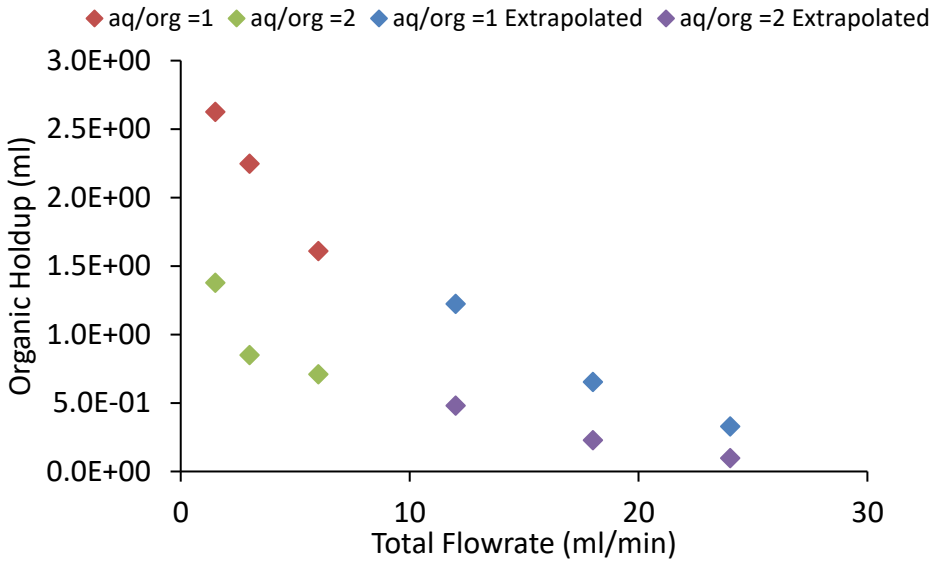

Fig.69. The organic holdup volume in the mixing zone as a function of total flowrate for the Robatel contactor at 4500 RPM

VI. Summary and Conclusions

In this study, the Robatel BXP012 centrifugal contactor with an inner rotor diameter of 12 mm was investigated in an attempt to predict the holdup ratio of the two phases in the mixing zone under various experimental parameters. To do so, the following strategy was adapted.

1- The efficiency of the contactor was investigated under various flowrates, flowrate ratios, and rotor speeds using two systems. Both in the cases of extraction of dysprosium from a nitric acid media with the acidic reagent cyanex 572 and the extraction of uranyl nitrate with tributyl phosphate, the extractions achieved equilibrium under all conditions.

2- Using residence time distribution analysis with the pulse method, the overall residence time of each phase in the contactor was measured and found to be relatively unaffected by rotor speed and accordingly change with flowrate.

3- To study the kinetics of the interfacial reaction responsible for the transfer of metal ions from the aqueous to the organic phase, a Nitsch cell was built and controlled experiments were performed. The unknown composition of cyanex 572 prompted the need to investigate a simple and well-known system. The kinetics of the HEH[EHP] was studied and a rate law was derived. The HEH[EH]P was not tested in the contactor however due to limited availability of chemicals.

4- Centrifugal contactors with radius of 20 mm and 10 mm and having a drain made by Argonne National Laboratories were provided. An overall mass transfer coefficient in the 20 mm contactor for the same system studied in the Robatel was obtained

through the use of correlations and measurements. Since the Reynolds, Taylor, and Weber numbers for the two contactors are close, the 20 mm contactor overall mass transfer coefficient was used to predict the holdup volume of the organic phase in the Robatel BXP012.

5- It was shown that by eliminating molecular diffusion through efficient mixing, the mass transfer coefficient in the Nitsch cell was comparable to the one in the Robatel BXP012.

6- Under aqueous to organic flowrate ratio of one, it was concluded that the organic phase would have a holdup volume of about 2-3 ml. For the case of flowrate ratio of 2, less organic is present in the mixing zone.

7- In the range of flowrates and rotor speeds studied, the Robatel has very sensitive hydrodynamics characterized by mid-operation flooding of the mixing zone. Also, the aqueous exit stream does not have a steady flow but rather one with an unsteady frequency. These random changes in the hydrodynamics of the Robatel have made this study particularly challenging.

8- Overall, it was demonstrated that this approach can be used to estimate the holdup volume of the mixing zone in annual centrifugal contactors.

Nomenclature

D: Distribution coefficient

C_i: Concentration of species i (M)

Subscripts: org: Organic phase

aq: Aqueous phase

M: Metal ion

L: Organic ligand

u_∞: Terminal velocity (m/sec)

d_p: Particle diameter (m)

ρ_p: Density of particle (kg/m^3)

ρ_c: Density of continuous phase (kg/m^3)

r_{in}: Radius of inner cylinder (m)

Ω: Rotation speed (sec^{-1})

μ: Dynamic viscosity (kg/m.sec)

η_M: Murphree efficiency

C_f: Feed concentration (M)

C_r: Raffinate concentration (M)

C_{eq}: Equilibrium concentration (M)

N_D: Dispersion Number

τ: Residence time (sec)

ΔZ: Emulsion thickness (m)

a: Acceleration (m/sec^2)

V: Volume (m^3)

$\overline{V}$: Volumetric flowrate (m^3/sec)

Ta: Tayler number

r_{out}: Radius of outer cylinder (m)

ν: Kinematic viscosity (m^2/sec)

Re: Reynolds number

η_0: Overall cascade efficiency

n: Number of stages

N: Number of theoretical stages

E_f: Extraction factor

N_i: Number of moles of species i (moles)

t: Time (sec)

r_i: Rate of reaction (M/sec)

K: Reaction rate coefficient

A: Interfacial area (m^2)

$J_{i,y}$: Molar flux (mol/m^2.sec)

k: Mass transfer coefficient (m/s)

a: Interfacial area per unit volume (m^2/m^3)

A_{rad}: Activity (disintegration/sec)

Φ: Neutron flux (neutrons/m^2.sec)

σ: Cross section (barns)

t_{irr}: Irradiation time (sec)

t_{hlf}: Half-life or radionuclide (sec)

t_{cool}: Cooling time (sec)

γ: Activity coefficient

$C_{1,2..}$: Constant

E: Residence time distribution function

D_c: Diffusion coefficient (m^2/sec)

D_L: Diffusion length (m)

$C_{i,int}$: Interfacial concentration (M)

$C_{i,b}$: Bulk concentration (M)

S: Rate of surface renewal (sec^-2)

ε: Rate of turbulent energy dissipation (m^2/sec^3)

u_i: Total velocity (m/s)

L_c: Characteristic length (m)

τ_s: Dynamic pressure stresses (N/m^2)

λ: Kolmogorov length scale (m)

u_i': Fluctuating Velocity (m/s)

$\overline{u_i}$: Time averaged velocity (m/s)

Oh: Ohnesorge number

We: Weber number

d: Droplet diameter (m)

σ_s: Interfacial tension (mN/m)

d_{max}: Maximum droplet diameter (m)

d_b: Stir blade diameter (m)

d_{in}: Inner rotor diameter (m)

Δr: Annular zone (m)

d_{32}:Sauter mean diameter (m)

f_i: Fraction of species i

ϕ_v: Volume phase ratio

P: Power (j/sec)

$\overline{V_D}$: Volumetric flowrate of dispersed phase (m^3/sec)

References

1. Schobert, H.H., *Energy and Society*. 2014: CRC Press.
2. GISELE O. DA ROCHA, J.P.D.A.a.J.B.D.A., *Energy trends and the water-energy binomium for Brazil.* Annals of the Brazilian Academy of Sciences, 2015. **87**: p. 569-594.
3. Administration, U.S.E.I. *International Energy Outlook 2013*. 2013; Available from: https://www.eia.gov/outlooks/ieo/pdf/0484(2013).pdf.
4. Layton, B.E., *A Comparison of Energy Densities of Prevalent Energy Sources in Units of Joules Per Cubic Meter.* International Journal of Green Energy, 2008. **5**(6): p. 438-455.
5. Le Quéré, C., et al., *The global carbon budget 1959–2011.* Earth Syst. Sci. Data, 2013. **5**(1): p. 165-185.
6. Greenpeace, *The Great Water Grab. How the Coal Industry is Deepening the Global Water Crisis*, 2016, Greenpeace International. p. 59.
7. Adams, M.L., *Sustainable Energy from Nuclear Fission Power.* National Academy pf Engineering, 2002. **32**(4).
8. J. Magill, V.B., D. Haas, J. Galy, R. Schenkel, H.-W. Wiese,G. Heusener, J. Tommasi and G. Youinou, *Impact limits of partitioning and transmutation scenarios on the radiotoxicity of actinides in radioactive waste.* Nuclear Energy, 2003. **42**(5): p. 263-277.
9. *Nuclear Fission.* https://www.nuclear-power.net/nuclear-power/fission/.
10. Dones, R., *Critical note on the estimation by Storm van Leeuwen J.W. and Smith P. of the energy uses and corresponding CO2 emissions from the complete nuclear energy chain*, 2007, Paul Scherrer Institut.
11. Kharecha, P.A. and J.E. Hansen, *Prevented Mortality and Greenhouse Gas Emissions from Historical and Projected Nuclear Power.* Environmental Science & Technology, 2013. **47**(9): p. 4889-4895.
12. Anil Markandya, P.W., *Electricity generation and health.* Energy and Health, 2007. **370**(9591): p. 979-990.
13. D. Weißbach, G.R., A. Huke, K. Czerski, S. Gottlieb and A. Hussein, *Energy intensities, EROIs (energy returned on invested), and energy payback times of electricity generating power plants.* Energy, 2013. **52**(C): p. 210-221.
14. Energy, S.o., *Blue Ribbon Commission on America' s Nuclear Future*, 2012.
15. *United States Nuclear Regulatory Commission* www.nrc.gov/waste.html.
16. *Advanced Separation Techniques for Nuclear Fuel Reprocessing and Radioactive Waste Treatment*. 2011: Woodhead Publishing.
17. *Critical Metals Handbook*. 2014: American Geophysical Union.
18. Griffiths, T.R., et al., *Reprocessing spent nuclear fuel using molten carbonates and subsequent precipitation of rare earth fission products using phosphate.* Journal of Alloys and Compounds, 2006. **418**(1-2): p. 116-121.
19. *Managing Spent Fuel from Nuclear Power Reactors. Experience and Lessons from Around the World*, Z.M. Harold Feiveson, M.V. Ramana and Frank von Hippel, Editor 2011, International Panel of Fissile Materials.
20. *http://www.separationprocesses.com/Extraction/SE_001.htm*.
21. REAS, E.R.I.a.W.H., *THE PUREX PROCESS -A SOLVENT EXTRACTION REPROCESSING METHOD FOR IRRADIATED URANIUM*, 1957: RICHLAND, WASHINGTON
22. Lewis, F.W., et al., *Highly Efficient Separation of Actinides from Lanthanides by a Phenanthroline-Derived Bis-triazine Ligand.* Journal of the American Chemical Society, 2011. **133**(33): p. 13093-13102.

23. Leonard, R.A., et al., *Annular Centrifugal Contactors for Solvent Extraction.* Separation Science and Technology, 1980. **15**(4): p. 925-943.
24. *Schematic cross-section of the CINC centrifugal Contactor* www.researchgate.net/figure/233416873_fig1_Fig-1-Schematic-cross-section-of-a-centrifugal-contact-separator-CINC-V02-courtesy-of, Editor.
25. G. J. Bernstein, D.E.G., J. F. Lenc, N. M. Levitz, *A High-Capacity Annular Centrifugal Contactor.* Nuclear Technology 1973. **20**(3): p. 200-202.
26. Leonard, R.A., *Recent Advances in Centrifugal Contactor Design.* Separation Science and Technology, 1988. **23**(12-13): p. 1473-1487.
27. Leonard, R.A., D.B. Chamberlain, and C. Conner, *Centrifugal Contactors for Laboratory-Scale Solvent Extraction Tests.* Separation Science and Technology, 1997. **32**(1-4): p. 193-210.
28. Vedantam, S. and J.B. Joshi, *Annular Centrifugal Contactors—A Review.* Chemical Engineering Research and Design, 2006. **84**(7): p. 522-542.
29. R. A. LEONARD, G.J.B., R. H. PELTO, A.A. ZIEGLER, *Liquid-Liquid Dispersion in Turbulent Couette Flow.* American Institute of Chemical Engineers 1981. **27**(3).
30. Stuart, J.T., *Taylor-vortex flow: a dynamical system.* Industrial and Applied Mathematics, 1986. **28**(3): p. 315-342.
31. Koschmieder, E.L., *Turbulent Taylor vortex flow.* Journal of Fluid Mechanics, 2017. **93**(3): p. 515-527.
32. Andereck, C.D., S.S. Liu, and H.L. Swinney, *Flow regimes in a circular Couette system with independently rotating cylinders.* Journal of Fluid Mechanics, 2006. **164**: p. 155-183.
33. Richard M Lueptow, A.D., Kyungyoon Min, *Stability of axial flow in an annulus with a rotating inner cylinder.* Physics of Fluids A, 1992. **4**(11): p. 2446-2455.
34. Davis, M.W. and E.J. Weber, *Liquid-Liquid Extraction between Rotating Concentric Cylinders.* Industrial & Engineering Chemistry, 1960. **52**(11): p. 929-934.
35. Watanabe, T., Y. Toya, and I. Nakamura, *Development of free surface flow between concentric cylinders with vertical axes.* Journal of Physics: Conference Series, 2005. **14**(1): p. 9.
36. Watanabe, T. and Y. Toya, *Vertical Taylor–Couette flow with free surface at small aspect ratio.* Acta Mechanica, 2012. **223**(2): p. 347-353.
37. J. D. Seader, E.J.H., D. Keith Roper *Separation Process Principles with Applications using Process Simulators*. 3rd ed. 2010: Wiley.
38. *Liquid extraction (2 ed.), Robert E. Treybal, McGraw-Hill, New York (1963). 621 pages. $16.50.* AIChE Journal, 1963. **9**(6): p. 863-863.
39. Leonard, R.A., et al., *The Centrifugal Contactor as A Concentrator in Solvent Extraction Processes.* Separation Science and Technology, 1993. **28**(1-3): p. 177-200.
40. Fogler, H.S., *Elements of chemical reaction engineering*. 1999: Third edition. Upper Saddle River, N.J. : Prentice Hall PTR, [1999] ©1999.
41. KneißI, F., A. Geist, and W. Nitsch, *EUROPIUM EXTRACTION INTO D2EHPA: KINETICS OF MASS TRANSFER IN A STIRRED CELL.* Solvent Extraction and Ion Exchange, 1999. **17**(3): p. 475-493.
42. Wang, Y., et al., *The novel extraction process based on CYANEX® 572 for separating heavy rare earths from ion-adsorbed deposit.* Separation and Purification Technology, 2015. **151**: p. 303-308.
43. Quinn, J.E., et al., *Solvent extraction of rare earth elements using phosphonic/phosphinic acid mixtures.* Hydrometallurgy, 2015. **157**: p. 298-305.
44. K. Lyon, M.G., R. S. Herbst, T. Garn, A. Welty, M. D. Soderstrom, B. Jakovljevic. *ENHANCED SEPARATION OF RARE EARTH ELEMENTS*. in *2016 International Mineral Processing Congress*. 2016.

45. Choppin, G., Jan-Olov Lilijenzin, and Jan Rydberg, *Radiochemistry and Nuclear Chemistry*. 3 ed. 1994.
46. Agarwal, V., M.S. Safarzadeh, and J.T. Bendler, *Solvent extraction of Eu(III) from hydrochloric acid solutions using PC88A and Cyanex 572 in kerosene.* Hydrometallurgy, 2018. **177**: p. 152-160.
47. Choppin, G.R. and K.L. Nash, *The kinetics and mechanisms of extraction of Am(III) and Th(IV) by HDEHP.* Revue de Chimie Minerale, 1977. **14**(2): p. 230-236.
48. A. H. SELKERl, C.A.S., *Factors Affecting which Phase will Disperse when Immiscible Liquids are Stirred Together* The Canadian Journal of Chemical Engineering, 1965.
49. Bin Hu, P.A., *Phase Inversion and Associated Phenomena in Oil-Water Vertical Pipeline Flow.* THE CANADIAN JOURNAL OF CHEMICAL ENGINEERING, 2006.
50. LUHNING, R.W., *PHASE INVERSION IN STIRRED LIQUID-LIQUID SYSTEMS*

1970, University of London.
51. Norato, M.A., L.L. Tavlarides, and C. Tsouris, *Phase inversion studies in liquid-liquid dispersions.* The Canadian Journal of Chemical Engineering, 1998. **76**(3): p. 486-494.
52. Leonard, R.A., *Solvent Characterization Using the Dispersion Number.* Separation Science and Technology, 1995. **30**(7-9): p. 1103-1122.
53. Wardle, K.E., et al., *Analysis of the effect of mixing vane geometry on the flow in an annular centrifugal contactor.* AIChE Journal, 2009. **55**(9): p. 2244-2259.
54. Wardle, K.E., et al., *Free surface flow in the mixing zone of an annular centrifugal contactor.* AIChE Journal, 2008. **54**(1): p. 74-85.
55. Wardle, K.E., et al., *Experimental study of the hydraulic operation of an annular centrifugal contactor with various mixing vane geometries.* AIChE Journal, 2010. **56**(8): p. 1960-1974.
56. Horner, D., et al., *Interphase Transfer Kinetics of Uranium Using the Drop Method, Lewis Cell, and Kenics Mixer.* Industrial & Engineering Chemistry Fundamentals, 1980. **19**(1): p. 103-109.
57. Bringer, M.R., et al., *Microfluidic systems for chemical kinetics that rely on chaotic mixing in droplets.* Philosophical transactions. Series A, Mathematical, physical, and engineering sciences, 2004. **362**(1818): p. 1087-1104.
58. Nichols, K.P., et al., *Toward Mechanistic Understanding of Nuclear Reprocessing Chemistries by Quantifying Lanthanide Solvent Extraction Kinetics via Microfluidics with Constant Interfacial Area and Rapid Mixing.* Journal of the American Chemical Society, 2011. **133**(39): p. 15721-15729.
59. Lewis, J.B., *The mechanism of mass transfer of solutes across liquid-liquid interfaces*

Part II.-The transfer of organic solutes between solvent and aqueous phases. Chemical Engineering Science, 1954. **3**: p. 260-278.
60. Lewis, J.B., *The mechanism of mass transfer of solutes across liquid-liquid interfaces*

Part I: The determination of individual transfer coefficients for binary systems. Chemical Engineering Science, 1954. **3**: p. 248-259.
61. McManamey, W.J., et al., *The influence of molecular diffusion on mass transfer between turbulent liquids.* Chemical Engineering Science, 1973. **28**(4): p. 1061-1069.
62. Olander, D.R. and M. Benedict, *The Mechanism of Extraction by Tributyl Phosphate-n-Hexane Solvents Part II. Nitric Acid Extraction.* Nuclear Science and Engineering, 1963. **15**(4): p. 354-365.
63. Davies, J.T. and G.R.A. Mayers, *The effect of interfacial films on mass transfer rates in liquid-liquid extraction.* Chemical Engineering Science, 1961. **16**(1): p. 55-68.
64. Geist, A., W. Nitsch, and J. Kim, II, *On the kinetics of rare-earth extraction into D2EHPA.* Chemical Engineering Science, 1999. **54**(12): p. 1903-1907.

65. Burger, L.L., *THE TRANSFER OF URANYL NITRATE ACROSS THE WATER - TRIBUTYL PHOSPHATE INTERFACE.* 1959.
66. Nitsch, W. and B. Kruis, *The influence of flow and concentration on the mass transfer mechanism in chelating liquid/liquid-extractions.* Journal of Inorganic and Nuclear Chemistry, 1978. **40**(5): p. 857-864.
67. Vandegrift, G.F. and E.P. Horwitz, *The mechanism of interfacial mass transfer of calcium in the system: Di(2-ethylhexyl)phosphoric acid in dodecane-dilute nitric acid.* Journal of Inorganic and Nuclear Chemistry, 1977. **39**(8): p. 1425-1432.
68. Danesi, P.R., et al., *Simulation of interfacial two-step consecutive reactions by diffusion in the mass-transfer kinetics of liquid-liquid extraction of metal cations.* The Journal of Physical Chemistry, 1980. **84**(26): p. 3582-3587.
69. Hughes, M.A. and V. Rod, *On the use of the constant interface stirred cell for kinetic studies.* Hydrometallurgy, 1984. **12**(2): p. 267-273.
70. El-Hefny, N.E., *Kinetics and mechanism of extraction and stripping of neodymium using a Lewis cell.* Chemical Engineering and Processing: Process Intensification, 2007. **46**(7): p. 623-629.
71. AUSTIN, L.J., *LIQUID — LIQUID MASS TRANSFER IN A STIRRED CELL*, in *Department of Chemical Engineering & Chemical Technology*1966, Imperial College of Science and Technology: London.
72. Bulička, J. and J. Procházka, *Mass Transfer between Two Turbulent Liquid Phases*. Vol. 31. 1976. 137–146.
73. Dong, J., et al., *Thermodynamics and kinetics of lutetium extraction with HEH(EHP) in hydrochloric acid medium.* Journal of Rare Earths, 2016. **34**(3): p. 300-307.
74. Hinze, J.O., *Fundamentals of the hydrodynamic mechanism of splitting in dispersion processes.* AIChE Journal, 1955. **1**(3): p. 289-295.
75. Zhou, G. and S.M. Kresta, *Correlation of mean drop size and minimum drop size with the turbulence energy dissipation and the flow in an agitated tank.* Chemical Engineering Science, 1998. **53**(11): p. 2063-2079.
76. Haas, P.A., *Turbulent dispersion of aqueous drops in organic liquids.* AIChE Journal, 1987. **33**(6): p. 987-995.
77. Tison, E., *Caractérisation de la zone de mélange d'un extracteur centrifuge à effet Couette utilisé en extraction liquide-liquide*, 1996. p. 1 vol. (190 p.).
78. Kadam, B.D., et al., *Dispersed phase hold-up, effective interfacial area and Sauter mean drop diameter in annular centrifugal extractors.* Chemical Engineering Research and Design, 2009. **87**(10): p. 1379-1389.
79. Andersson, R. and B. Andersson, *On the breakup of fluid particles in turbulent flows.* AIChE Journal, 2006. **52**(6): p. 2020-2030.
80. Tamhane, T.V., et al., *Measurement of drop size characteristics in annular centrifugal extractors using phase Doppler particle analyzer (PDPA).* Chemical Engineering Research and Design, 2012. **90**(8): p. 985-997.
81. Wyatt, N.B., T.J. O'Hern, and B. Shelden, *Drop-size distributions and spatial distributions in an annular centrifugal contactor.* AIChE Journal, 2013. **59**(6): p. 2219-2226.